Politecnico di Torino

Master's Degree in Biomedical Engineering – Bionanotechnology

Academic year 2024/2025

Optimization of Polymeric Coatings for Vascular Balloon Deployment

Supervisors:
Valentina A. Cauda
Carly S. Filgueria

Candidate:
Marta Aguglia

Abstract

Approximately 12-14% of the world's population experiences peripheral arterial disease (PAD), a progressive atherosclerotic condition that can lead to serious complications such as ischemia, ulceration, and limb amputation if untreated. When lifestyle changes and medications fail, clinicians often use percutaneous transluminal angioplasty (PTA) —a minimally invasive procedure where a balloon, uncoated or coated with an antiproliferative drug (drug-coated balloon, DCB), is inflated at the occlusion site to restore blood flow. Although effective, restenosis and thrombosis limit PTA's long-term success. DCBs directly address restenosis and indirectly address thrombosis by releasing an antiproliferative drug (e.g., Paclitaxel, PTX) to prevent neointimal hyperplasia and impede clot formation. Compared to uncoated balloons, DCBs improve outcomes and reduce lesion failure rates (28.6% vs 17.9%); yet, clinical efficacy remains limited by restenosis (20–45%) and thrombosis (3–10%) within six months. Moreover, commercial DCBs suffer from poor drug transfer to the vessel wall (<10%), limited retention at the target site, and short shelf life.

To overcome these limitations, this work presents a customizable, "off-the-shelf" hydrogel-based coating for commercial uncoated balloons, designed for patient-specific intraoperative application, enabling tailored, sustained drug delivery. The study focused on formulation optimization to achieve adequate mechanical properties, vessel adhesiveness, and prolonged PTX drug release.

Calcium alginate (CA) hydrogels were generated by combining sodium alginate (SA) with calcium carbonate ($CaCO_3$) and glucono-δ-lactone (GDL), added in a fixed 1:2 GDL-to-$CaCO_3$ molar ratio to gradually lower the pH and promote internal gelation. High and medium viscosity SA (HV, 1000-1500 mPa·s; MV, 350–500 mPa·s) were compared in terms of mechanical and coating performance; MV-SA was selected based on its easier handling and greater uniformity in coating the balloon. Five 1% MV-SA formulations with increasing concentrations of $CaCO_3$ (15–75 mM, 1X–5X) and GDL (30–150 mM) were tested, demonstrating that the 4X formulation (60 mM $CaCO_3$ and 120 mM GDL) had optimal crosslinking time (~12 min) and good mechanical performance (cross-over point: 3.21 ± 0.27%). Adding 5% polyvinyl alcohol (PVA), in a 1:1 ratio with CA, significantly enhanced mechanical stability and adhesion, as confirmed by amplitude

sweep and probe tack tests. A thermal cycling protocol (−20 °C for 10 min, 55 °C for 60 min) further improved mechanical properties. FTIR confirmed hydrogen bonding between PVA and CA.

As a proof of concept, PTX-loaded 4X hydrogels (0.25 mg/ml) were applied onto 3D-printed balloon phantoms (100 mm x 6 mm) mimicking a clinical scenario. Formulations with either low (13–23 kDa) or high (146–186 kDa) molecular weight (MW) PVA were tested. UV–vis spectroscopy showed that low MW PVA enabled a sustained release of 53% over 5 days, while high MW PVA led to a faster, near-complete release within 8 hours. These results confirm the versatility of the coating, as parameters such as polymer molecular weight can be adjusted.

In conclusion, among the different formulations tested, the 4X + 5% low MW PVA hydrogel demonstrated favorable mechanical properties, strong adhesion, and sustained PTX release, supporting its use as a candidate coating for intraoperative application on off-the-shelf vascular balloons. This approach enables tailored drug delivery profiles aligned with patient-specific clinical needs.

Acknowledgments

First and foremost, I would like to express my deepest gratitude to my Italian supervisor, Valentina Alice Cauda, without whom this wonderful opportunity to pursue my thesis in the United States would never have materialized. I am also sincerely thankful to Dr. Maham Rahimi, whose vision and invaluable medical support made this multidisciplinary project possible. A special and heartfelt thank you goes to my American supervisor, Carly S. Filgueira. Her unwavering support over these nine months has been absolutely essential. Thanks to her, I discovered the beauty of research—with all its challenges and complexities that make it so fascinating. I am deeply grateful for her involvement, warmth, and kindness; for believing in me even when I doubted myself; and for encouraging me to keep going even during the hardest moments. I would not be where I am today without her, and I will be forever thankful.

I would also like to thank all my lab colleagues who made each day more enjoyable and lighthearted. A special mention goes to Antonio Martino, a true source of inspiration and a constant support throughout these months. Thank you for trusting my instincts, for encouraging me to pursue my ideas, and for guiding me through both scientific and personal growth. You have been a fundamental mentor to me.

Another special thanks go to Cesare Farina, both a colleague and a housemate, who shared every single hour of this experience with me—through laughter, frustration, and moments of madness when research seemed impossible. I truly appreciate his support in this project, including his contribution to key experiments reported in this thesis, which were essential to drawing final conclusions. I already miss his contagious laughter, his "selective hearing", and the strange noises he used to make every morning. While on the topic of housemates, I would like to thank Danilo, our private chef at home—without whom I probably would have starved. He has been a wonderful friend, with whom I spent countless evenings talking late into the night. He was also a trusted advisor throughout my thesis work, always ready to offer guidance whenever I faced a problem and didn't know what to do. And my roommate Matilde, whose presence, though limited to the first few months, was crucial to my experience. She was not only a great roommate, but also a great friend, and I missed her deeply during the rest of the stay. I even missed having to worry about Cesare and his contaminations! I am also grateful to all the amazing people

I met along the way, each of whom contributed—some in small ways, some in great—to making these nine months unforgettable.

My gratitude extends not only to those who stood by me during this journey, but also to those who have always been there before. I want to thank my friends from the "Destinazione Laurea" group, who have become much more than just colleagues. Together we laughed, cried, and shared countless aperitivi—an essential ritual that helped us survive the ups and downs of the past two years. They made lectures less tedious, studying more bearable, and this path far more enjoyable. I also want to thank Alice, Giorgia, and Davide, with whom every group project became fun, and without whom I doubt I would have made it through the many difficult and stressful times. A special mention goes to Ferdinando, a classmate from the very beginning and a dear friend who hosted me countless times. Studying with him turned every exam into a team effort. His support has been crucial throughout this journey, and I would not have completed my degree without him.

My heartfelt thanks also go to those who have known me for much longer and have stood by me since the days when I had no idea what I wanted to do in life. To Massimo, my best friend, who has always been there through every hardship, helping me manage my frequent meltdowns, and with whom I have considered quitting university more times than I can count. Even though we didn't talk as often while I was in the US, nothing between us has changed — a clear sign of how strong and lasting our friendship is. Your emotional support during these last few weeks has meant the world to me.

To Vittorio—high school classmate, friend for over ten years, now my partner, confidant, shoulder to cry on, and source of strength—thank you for everything. You've been a pillar throughout this entire journey. With you, I've grown and matured, discovering what truly matters to me. I wouldn't have made it through these months—an emotional rollercoaster with you 8,665 km away—without your love and support. Thank you for helping me pick up the broken pieces when everything felt like too much. If I'm here today, having finally reached this milestone, it's also thanks to you.

Finally, I wish to thank my wonderful family, who have supported every choice I've made. I am especially grateful to my uncle, aunt, and my sweet little cousin, who made me feel at home even on the other side of the world—sharing American-style Sundays, outings,

and unforgettable experiences. To my grandmother, who has been a constant presence in my life since I was little. Thank you for your endless support and the comfort of your home-cooked meals. To my little brother, whom I've seen grow up day by day and who is now, incredibly, becoming a young adult. Whom I missed dearly and who now owes me updates on all the music I've missed while I was away. Even if I don't say it often—I love you deeply. To my mom, always by my side, encouraging me to take on this experience even when I was unsure. She has been not only a mother, but also a true friend and confidant. And even though we grew a little distant over the past few months due to some minor misunderstandings, we are now closer than ever — something that means the world to me.

And last but certainly not least, to my amazing dad, to whom I dedicate this achievement. Every sacrifice, every exam, every step forward has been guided by his unwavering belief in me. He always spoke proudly of me to everyone, no matter how small the accomplishment, and I know that finally earning this degree would have made him even prouder and would have filled him with immense joy. Although he is no longer here to celebrate this milestone, his presence is felt in every success and in every future plan. Every celebration will be for him, who may not be here physically, but whom I know is always by my side in spirit, and forever in my heart. I love you deeply and always will. Thank you for being my greatest supporter.

Table of Contents

List of Figures

List of Tables

List of Abbreviations

1. PAD: Peripheral Arterial Disease
2. DALY: Disability-Adjusted Life Year
3. LDL: Low-Density Lipoprotein
4. VSMC: Vascular Smooth Muscle Cell
5. ABI: Ankle-Brachial Index
6. PTA: Percutaneous Transluminal Angioplasty
7. DCB: Drug Coated Balloons
8. DES: Drug-Eluting Stents
9. PTX, $C_{47}H_{51}NO_{14}$: Paclitaxel
10. SRL, $C_{51}H_{79}NO_{13}$: Sirolimus
11. FDA: Food and Drug Administration
12. CE: Conformité Européenne
13. PEG: Polyethylene Glycol
14. SA: Sodium Alginate
15. $CaCl_2$: Calcium Chloride
16. $CaCO_3$: Calcium Carbonate
17. GDL: Glucono-δ-lactone
18. CA: Calcium Alginate
19. PVA: PolyVinyl Alcohol
20. G': Elastic or Storage Modulus
21. G'': Viscous or Loss Modulus
22. Tanδ: Loss or Damping Factor
23. LVR: Linear Viscoelastic Region
24. G'_{eq}: Equilibrium Storage Modulus
25. MW: Molecular Weights
26. SEM: Scanning Electron Microscopy
27. MV: Medium Viscosity
28. HV: High Viscosity
29. RT: Room Temperature
30. FT-IR: Fourier Transform Infrared Spectroscopy

31. IR: Infrared
32. ATR: Attenuated Total Reflectance
33. UV-vis: Ultraviolet-Visible Light Spectroscopy
34. Sem: Standard Error of the Mean
35. ANOVA: Analysis of Variance
36. ESEM: Environmental Scanning Electron Microscopy
37. Cryo-SEM: Cryogenic Scanning Electron Microscopy

1. Introduction

1.1 Clinical Overview of PAD

Peripheral arterial disease (PAD) is a chronic vascular disease characterized by the blockage of peripheral arteries, principally in those supplying blood to lower extremities. This obstruction arises from the progressive accumulation of atherosclerotic plaques, composed mainly of cholesterol, within the inner layer of arterial walls.

PAD affects at least 113 million individuals worldwide, with an estimation of 74,100 deaths per year and an increase of about 70% since 1990, attributed to population growth and aging.[1] PAD prevalence rises with age, leading to higher rates in women compared to men; however, men exhibit higher mortality.[1] The economic burden is about $4.37 billion annually,[2] making it a relevant public health concern. The overall impact of PAD can also be assessed through disability-adjusted life years (DALYs), a parameter that quantifies the total number of years lost due to premature death and time lived with disease and disability. One DALY corresponds to one year of healthy life lost. As shown in Figure 1, life expectancy is significantly reduced in many countries due to PAD.

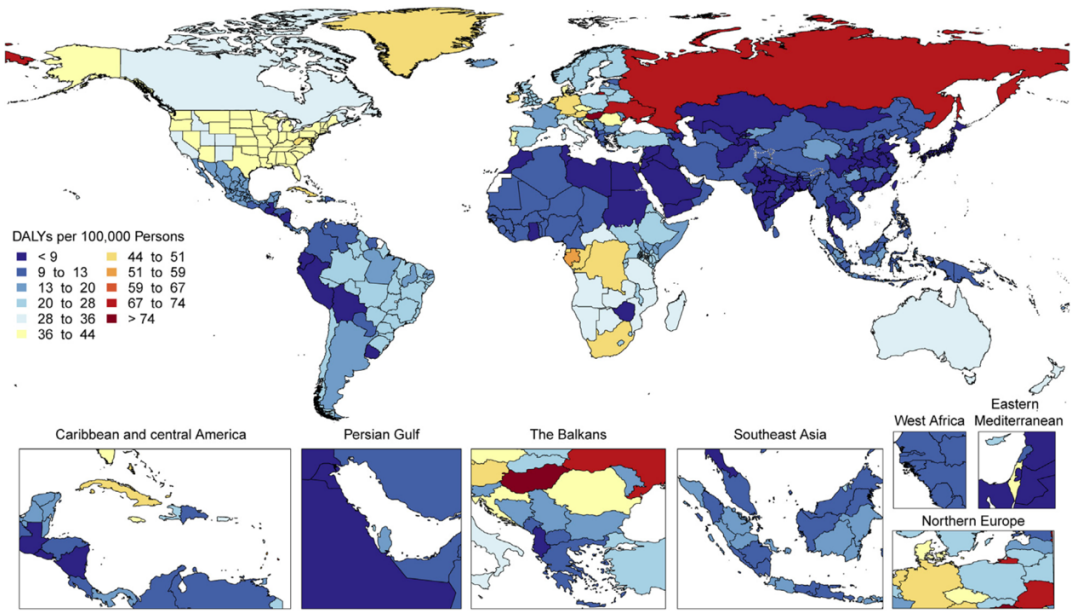

Figure 1. Map of disability-adjusted life years (DALYs) due to PAD in 2019.
More intense colors tending toward red denote regions where PAD leads to a significant reduction in patients' life expectancy.
Figure adapted from Roth et al.[1]

The main cause of PAD is *atherosclerosis*, which is a build-up of fat and other substances on artery walls that leads to plaque formation. As shown in Figure 2, plaques cause narrowing of the arteries, reducing blood flow, and in more severe cases leading to blood clot formation. The progression of the condition is a multistep process that involves chronic inflammation, lipid deposition inside the vessels, endothelial dysfunction and vascular remodeling. The process begins with endothelial damage, which promotes the recruitment of monocytes and T-cells to the site of injury, where low-density lipoprotein (LDL) infiltration also occurs. This triggers an inflammatory cascade, with macrophage activation and foam cell formation, resulting in an excessive fat accumulation. The inflammatory microenvironment leads to vascular smooth muscle cells (VSMCs) proliferation, which begin to deposit extracellular matrix around the lipid core, forming a fibrotic cap. The cap induces apoptosis of foam cells, until a necrotic core is formed. Over time, these plaques, called atheroma, expand until the arteries become occluded, preventing the proper supply of oxygen and nutrients to the tissues. This hypoperfusion can eventually degenerate into ischemia, which manifests with symptoms of varying severity depending on the degree of vessel occlusion and the ability of healthy vessels to compensate for the reduced blood flow.[3,4]

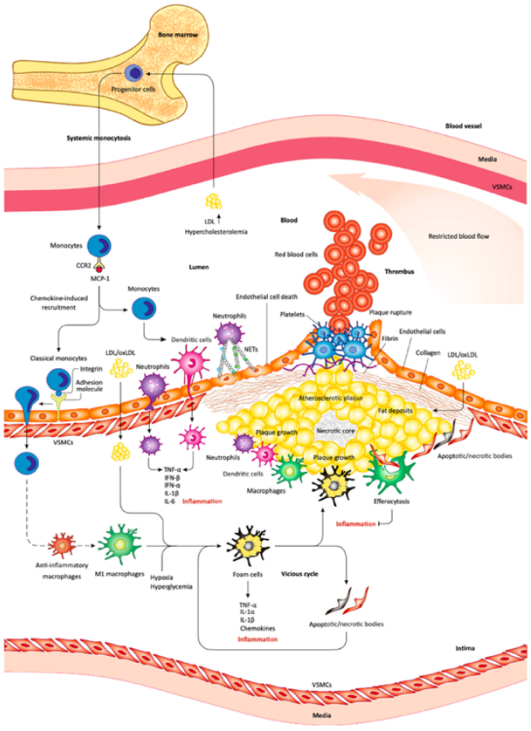

Figure 2. Diagram of atherosclerotic plaque formation.
The schematic shows the different developmental stages of atherosclerosis. Figure adapted from Turner et al.[4]

The major risk factors, that lead to the development of this pathology, are:

- *Hypertension and hyperlipidemia*: these are conditions that contribute to the dysfunction of blood vessel endothelial tissue and the development of atherosclerotic plaques.[5]
- *Smoking*: smoking is one of the biggest risk factors for PAD, which is easier to intervene on. Smokers show a significantly higher risk of developing ischemia, needing amputation, and experiencing death than nonsmokers.[6]
- *Diabetes mellitus*: Diabetic patients are particularly susceptible to PAD, and often have more serious complications, such as foot ulcers and gangrene.[7]
- *Advanced age*: The risk of developing PAD increases with age, particularly in individuals older than 65-70 years.[6]

Considering these risk factors, *prevention* plays a crucial role in slowing the progression of the disease. It has been shown that the probability of death or amputation in smoking patients is higher than in non-smoking patients,[5] so smoking cessation is a critical step. In addition, maintaining an active lifestyle, and a healthy diet rich in fruits and vegetables can further reduce the risk of developing PAD.

Given the impact of these risk factors, the first key step in the management of PAD is diagnosis, to try to identify patients early and define the appropriate treatment to avoid serious side effects. Among the simplest and non-invasive methods for diagnosing PAD is the *ankle-brachial index* (ABI). This index is calculated as the ratio of the systolic pressure measured at the ankle (posterior tibial or dorsal foot artery) to that measured at the arm (brachial artery). Normally the ABI is between 0.90 and 1.40, but a value below 0.90 indicates the presence of PAD. This index allows assessment of arterial perfusion of the lower limbs but provides no information on the anatomical location of the occlusion. Moreover, its accuracy is limited in the presence of noncompressible arteries, as the ABI may be falsely elevated (>1.40). In these cases, it is preferable to use the *toe-brachial index*, which uses the measurement of systolic toe pressure. Other tests such as duplex ultrasonography, magnetic resonance angiography, and computed tomographic angiography could be used to obtain information on the location of the occlusion.[8] Through diagnosis, patients can be classified into four categories,[9] according to the severity of symptoms:

1. *Asymptomatic Patients*: in these individuals detecting the presence of obstruction is more complicated due to the absence of noticeable symptoms. This implies that in this category of patients PAD is often identified incidentally through routine screening, so it often remains undiagnosed for years, increasing the risk of serious complications, such as limb ischemia or major adverse cardiovascular events. 59% of patients with PAD belong to this category.
2. *Chronic Symptomatic Patients*: in these individuals the presence of symptoms allows earlier detection of the pathology. The most common clinical manifestations are intermittent claudication and discomfort in legs and feet localized around the vascular occlusion.
3. *Chronic Limb-Threatening Ischemia Patients*: in these individuals the most common symptoms are ischemic rest pain, tissue loss or non-healing ulcers. This category of patients is associated with a high risk of amputation and often presents other comorbidities such as renal failure or diabetes.
4. *Acute Limbe Ischemia Patients*: the latter category occurs due to acute thrombosis or embolism resulting in limited perfusion with symptoms such as paresthesia, paralysis, and absence of peripheral pulse. Even in this case, the probability of amputation is extremely high.

The primary difference between symptomatic and asymptomatic patients is prognosis, because in symptomatic PAD is associated a higher probability of developing adverse cardiac events. However, the mortality rate is comparable between the two groups. The disease progression is often slow and insidious, especially in the case of women who show more atypical symptoms, such as burning or fatigue, greater functional impairment, and higher risks of complications. Despite this gender difference, to date women are underrepresented in clinical trials.[9]

Early and accurate diagnosis not only identifies the presence of PAD but also guides in appropriate treatment approaches. Indeed, it is essential to tailor therapy to the severity of occlusion, to prevent major adverse cardiovascular events, slow down disease progression and improve patients' quality of life. In addition to prevention, several treatments are currently available for PAD. In the early stages of the disease an option is the p*harmacological treatment*, through the administration of drugs to limit the progression of PAD. The main pharmacological treatments include the use of antiplatelet and

anticoagulants such as Aspirin, Clopidogrel, and Heparin. It is also possible to administer drugs with the aim of reducing symptoms, such as those of intermittent claudication. In the advanced stages, a *surgical procedure* may be necessary. Common treatments include (I) surgical bypass, in which an alternative pathway for blood flow is created; (II) angioplasty, a minimally invasive procedure in which a balloon catheter is used to dilate the occluded artery; (III) stent placement, in which a permanent device is inserted inside the damaged blood vessel to restore blood flow; (IV) atherectomy, which involves the physical removal of atherosclerotic plaque; (V) amputation, which occurs in the most severe cases and as a last resort, involving total removal of the limb.[10] Minimally invasive approaches are currently considered the treatment of choice in suitable patients, due to their limited invasiveness, lower surgical risk and shorter recovery. The choice of technique to be used depends on several criteria such as comorbidities, extension of occlusion, previous failed interventions, and other factors.[11]

In conclusion PAD is a widespread and debilitating disease with significant clinical and economic impact. Therefore, research is focusing on identifying new strategies to address the challenges associated with PAD and to reduce its overall burden. Among the various existing treatment options, minimally invasive techniques are widely preferred due to their reduced procedural risks and faster recovery times. In particular, *percutaneous transluminal angioplasty* (PTA) is a standard procedure for revascularization in patients with PAD.

1.2 PTA as Minimally Invasive Procedure for PAD Treatment

PTA is a minimally invasive procedure, widely used to restore blood flow in occluded arteries. During this intervention, a catheter with an inflatable balloon is inserted in the site of occlusion. By inflating the balloon, the atherosclerotic plaque is compressed against the arterial wall, increasing the luminal diameter and restoring proper blood flow,[12] as shown in Figure 3.

PTA is particularly effective in the early stages of PAD, where timely intervention can prevent further vascular deterioration and reduce the need for major surgical procedures such as bypass or limb amputation, which is only performed in the most extreme cases. Compared to surgical amputation, PTA is hence associated with lower morbidity and mortality rates. Additionally, it allows a faster recovery time of the patients, returning to normal activities in 24 to 48 hours.[13] Another advantage is that this technique reduces the procedural complexity compared to other options such as bypass or endarterectomy, and can be safely repeated multiple times if needed.[14] This highlights the crucial role of early diagnosis and immediate intervention in changing the course of the disease.

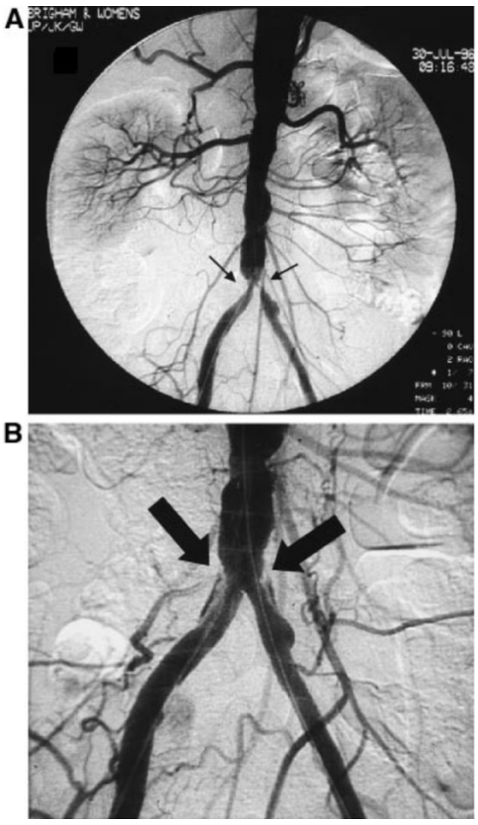

Figure 3. Picture of an angiogram of the iliac arteries.
A) Iliac artery occluded due to atherosclerotic plaque formation, with poor blood flow, B) artery after PTA, with increased vessel diameter. Figure adapted from Gornik et al.[6]

Depending on clinical factors, PTA may involve the exclusive use of a balloon or involve the placement of a permanent stent.[12] Regardless of the approach, PTA has several drawbacks and potential risks like all medical procedures. *Balloon angioplasty* may cause mechanical injury to the arterial wall, leading to complications such as vessel dissection, acute thrombosis, and restenosis, especially in the case of extensive and highly calcified

plaques.[15] In the case of *stent angioplasty*, some of the most common issues include stent fracture, especially for longer lesions, persistent inflammation due to the presence of a foreign body, acute thrombosis and restenosis.[14,16] Regardless of the chosen approach, the main complications that limit the long-term effectiveness of PTA are acute thrombosis and restenosis, both contributing to treatment failure.

Both conditions can compromise vessel patency, reducing the benefits of the surgery and increasing the risk of adverse events. *Acute thrombosis* is defined as the formation of a thrombus at the site of vascular injury, x. Its manifestation involves three main mechanisms described in Virchow's triad, based on three interdependent conditions, as shown in Figure 4: endothelial injury, hemodynamic changes, and hypercoagulability.[17,18] *Endothelial injury* is the first element of the triad and arises from the mechanical injuries generated by the insertion of the balloon or stent in the site of occlusion. The damage causes exposure of subendothelial collagen and other thrombogenic components, triggering platelet adhesion and activation of the coagulation cascade. The second element of the triad is the *hemodynamic change* characterized by a reduction in the shear stress. This leads to decreased nitric oxide production, increased leukocyte adhesion, and increased expression of inflammatory molecules such as ICAM-1 and VCAM-1, which promote thrombogenesis. Finally, there is *hypercoagulability* due to an imbalance between clotting, fibrinolytic, and aggregating factors.

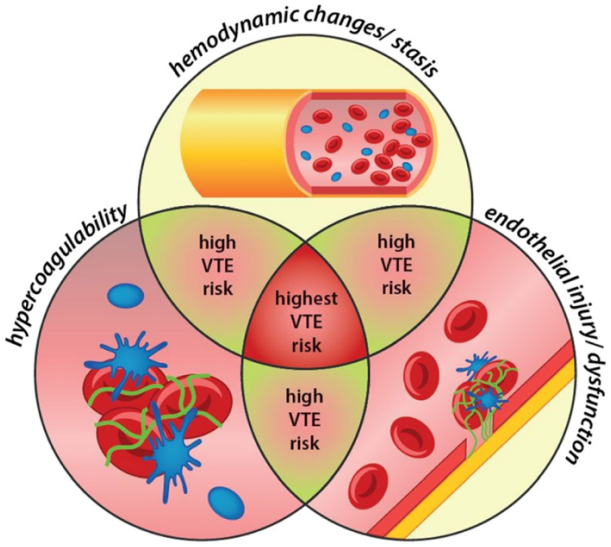

Figure 4. Diagram describing Virchow's triad.
There are three broad categories of factors that contribute to the risk of venous thrombosis (VTE): endothelial injury, hemodynamic changes, and hypercoagulability. Figure adapted from Kovačič et al.[17]

Restenosis, instead, is the re-narrowing of the treated artery, as shown in Figure 5, occurring typically within 3-12 months after the intervention.[19] Balloon insertion into blood vessels can disrupt endothelial cells and induce a local inflammatory response. This results in the recruitment of inflammatory cells, triggering the proliferation and migration of VSMCs. All these processes culminate in intimal hyperplasia, a thickening of the wall that contributes to restenosis.[20] In ballon angioplasty, restenosis evolves through three stages: (I) early elastic recoil, (II) negative arterial remodeling and (III) neointimal hyperplasia. In contrast, stent angioplasty prevent recoil and remodeling, but neointimal proliferation remains the dominant mechanism.[21]

The drawbacks of PTA have led to the development of different therapeutic strategies aimed to address these post-procedural complications, releasing antiproliferative or anticoagulant drugs. Among the first approaches explored were systemic drug therapies, including intravenous or oral administration. Despite their theoretical potential, these strategies have proven inadequate mainly due to their inability to achieve sufficient drug concentration at the site of injury. In addition, it has been observed that this approach exposes patients to an increased risk of side effects due to the possible distribution of the drugs to non-target organs.[22] To overcome these limitations, research has increasingly focused on strategies aimed to locally release drugs, maximizing therapeutic concentrations while minimizing systemic side effects. Consequently, drug coated balloons (DCB) and drug-eluting stents (DES) have been developed as a possible solution.

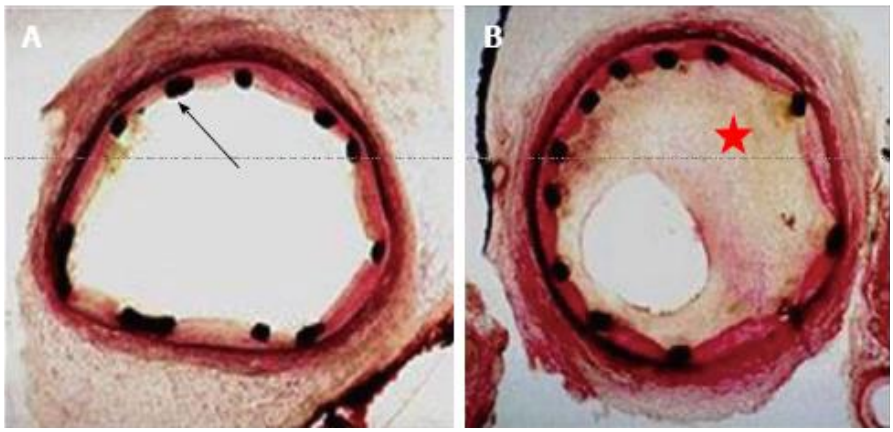

Figure 5. Cross-section of coronary artery.
A) Healthy artery, B) neointimal hyperplasia and narrowing of the vessel lumen due to restenosis. Figure adapted from Alraies et al.[16]

1.3 DCB and DES as Possible Therapeutic Devices for PAD

DCBs and DESs are standard devices designed to release, in extended period, anti-proliferative drugs, such as Paclitaxel or Sirolimus, to inhibit the proliferation of VSMCs reducing the risk of restenosis. The main difference lies in the mechanism of deployment. As shown in Figure 5, in the case of DCBs, the balloon is temporarily inserted into the vessel and inflated corresponding to the occlusion. During this short time window, the drug is transferred to the vessel wall by direct contact. Once the balloon is deflated and removed, there is no further release. In contrast, DESs are implantable devices that remain in place within the vessel. The drug is embedded within a polymer coating on the surface of the stent, which degrades over time and allows for prolonged drug release over time.

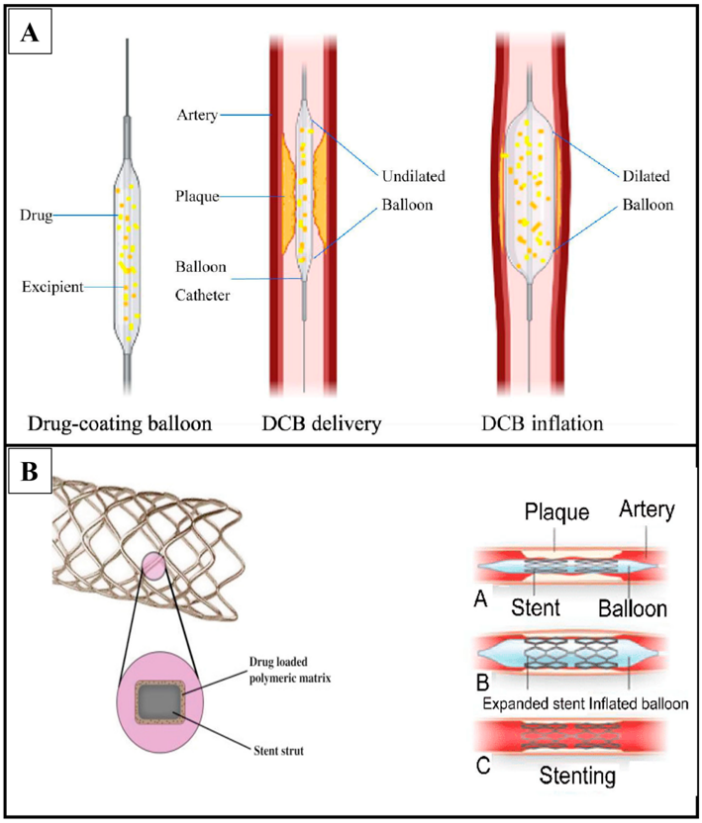

Figure 5. Diagram of the different drug release mechanism for DCBs and DESs.
A) For DCBs, the drug is placed on the surface of the device. When the balloon comes into contact with the artery wall, the drug diffuses from the DCB to the vessel tissue. B) For DESs, the drug is inserted inside a polymer layer. In this case, drug release occurs mainly by diffusion within the polymer and by erosion/degradation of the polymer itself. Figure adapted from Qamar et al.[23]

Both DCB and DES are proposed as therapies to ensure more targeted and effective treatment: studies have demonstrated that DESs have a restenosis rate of 3-20%, compared with 16-44% for bare-metal stents after 20 months from the stent placement.[16] The multicenter randomized AcoArt II-BTK trial with 105 participants demonstrated, at a 5-year follow-up, a complete wound healing of 89.4% in the DCB-treated group compared to the one treated with traditional balloons, in which the rate is 57.2% ($p = 0.04$). In addition, 34.5% major adverse events are shown in the DCB-treated group, compared with 56.1% in the second group ($p = 0.013$).[24] Several studies have also compared the effects of DCB and DES. The DRASTICO trial tested 192 patients randomized to be treated with DCB or DES, for a 12-month follow-up. The results showed no significant differences in incident restenosis between the DES and DCB groups, occurring in 21% of DES patients and 22% of DCB patients over the course of 12 months.[25]

Despite similar outcomes, DCBs offer several advantages over DESs. Indeed, DCBs overcome some specific complications associated with stent implantation, such as allergic reactions, chronic inflammation caused by the presence of foreign materials, or stent fracture.[26] Another important advantage of DCBs is the great procedural simplicity: by not requiring a permanent device inside the artery, the use of DCBs allows less invasive procedures and the use of smaller sheaths. They allow more precision in positioning, since in the case of stents it is challenging to align the device perfectly parallel to the vessel walls. Moreover, they have the theoretical advantage of greater drug release per square millimeter of surface area than surface doses of DESs, and this may translate into greater therapeutic efficacy. Finally, DCBs have the potential to improve the outcomes of some treatments where DESs have been ineffective, such as areas where restriction is particularly problematic (e.g., in arteriovenous fistulas for dialysis access).[27] On the other hand, DESs also offer several advantages that make them relevant in a clinical context. First, they provide sustained mechanical support, especially in the case of calcified or extensive occlusions, where the use of DCBs may no longer be adequate. Another important advantage lies in the duration of drug release: current DCBs release the drugs only during the operative window (approximately 3 minutes), when the balloon is placed in contact with the vessel. In contrast, since stents are permanent devices, they allows a prolonged release over time.[28] Thus, both DESs and DCBs have advantages and

disadvantages, and their use is selected based on patient's clinical factors, extent of occlusion, and therapeutic goal. In light of this, research has increasingly focused on the development of innovative balloon coating strategies to ensure new therapeutic approaches tailored to patient-specific needs. By selecting different materials and coating techniques, the goal could be to obtain sustained, device-free drug release capable of combining the procedural advantages of DCBs with therapeutic effects of DESs. This line of thinking has the potential to overcome current limitations and expand the applicability of DCBs in clinical practice.

1.4 DCBs Technologies

DCBs are medical devices designed to deliver anti-restenosis pharmacological directly to the area of occlusion during balloon PTA. The effective use of DCBs starts with proper lesion preparation and appropriate selection of the balloon diameter to match the size of the occluded vessel. During handling, it is essential to avoid the contact with the coating surface to prevent loss or degradation of the active pharmaceutical ingredients. Additionally, the catheter should be positioned as rapidly as possible to avoid unwanted drug leakage. Once deployed, the balloon should be inflated for a sufficient time: normally a minimum of 30-120 seconds is required to ensure proper drug release.[29] The effectiveness of DCBs depends not only on proper procedural technique, but more importantly on device design. The performance of a DCB depends on several factors such as the choice of pharmacological agent, the coating technology used, and the type of coating used. Each of these aspects is critical in determining drug release kinetics and clinical outcome.

1.4.1 Therapeutic Agents

An important element in the design of DCBs is the type of therapeutic agent incorporated into the balloon's coating. The chosen drug must exhibit suitable biological properties, such as the ability to inhibit VSMCs proliferation and migration, but also adequate manufacturing properties to allow easier functionalization of the balloon. Commercially

available DCBs aim to deliver a high concentration of antiproliferative drugs, during the procedural timeframe, directly to the target vessel, minimizing systemic exposure. This localized drug release greatly reduces the risk of neointimal hyperplasia, and thus restenosis, improving patient outcomes. To date, the most widely used drugs are Paclitaxel and Sirolimus.

Paclitaxel (PTX, $C_{47}H_{51}NO_{14}$) was initially developed as a chemotherapeutic agent, due to its cytostatic and antiproliferative properties. These same properties make it effective in the vascular field to reduce restenosis rates after angioplasty. It is a complex diterpenoid with, as shown in Figure 6, has a tricyclic taxane core, i.e., a 6-8-6 membered ring, an ester group at C13 with a benzoylated side chain containing an aromatic amide group and several acetylated hydroxyl and hydroxyl groups. The presence of these groups makes PTX a lipophilic drug, which can inhibit key cellular processes, such as mitosis and proliferation, keeping cells in a cytostatic state.[30]

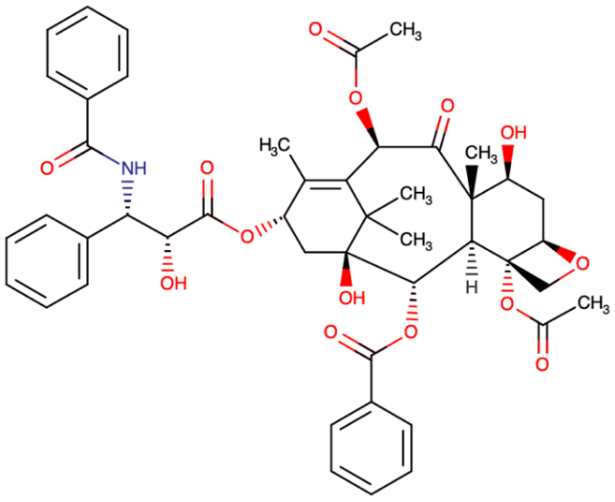

Figure 6. Chemical structure of Paclitaxel.
Figure adapted from DrugBank.

Specifically, it exerts its antiproliferative effects binding to tubulin, a structural protein present in high quantities in the cytoplasm and involved in microtubule formation. Microtubules play a crucial role in numerous cellular functions, including motility, cell division, and signal transduction. PTX stabilizes microtubules and prevents their disassembly, inhibiting cell division, particularly in the G0/G1 and G2/M phases of the cell cycle.[31] Additionally, this drug induces cell apoptosis due to its ability to bind and inhibit the function of B-cell Leukemia apoptosis inhibitor protein 2 (Bcl-2), a key protein

that regulates cell survival. The combination of these mechanisms makes PTX an effective drug for use in vascular interventions. The high lipophilicity of this agent facilitates its rapid uptake into cells, as it can easily cross the phospholipid membrane, resulting in a rapid onset of action.[31] However, this drug is associated with an increased risk of late thrombosis (especially in drug-eluting devices), systemic toxicity (particularly for high doses) and fast pH-sensitive degradation, leading to several adverse reactions that make the therapeutic effect of this drug unsatisfactory.[20,32,33] These issues have led to a growing interest in alternative medicines.

A second option is *Sirolimus* (SRL, $C_{51}H_{79}NO_{13}$), also known as rapamycin, is a macrolide lactone as shown in Figure 7, which was initially isolated and identified as an antifungal agent.

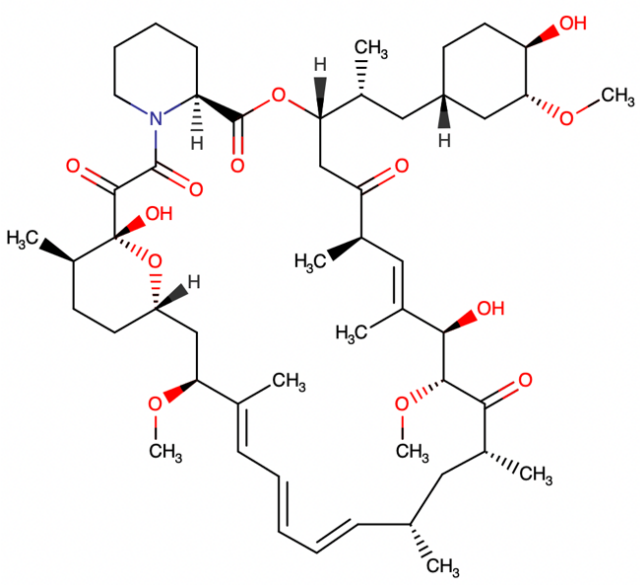

Figure 7. Chemical structure of Sirolimus.
Figure adapted from DrugBank.

Over time, its excellent antitumor and antiproliferative properties have been evaluated, making it an excellent candidate for the vascular field. Inside the cell, SRL binds reversibly to the receptor of the cytosolic protein FKBP12, creating a stable drug-protein complex. The complex inhibits the activity of mTOR (mammalian target of rapamycin), a cell cycle-specific kinase that plays a crucial role in different cell functions, such as cell growth and proliferation. Specifically, this inhibits cell proliferation through the block of the cell cycle evolution at the G1 and S phases[34,35]. SRL provides a prolonged window of action

compared with PTX. Additionally, it has been associated with a lower risk of late thrombosis [32,36], resolving one of the main concerns associated with PTX treatments. However, SRL has a low lipophilicity, and therefore the penetration of the drug into the vessel walls is more challenging. Indeed, the drug has a low affinity for the cell membrane, which is lipid in nature, making it difficult to release directly into the vascular tissue.

Among the two drugs, the most promising appears to be SRL, as it addresses several of the limitation associated with PTX, including the increased risk of late thrombosis, its high degradation rate in the human body, and cytotoxic effects. Despite these advantages, Paclitaxel remains the most widely used drug, and the only agent currently approved by the U.S. *Food and Drug Administration* (FDA) for DCBs, as shown in Table 1, which lists the six FDA-approved DCBs commercially available, all PTX-based. This is mainly due to the higher lipophilicity of PTX, which allows for easier internalization at the cellular level. Moreover, PTX was the first agent to be clinically tested for DCBs, so there are numerous clinical trials demonstrating its efficacy. In contrast, clinical trials on SRL-DCBs remain limited. Despite this, in Europe there are fifteen *Conformité Européenne* (CE) approved DCBs,[29] as shown in Table 2, of which four SRL-based.

Table 1. CE approved DCBs.
This table summarizes the main drug-coated balloon devices approved by the EC for clinical use. It includes the company, the drug used in the coating, and the surface drug concentration. From Verde et al.[29]

Device Name	**Company**	**Composition**
IN.PACT	Medtronic	Paclitaxel (3.5 $\mu g/mm^2$)
AGENT™	Boston Scientific	Paclitaxel (2 $\mu g/mm^2$)
Elutax SV	Aachen Resonance	Paclitaxel (2.2 $\mu g/mm^2$)
SeQuent Please	BBraun	Paclitaxel (3 $\mu g/mm^2$)
Pantera Lux	Biotronik	Paclitaxel (3 $\mu g/mm^2$)
Danubio	Minvasys	Paclitaxel (2.5 $\mu g/mm^2$)
Dior II	Eurocor	Paclitaxel (3 $\mu g/mm^2$)
RESTORE	Cardionovum	Paclitaxel (3 $\mu g/mm^2$)
AngioSculpt X	Spectranetics	Paclitaxel (3 $\mu g/mm^2$)
Essential	iVascular	Paclitaxel (3 $\mu g/mm^2$)
Chocolate Touch	QT Vascular	Paclitaxel (3 $\mu g/mm^2$)
Selution	Med Alliance	Sirolimus (1 $\mu g/mm^2$)

SeQuent Please SCB	BBraun	Sirolimus (4 μg/mm^2)
MagicTouch	Concept Medical	Sirolimus (1.27 μg/mm^2)
Mozes SEB	Meril	Sirolimus (3 μg/mm^2)

Table 2. FDA approved DCBs.
This table summarizes the FDA-approved drug-coated balloons, highlighting that all approved DCBs exclusively use Paclitaxel as the antiproliferative agent. From FDA website.

Device Name	**Company**	**Composition**
AGENT	Boston Scientific	Paclitaxel (2 μg/mm^2)
SurVeil	Surmodics	Paclitaxel (2 μg/mm^2)
IN.PACT	Medtronic	Paclitaxel (3.5 μg/mm^2)
Stellarex	Philips	Paclitaxel (2 μg/mm^2)
Lutonix	BD Bard	Paclitaxel (2 μg/mm^2)
Ranger	Boston Scientific	Paclitaxel (2 μg/mm^2)

Although several clinical studies have shown that DCBs reduce the rate of restenosis compared with uncoated balloon angioplasty (17.9% vs 28.6%),[37] the positive effects remain limited. In fact, recent studies show restenosis rates of 20-45% within 6-12 months of DCB treatment.[38] In addition, acute thrombosis is not completely treated, with a rate of 3-10%.[39] These limitations, along with the fact that current DCBs rely on a single pharmacological agent, underscore the need to improve DCB technologies so as to treat not only restenosis but other mechanisms such as acute thrombosis with the addition of antithrombogenic agents to prevent thrombin formation. It might also be possible to include antiplatelet drugs to reduce blood clot formation, anti-inflammatory elements to inhibit the action of macrophages and monocytes, and that cytotoxic antibiotics that inhibit the G1 phase of cell proliferation.[40] Furthermore, significant drug losses often occur during balloon manipulation and deployment, which can reduce the effective dose administered to the patient and compromise therapeutic outcomes.[41]

1.4.2 Coating Technologies

A second important element in the design of DCBs is the coating system, which greatly influences drug release. An ideal coating technology should provide a thin, uniform layer across the entire balloon surface, exhibit mechanical stability during deployment, be industrially scalable, and cost-effective. However, current coating methods often fail to achieve these requirements, resulting in uneven drug distribution and coating detachment during handling. This instability could result in unwanted drug release during balloon positioning in the vessel, compromising therapeutic efficacy. These limitations have led to the development of innovative coating strategies designed to improve drug stability, adhesion and reproducibility. Some of the most studied techniques, showed in Figure 8, are:[40]

- *Spray coating*: this is one of the most widely used techniques, in which a device sprays a solution containing the drug onto the surface of the balloon, ensuring uniform deposition. Usually, this technique exhibits a biphasic type of release, with an initial burst release followed by a slower release that allows for long-term therapeutic effects. This coating strategy enables precises control over thickness and is suitable for large-scale production with minimal drug loss. However, it requires expensive equipment and high process optimization to achieve a good coating. Spray coating was used in Turner *et al.* study,[2] in which this technique was used to coat several balloons with paclitaxel and iohexol as an excipient. A drug loading of about 4.0 µg/mm² was achieved, and effective drug release was demonstrated using ex vivo pig arteries. This test proves good scalability and reproducibility of the method.
- *Dip coating*: in which the balloon is dipped in a solution containing the drug and any excipients. The balloon is then dried to evaporate the solvent and fix the coating on the surface. This is a very simple and cheap technique that can be applied even on complex geometries, but it is difficult to control the thickness and uniformity of the coating. This technique has also been tested in the preclinical context. For example, one study performed by Anderson *et al.*[42] exploited polyethylene oxide (PEO)-based dip coating into which PTX was embedded. This approach demonstrated controlled drug release in a porcine arterial model and allowed the creation of a multi-layer coating to achieve customized release profiles.

- *Micro-pipetting coating*: in which small volumes of solution, containing the drug and excipients, are applied, either manually or automatically, directly to the length of the balloon, using precision micropipettes. This technique provides very accurate control of drug quantity and distribution and ensures high efficiency. On the other hand, it is difficult to scale up, so it is not used on large-scale production, and requires high control to ensure coating uniformity. In a study performed by Fuglsby *et al.*[43] an automated micro-pipetting method was designed. Again, ballons were coated with PEO and PTX, and the system was then tested in vitro in an arterial flow model, showing good release.
- *Microcapsule Coating*: in which biodegradable microcapsules containing the drug are used and placed on an adhesive layer provided on the surface of the balloon. Drug release can occur either during balloon inflation, in which mechanical stresses disrupt the microcapsules, or over time through degradation of the material. This is an innovative technique but shows high costs and complex design.
- *Hydrogel-Based Coating*: in which a hydrogel is used as a matrix for drug incorporation, which is then released by diffusion and/or degradation. This technique is considered among the most promising, as the hydrogel composition can designed to allow for controlled releases, good adhesion with the blood vessel, and the delivery of different therapeutic agents. However, it is difficult to ensure coating stability during insertion into the vessel, to achieve adequate mechanical performance, and to prevent premature wash-out of the hydrogel into the bloodstream.
- *Polymer-Free Coating*: in which the drug is introduced directly onto the ballon surface in (micro)crystalline form or by introducing excipients such as urea, shellac, butylated hydroxytoluene, etc. This technique reduces the risk of late thrombosis, avoids the risks related to the use of hydrogels, and requires a simple fabrication process. However, it provides a rapid release that is not always desired, low adhesion and difficulty in achieving a uniform coating. Regarding this approach, direct addition of crystalline PTX to the balloon surface has been proposed by exploiting solvent-induced crystallization. This strategy, besides being extremely simple, ensured the formation of a uniform coating over the entire surface.[44]

Although microcapsule and hydrogel-based coatings are promising, to date there are no preclinical examples carried out explicitly in DCBs. Nevertheless, several studies suggest their potential for controlled drug delivery for use in this setting.

Currently, the available technologies are based on standardized, industrial processes that result in identical, ready to use coatings, leaving no opportunity for personalization. Hence the need to develop new customizable and modular coating technologies that could be used directly by the surgeon during the procedure, allowing for the selection of the drugs and concentrations to be used according to the patient's need. Also interesting is the possibility of developing multilayer coating systems that allow incorporation of different therapeutic agents and ensure release over time with different kinetics. Moreover, it would be useful to design user-friendly coating systems to ensure their translation into the clinical setting. In conclusion, there are still many viable avenues for improving coating technologies, each with the potential to increase therapeutic efficacy and improve patient outcomes.

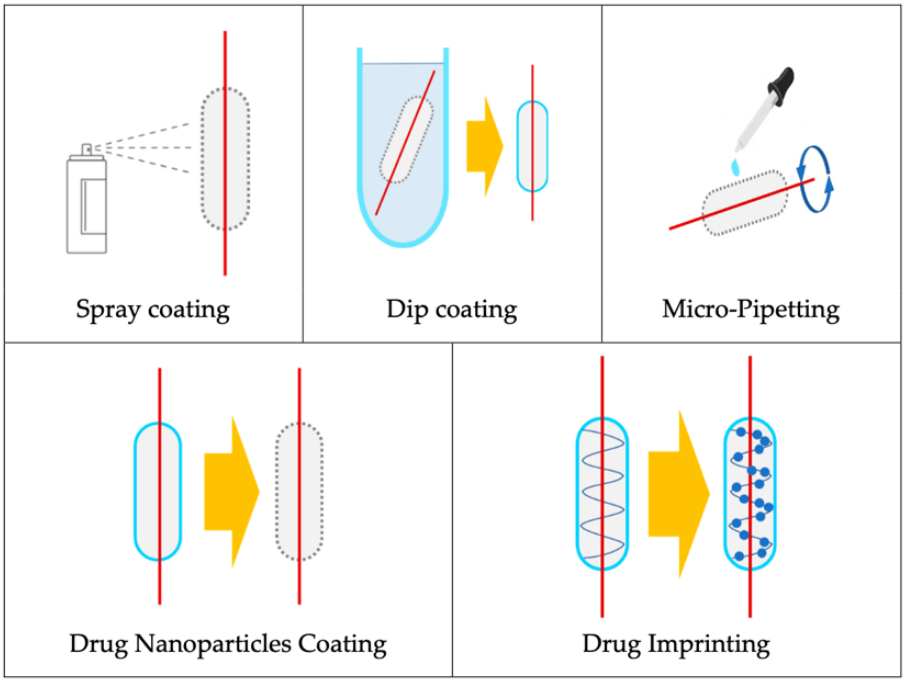

Figure 8. Schematic of different coating techniques for drug loading.
This figure provides an overview of the main methods used to coat balloons with therapeutic agents. Techniques include spray, dip, micropipette, and hydrogel-based coatings. Figure adapted from Rykowska et al.[40]

1.4.3 Coating Properties

A third important element in the design of DCBs are the physical and chemical properties of the coating. Material choice is critical to ensure controlled and efficient drug release, while also provide adequate mechanical performance. Current coatings are designed to withstand the mechanical stresses of the procedure, maintain a well-adhered coating on the balloon surface during use, and exhibit a sufficiently long shelf life. These materials are biocompatible and hemocompatible, designed to avoid unwanted inflammatory or immune responses as well as coagulative effects.

In the current commercial available DCBs, the most commonly used materials to fulfill these requirements are:[45] (I) *Urea*, a hydrophilic excipient that facilitates rapid dissolution of PTX in contact with blood, allowing efficient transfer of the drug from the balloon surface to the target vessel wall. (II) *Shellac*, a natural resin used in some polymer-free DCBs that acts as a dispersing agent for PTX crystals, also improving their adhesion. (III) *Polyethylene Glycol* (PEG), a hydrophilic excipient that modulates the release kinetics of PTX while improving the stability of the coating. (IV) *Polysorbate* and *Sorbitol*, excipients that used in combination enable the creation of a uniform, well-adhered coating on the balloon surface, enhancing the solubility of PTX. Polysorbate is a surfactant, while sorbitol a sugar alcohol.

Despite their wide use, these coatings have several drawbacks. A major limitation of current coatings is their mechanical instability, due to which during the procedure there is partial loss of drug before the DCB reaches the lesion. This unwanted leakage can significantly reduce therapeutic results.[46] Another limitation of current DCB coatings is the release time of the anti-proliferative drugs. As specified earlier, all commercially available devices deliver the drug only exclusively during the balloon inflation phase, but restenosis occurs about 3 months after PTA procedure. [47] Another important aspect, often overlooked, is the limited shelf life of current DCB coatings. Many of the excipient-drug formulations are sensitive to different environmental factors such as humidity, temperature and exposure to light, which can cause degradation of the drug over time. As a result, DCBs typically have a shelf life of only 6-12 months. This short life increases manufacturing costs and may limit the availability of the device in some clinical settings.[47]

These limitations highlight the need to explore new coating materials. In this context, hydrogels have emerged as highly promising materials due to their tunable properties. The study by Kaule *et al.*[48] compared various hydrogels as coating systems, showing that these materials significantly reduce drug loss during DCB placement, improving also the efficiency of drug release. Moreover, Consigny *et al.*[49] demonstrated that hydrogel-coated balloons loaded with antiproliferative agents were able to release sufficient amounts of drug to inhibit the proliferation of VSMCs in vitro. Similarly, Glazier *et al.*[50] evaluated the clinical performance of hydrogel-based coating for delivering antithrombotic agents on 95 patients, showing significant improvements in therapeutic outcomes. Together, these studies highlight hydrogels as promising candidates for controlled drug delivery applications, with the potential for incorporating multiple therapeutic agents without inducing toxicity.

1.5 Hydrogel and Excipients as Advanced Coating Materials

1.5.1 Introduction to Hydrogel

Hydrogels are three-dimensional polymeric networks capable of absorbing large amounts of water or biological fluids, maintaining a solid-like behavior in a stationary state.[51] A hydrogel is defined as such when at least 10% of its total weight is composed of water. One of the major advantages of hydrogels lies in their tunable properties, thus the possibility to significantly modify their characteristics depending on crosslinking agents used, composition, configuration, origin (natural, synthetic or hybrid), preparation method and other factors. By carefully selecting these parameters, it is possible to obtain biocompatible materials with good mechanical properties that are also biodegradable and biomimetic. Another interesting aspect is the possibility to modulate the release of any therapeutic agent encapsulated within the hydrogel depending on the network porosity and the degree of polymer crosslinking. In addition, hydrogels are typically non-Newtonian fluids with shear-thinning behavior: as mechanical stresses increase, viscosity decreases. These features make hydrogels an excellent option to consider in various biomedical applications, which can range from regenerative medicine to tissue and

biomedical engineering to delivery of therapeutic agents and injections,[52,53,54] as shown in Figure 9.

Based on the nature of crosslinking, hydrogels can be classified into:[54]

- *Physical hydrogels*, in which polymer chains interact through weak forces such as hydrogen bonding, ionic forces, and hydrophobic/hydrophilic interactions. These hydrogels do not require toxic crosslinkers and/or additives, do not involve organic solvents, possess sufficiently long degradation times and are easy to prepare. However, the presence of non-covalent bonds results in less unstable structure.
- *Chemical hydrogels*, where polymer chains interact through covalent bonds, which can be formed by various methods such as photopolymerization or thermal polymerization. These hydrogels possess superior mechanical performance, good degradability and controlled gelation. However, their synthesis often requires toxic crosslinkers and/or additives, and the reaction times are generally long, posing limitations for certain biomedical applications.

It is also possible to combine two or more components to create *composite hydrogels*. The advantage of this strategy is that the properties of the individual components can be combined, resulting in a material with increased performance, especially in terms of mechanical properties.

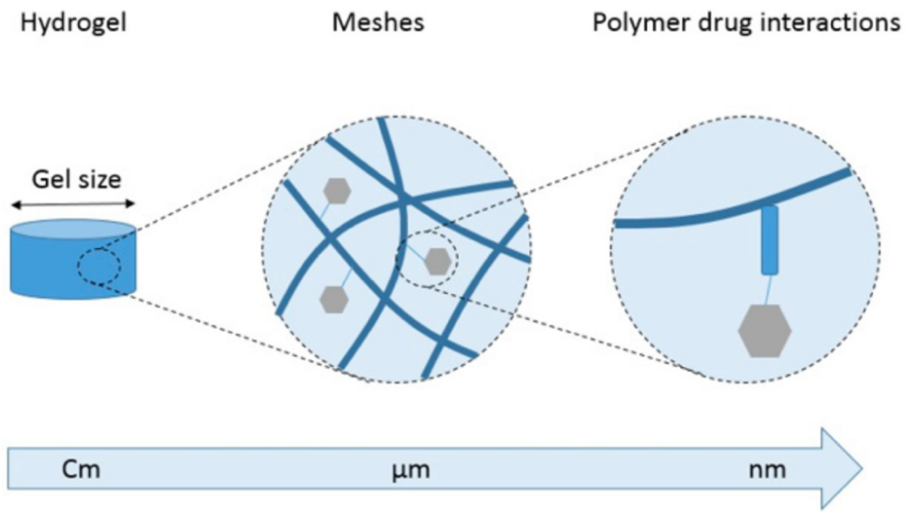

Figure 9. Diagram of a hydrogel at different scales.
This schematic shows the structure of the hydrogel at multiple levels of magnification, from macroscopic to nanoscale. The 3D polymer matrix and its ability to retain water and incorporate drugs are observed. Figure adapted from Chamkouri et al.[55]

The primary challenge in developing custom DCB coatings is to select a hydrogel with a simple and controllable crosslinking mechanism: the gelling process should not occur too quickly, as this could result in an inadequate coating, but at the same time it should not occur too slowly, as it should be used effectively and promptly during surgery procedure. Additionally, the hydrogel should possess adequate mechanical strength to remain undamaged during the inflation and deflation phases, and, if required, to provide structural support to the blood vessel walls. It should also ensure high encapsulation efficiency for different types of cargo, to provide effective treatment of patients. At the same time, the coating should be thin and uniform to ensure precise drug delivery and to avoid excessive material buildup, which could interfere with balloon performance.

Achieving these characteristics requires a careful selection not only of the primary hydrogel material, but also of the excipients, each of which can provide specific characteristics to the overall performance of the hydrogel.

1.5.2 Sodium Alginate as Primary Hydrogel Component

Among the polymers available for hydrogel formation in DCBs application, sodium alginate stands out for its high biocompatibility, its reversible sol-gel transition that is independent of both pH and temperature, and the high tunability of its properties by changing several parameters.

Presently, alginate is widely used in various biomedical fields, such as wound dressings, drug delivery, and tissue engineering, which demonstrates its potential for clinical translation. For example, FDA-approved alginate dressings, such as Algisite™ and Kaltostat™, are routinely used in clinical settings to treat wounds, because alginate dressings maintain a moist environment, promote angiogenesis and facilitate tissue regeneration.[56] A less known but widely used application of sodium alginate is in the treatment of gastroesophageal reflux. In fact, alginate is contained in Gaviscon™, a commercially available drug. Sodium alginate, in the presence of stomach acid, is able to form a gelatinous barrier floating above the stomach contents, preventing reflux into the esophagus.[57] Several pre-clinical studies have also shown the positive effect of alginate in the vascular field. This hydrogel can be used to release proangiogenic factors such as

VEGF by inducing neovascularization.[56] In particular, the ability of alginate-based hydrogels to encapsulate and control the release of bioactive molecules has gained increasing attention for cardiovascular applications, which could be translated into the delivery of anti-proliferative agents. Currently, no clinical trials using alginate as a component in DCBs have emerged, but its characteristics make it an ideal candidate. To understand its potential, however, it is necessary to understand its composition and behavior.

Sodium alginate (SA) is a natural, linear, hydrophilic, anionic polysaccharide derived from brown seaweed, brown algae, and in metabolic compounds of some bacteria. This biocompatible polysaccharide is composed of β-D-mannuronic acid (M-blocks) and α-L-guluronic acid (G-blocks), linked through glycosidic bonding. Depending on the extraction origin of the alginate, the content of G and M groups as well as their length can significantly change influencing the hydrogel characteristics. Specifically, a high content of G groups generates stiffer gels, while a high content of M groups generates softer and more elastic gels.[58] Other very important parameters that can be modified to achieve tunable properties are molecular weight and viscosity. The molecular weight of commercially available sodium alginate can vary between 32,000 and 400,000 g/mol.[56] High molecular weight alginates produce hydrogels with increased mechanical strength and lower degradability, while low molecular weight alginates produce softer gels with lower mechanical strength. However, it should be considered that as the molecular weight increases, the viscosity of the material also increases, which is usually desired to not be too high during processing or injections. Another important factor is the concentration of alginate in a solution, often expressed as weight/volume (% w/v). In general, as the concentration increases, viscosity, crosslink density and mechanical stiffness increase, while porosity decreases and therefore the release of molecules becomes slower. Finally, another very important factor that determines the final properties of hydrogel is the method of gelation.

SA can form gels either by lowering pH or in presence of multivalent cations. In the second case, crosslink formation is described by the "egg box model," as show in Figure 10, according to which cations form ionic bridges by interacting with the carboxyl groups of G-blocks, arranging themselves in cavities like eggs in egg box.[58,59]

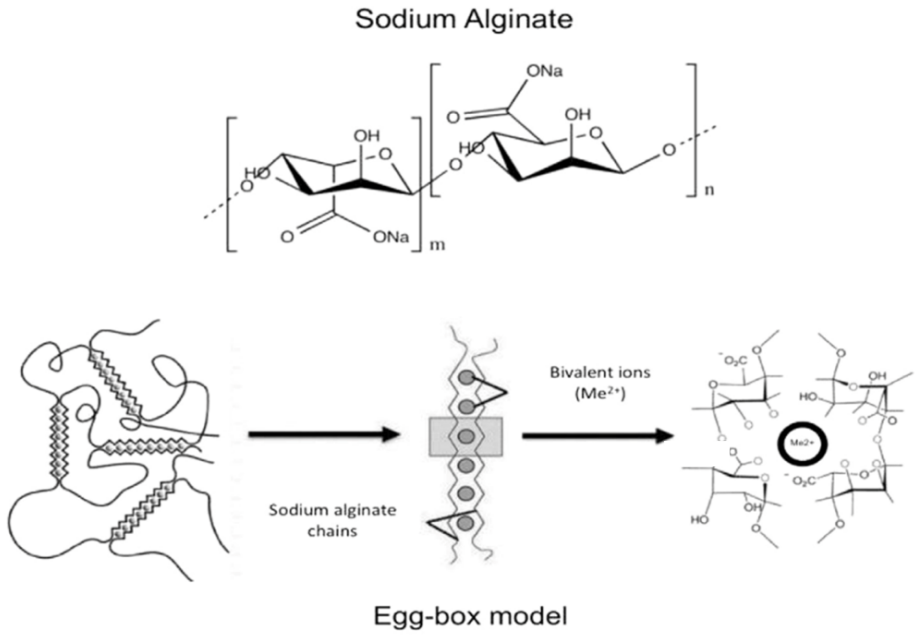

Figure 10. Chemical structure of SA and schematic of "egg box model".
The image shows the repeated units of sodium alginate and the ion cross-linking process with divalent cations, which form the characteristic "egg-box" structures that stabilize the hydrogel network. Figure adapted from Dodero et al.[58]

Crosslinking can occur externally if there is diffusion of ions from the outside to the inside, leading to inhomogeneous gelation. However, it can also occur internally, and in this case ions release takes place gradually throughout the solution leading to more homogeneous gelation.[60]

The affinity between alginate chains and cations decreases in the following order: Pb^{2+} > Cu^{2+} > Cd^{2+} > Ba^{2+} > Sr^{2+} > Ca^{2+} > Co^{2+}, Ni^{2+}, Zn^{2+} > Mn^{2+}, while Mg^{2+} ion does not promote gelation.[59] Usually, calcium chloride ($CaCl_2$) is used as crosslinking agent; however, this solubilizes rapidly in water and leads to instantaneous gelation when it comes in contact with the SA solution. Therefore, shaping hydrogel with required geometries is extremely difficult, as is the encapsulation of therapeutic agents. To overcome this issue, the alternative proposed is *calcium carbonate* ($CaCO_3$) as crosslinker agent. Specifically, $CaCO_3$ is an insoluble salt, consisting of calcium ions Ca^{2+} and carbonate ions CO_3^{2-}, as shown in Figure 11. It dissolves only in an acidic environment by releasing Ca^{2+} ions:

$$CaCO_3 + 2H^+ \rightarrow Ca^{2+} + CO_2 + H_2$$

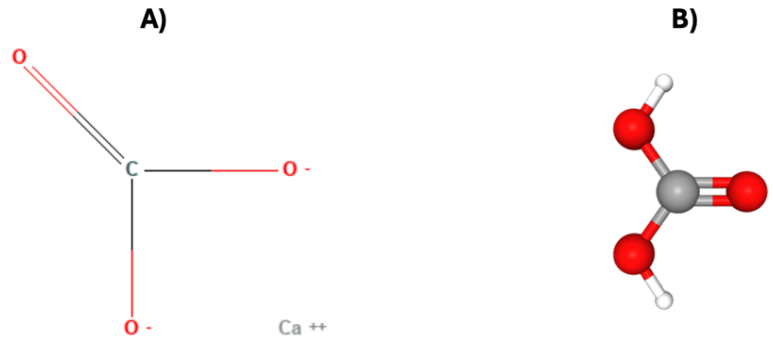

Figure 11. Chemical structure of calcium carbonate.
A) 2D and B) 3D chemical structure. The carbon atom is represented in gray, the oxygen atoms in red, and the calcium atoms in white. Figure adapted from Pubchem.

To lower the pH, *Glucono-δ-lactone* (GDL, $C_6H_{10}O_6$) is added into the formulation. GDL is a cyclic lactone, as shown in Figure 12, that in contact with water is transformed into gluconic acid by a hydrolysis reaction. This weak acid dissociates in gluconate and H^+ ions, lowering the pH of the solution and allowing the release of Ca^{2+} ions. The reaction follows the equation:[60,61]

$$GDL + H_2O \leftrightarrow HGluc \leftrightarrow Gluc^- + H^+$$

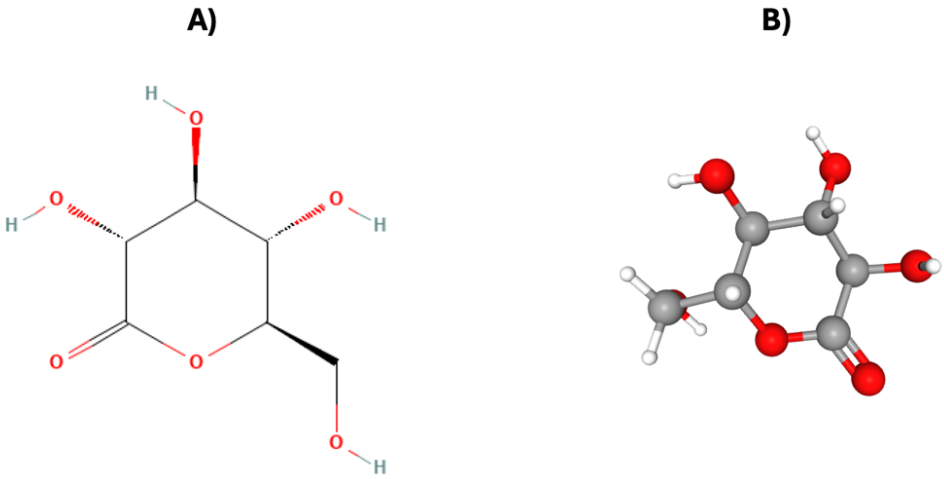

Figure 12. Chemical structure of glucono-δ-lactone.
A) 2D and B) 3D chemical structure. The carbon atom is represented in gray, the oxygen atoms in red, and the hydrogen atoms in white. Figure adapted from Pubchem.

After being released, these Ca^{2+} ions interact with the carboxyl groups of the alginate, forming a three-dimensional ionic network known as *Calcium Alginate* (CA). This in situ

crosslinking process allows for better control of the gelation kinetics, improving structural uniformity and facilitating the encapsulation of drugs within the hydrogel.

1.5.3 Polyvinyl Alcohol as Functional Excipient

Although SA offers excellent properties, its adhesiveness, especially when used in dynamic aqueous environments such as the vascular system, remains limited. To improve the adhesive characteristics of hydrogel, an excipient can be introduced. Literature research has led to the selection of polyvinyl alcohol, which in several studies has demonstrated adhesive properties in various biomedical applications when mixed with alginate.[62]

Polyvinyl alcohol (PVA, $(C_2H_4O)_n$) is a water-soluble synthetic polymer that is derived from the hydrolysis of polyvinyl acetate. As shown in Figure 13, each repeating unit consists of a methylene group and a carbon bonded to a hydroxyl group in the backbone. The presence of these hydroxyl groups ensures properties such as hydrophilicity, degradability and reactivity. PVA is a colorless, odorless polymer characterized by biocompatibility, adhesiveness, good mechanical stability, making it suitable for DCBs application. PVA can be classified according to molecular weight (typically ranging from 20,000 to 400,000 Da) or according to the concentration of acetate groups in the chain, which goes to define the degree of hydrolysis:

- *Partially hydrolyzed* (10-15 mol% acetate groups);
- *Intermediate hydrolyzed* (3-7 mol% acetate groups);
- *Fully hydrolyzed* (1-2 mol% acetate groups).

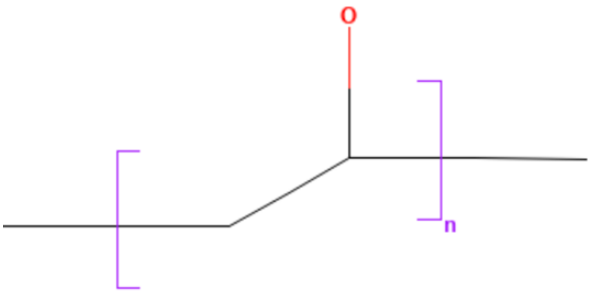

Figure 13. Chemical structure of PVA.
Figure adapted from PubChem.

Many properties of PVA depend on the degree of hydrolysis, also referred to as degree of saponification of polyvinyl acetate. As hydrolysis increases, crystallinity rise, leading to higher mechanical performance and a reduced solubility.[63] Another interesting property of PVA is that, subjected to multiple freeze/thaw cycles, it can crystallize acting as a physical cross-link, creating a stable network.[64] These characteristics make PVA a promising functional excipient to overcome the limitations of alginate alone, enabling the creation of more effective and durable drug delivery systems.

1.6 Rheology

1.6.1 Introduction to Rheology

In designing hydrogels for biomedical applications, such as in the case of DCBs, it is essential to understand and tune the physicochemical properties of the material. Among these, mechanical performance is particularly critical, as it affects not only the stability of the hydrogel during its handling and use, but also its interaction with cells and tissues. This aspect is relevant when working with materials such as SA and PVA, whose characteristics can vary significantly depending on the parameters described in the previous sections. For this reason, the use of accurate and reproducible characterization methods is essential to evaluate the hydrogel's behavior. In this context rheology arises as a method of choice.

Rheology is the science that study the flow and deformation of liquid and solid materials, and the role played by force, stress, strain and frequency in their viscoelastic behavior. Rheological analyses are extremely versatile, as they can determine a variety of material properties, such as thermal transitions, degree of network development, mechanical properties and more. Furthermore, these tests enable the study of the behavior of a wide range of materials, which can differ from low-viscosity fluids to solid gels.[65]

The rheometer is an instrument composed of a motor to which are connected attachments that act as sample holders. The upper attachment (rotor) is free to move and stress the sample, while the lower attachment (stator) is static. In addition, there is a temperature control system, which allows the temperature to be adjusted as needed. Another

important component is the transducer, which converts mechanical information into electrical ones, then processed into data. Finally, there is a software interface to set test parameters and display results. The attachments possess different geometries depending on the type of material being analyzed: there are smooth and crosshatch plates, and different configurations can be used, as shown in Figure 14, such as cone and plate suitable for low and high viscosity materials, parallel flat plates suitable for low viscosity or soft materials, and concentric cylinders suitable for very low or medium viscosity materials. By selecting the correct attachments, it is possible to evaluate the viscoelastic properties of any type of material.

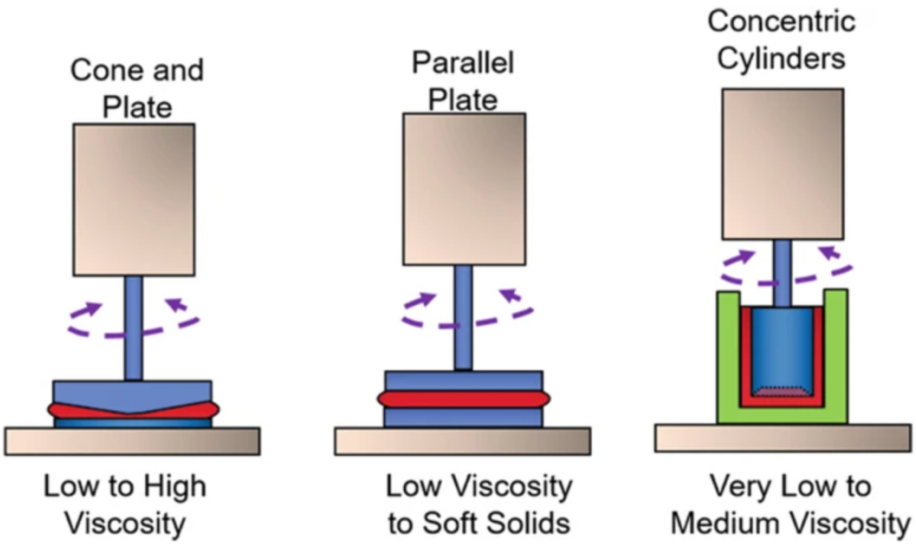

Figure 14. Schematic representation of the different attachments used in rheometry.
This figure outlines the various geometries used in rheological testing: (I) cone and plate, (II) parallel plates and (III) concentric cylinders. Figure adapted from Whaley et al.[66]

Based on the type of motion performed by the top plate, two macro-families of techniques can be identified:

- *Oscillatory analysis* → sinusoidal stresses are applied to evaluate the viscoelastic behavior of a material.
- *Rotational analysis* → constant stresses are applied to evaluate the steady-state shear behavior.

Among the most interesting properties that can be derived from rheological tests is the nature of the material, which can be elastic, viscous or viscoelastic. An elastic material can deform during the application of a stress and return to its initial shape and size when the

stress is removed. A viscous material, instead, exhibits resistance to flow and deformation during the application of a stress. Finally, a viscoelastic material exhibits both elastic and viscous behavior. Specifically, the nature of a material can be defined by considering the following parameters:

1. *Elastic or storage modulus* G', which represents the elastic behavior of the material and thus its ability to store energy.
2. *Viscous or loss modulus* G", which represents the viscous behavior of the material and thus its ability to dissipate energy and heat.
3. *Loss or damping factor tanδ*, which represents the ratio of the viscous modulus to the elastic modulus:

$$\tan\delta = \frac{G''}{G'}$$

The trend of these parameters allows the behavior of the material to be studied. When $G' > G''$ the sample behaves more like a solid and therefore the elastic component prevails. When $G'' > G'$ the sample behaves more like a liquid and therefore the viscous component prevails.[51] Whereas the point at which the two moduli cross, that is when $G' = G''$, is called *cross-over point* and represents the point at which the behavior of the sample shifts from solid-dominant to liquid-dominant and is the stability limit of the material. Similarly, $\tan\delta$ provides an assessment of the sample's performance. When $\tan\delta < 1$ the behavior is predominantly elastic, when $\tan\delta > 1$ the behavior is predominantly viscous, while when $\tan\delta \approx 1$ the material exhibits balanced viscoelastic properties.

1.6.2 Amplitude Sweep Test

Among the first rheological tests during the characterization of a hydrogel are amplitude sweep tests, also called strain sweep tests, in which increasing oscillatory strain is applied at a given frequency and temperature that remain constant throughout the test. It is the first test performed as it allows to study the strength limit of the material.

As a result of the test, a graph of G' and G" in logarithmic scale is obtained. There is a first constant area, which is called linear viscoelastic region (LVR), where the moduli are independent of the applied stress and the elastic behavior predominates. This region ends

at a shear stress value called the yield point, where the moduli lose linearity and begin to decrease. At the microscopic level, the loss of linearity corresponds to the formation of internal cracks in the material, which continue to grow until the mesh of the network ruptures. The rupture occurs at the cross-over point. This test is performed to define the LVR of the material: in fact, all rheological tests require being within the LVR of the material to be sure that there are no changes in structure during the analysis.

1.6.3 Time Sweep Test

Another rheological analysis frequently performed is the time sweep test, which is used to evaluate the behavior of a hydrogel over time. Changes in structure such as degradation, recovery, or crosslinking time can be observed. The test is conducted while maintaining constant temperature and frequency, within the LVR region, so an amplitude sweep test must first be conducted before this type of analysis can be performed. This technique allows the evaluation of the trend of G' and G" in logarithmic scale, but usually only the trend of G' is observed.[54]

The instant at which G' crosses G" is considered the gel point, at which there is a transition from sol to gel; instead, the point at which G' reaches a plateau, and thus stabilizes, is considered the time of complete crosslinking. The value of G' at which plateau is reached is called *equilibrium storage modulus* G'_{eq}, and from this point onward the material, having completed crosslinking, reaches a stable final structure.[67] The slope of the section where an increase in G' occurs gives information about the speed of the process: the steeper it is the faster the crosslinking will be.

1.6.4 Probe Tack Test

Probe tack test is a widely used method for evaluating the adhesive properties of soft and pressure-sensitive materials. In this test, a probe is placed in contact with the sample for a certain amount of time, as shown in Figure 15, and then the force required to detach the probe from the material is quantified. In fact, tack, by definition, is the ability of a material to adhere in a very short time to the surface of another solid material brought into contact

with not very high pressure. With this test what is evaluated is not the formation of adhesive bonds but the disruption of the bonds that have formed.

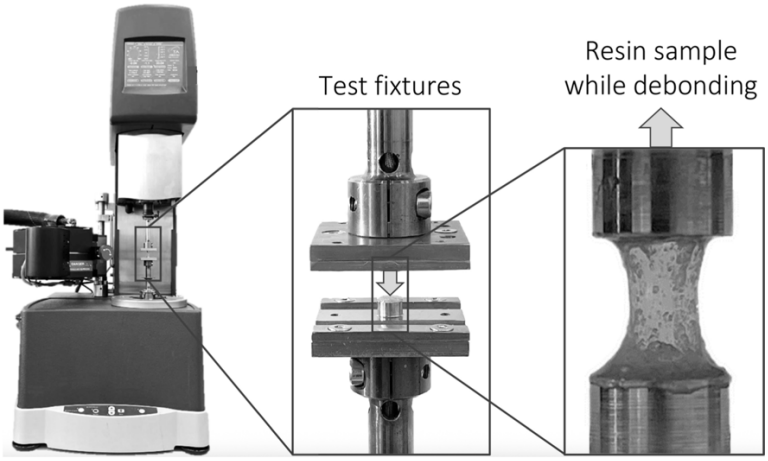

Figure 15. Probe tack test setup.
Figure adapted from Budelmann et al.[68]

Traditionally, probe tack tests are performed using universal testing machines equipped with dedicated testing equipment, but it is also possible to conduct these tests using rheometers. In this case, three stages of analysis are identified:

1. *Probe contact* in which a spherical or flat probe is pressed over the surface of the sample by applying a given force;
2. *Dwell time* in which the probe remains in contact with the sample for a certain amount of time to ensure adhesion between the two parts;
3. *Separation* in which the probe is pulled away from the sample and the force required for detachment is measured.

A linear force vs. time plot is obtained, and the area under the curve is evaluated: a high area indicates higher adhesiveness because the force required to ensure detachment is greater, while a smaller area indicates lower adhesiveness.

1.7 Aim of the Work

The specific objective of this thesis is to formulate and characterize hydrogel coatings composed CA and PVA, in order to identify the optimal composition for coating an off-

the-shelf vascular balloon that can be used in the scenarios of PAD treatment. The system is based on SA and $CaCO_3$ as hydrogel precursors, with crosslinking triggered by GDL to enable time-controlled internal gelation for the formation of a CA hydrogel. This strategy should allow the formation of a uniform, optimally distributed coatings directly on the surface of the balloon, ensuring consistent thickness and coverage. The hydrogel coating is engineered to achieve dual functionality: first, to adhere effectively to the vascular wall upon balloon inflation, thus ensuring prolonged retention and sustained therapeutic action; second, to possess adequate mechanical stability to withstand the stresses associated with deployment in the vessel and physiological conditions. To enhance both adhesion to the vascular wall and the mechanical robustness of the coating, PVA is incorporated as a functional additive within the hydrogel matrix.

Different formulations were developed and tested by changing key parameters including polymer concentrations, molecular weights, and viscosities to evaluate their impact on the behavior of the hydrogel. The formulations were assessed in terms of rheological behavior, mechanical stability under simulated deployment stress, and adhesiveness. Tests consisted in the empirical evaluation of the uniformity, stability, and the coating's ability to remain attached to balloon surfaces under conditions representative of the vascular environment. In addition to mechanical and adhesive evaluations, the hydrogels 'ability to encapsulate and release therapeutic agents was investigated. To accurately reproduce clinically relevant conditions, release experiments were conducted using 3D-printed balloons models designed to mimic the geometry and the morphology of standard vascular balloons.

These tests are designed to verify whether the coating can withstand the mechanical stresses that occur during deployment, as well as the dynamic forces imposed by blood flow and vascular wall pulsations following positioning, and whether it can allow the release of therapeutic agents. Further attention was given to the intraoperative applicability of the system, with particular focus on optimizing the cross-linking kinetics to ensure that uniform, reproducible hydrogel coatings could be formed directly on the surface of the balloon prior to vascular insertion.

Overall, this work contributes to the broader development of a *multilayer*, "*off-the-shelf*" hydrogel-based coating system for vascular balloon applications, designed for

intraoperative applications, as shown in Figure 16. This technology aims to enable targeted, controlled delivery of antiproliferative and antithrombotic agents, providing a personalized therapeutic approach tailored to the patient's specific clinical needs.

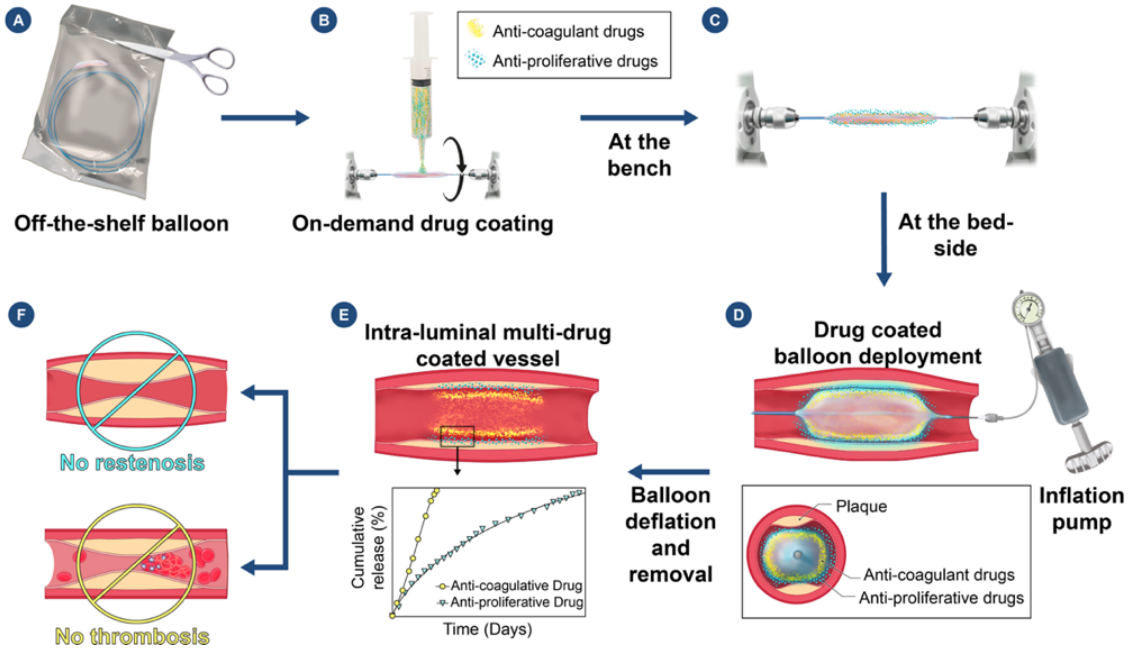

Figure 16. A schematic of the custom coated balloon for a controlled drug delivery.
This image shows the realization of an intraoperatively custom-made bilayer hydrogel-coated balloon. The inner layer contains an antiproliferative drug that is released for longer times, while the outer layer provides faster release of an antithrombotic agent. Image generated with BioRender.

2. Materials and Methods

This chapter describes the materials, protocols, and experimental methods used to characterize the hydrogel-based coating system. The experimental methods were divided into two main parts: physical-chemical characterization of the hydrogel and evaluation of drug release.

The first part focused on the rheological characterization of hydrogels to identify the optimal viscosity of SA and to evaluate the effect of $CaCO_3$ and GDL concentrations on the mechanical and adhesive properties of the formulation. At the same time, Fourier transform infrared spectroscopy was performed to analyze the chemical composition of the selected formulation and verify the presence of covalent bonds between CA and PVA. The second part analyzed the PTX encapsulation and its release profile from the formulation, specifically studying the influence of the molecular weight (MW) of PVA on both the mechanical properties and drug release profiles. Finally, scanning electron microscopy (SEM) was performed to examine the surface morphology of the hydrogels. Samples were subjected to a thermal cycle consisting of a freezing phase followed by a drying phase in an oven for preparing the hydrogel coating for practical use. The process begins with an initial freezing phases that induces turgidity in the hydrogel, allowing it to adapt perfectly to the balloon surface. This is followed by a drying phase in the oven, which dehydrates and stabilizes the hydrogel in position. The resulting coating maintains its adhesion and structural integrity both during handling and during balloon deflation. This property is particularly important before insertion into the protective sheath, a device used during PTA procedures to guide the balloon through the vasculature to the treatment site.

2.1 Materials

SA powders with different viscosities were used in this study. A SA with a viscosity of 350–500 mPa·s was purchased from Thermo Scientific (Thermo Fisher Scientific Inc., Waltham, MA, USA; Catalog No. 177775000, Lot No. A0453497), and a second type with a viscosity of 1000–1500 mPa·s was obtained from the same company (Catalog No.

J61887.30, Lot No. T25K027). For consistency throughout this thesis, these two materials are referred to as medium-viscosity (MV) and high-viscosity (HV) SA, respectively. $CaCO_3$ was purchased from Thermo Scientific (Catalog No. 012365.36, Lot No. Q20J31), while GDL from Sigma-Aldrich (Merck KGaA, Darmstadt, Germany; Product Code 1003608514, Source SLCQ7237). PVA with two different molecular weights (MW) and degrees of hydrolysis was used. A low MW PVA (13–23 kDa, ≥98% hydrolyzed) was purchased from Aldrich (Lot No. MKBP5691V, Product No. 348406-500G), while a high MW PVA (146–186 kDa, 87–89% hydrolyzed) was obtained from Sigma-Aldrich (Product No. 363103-500G). FD&C Blue #1 and Red #3 food dye was purchased from Innovating Science™ (Aldon Corporation, Avon, NY, USA; IS35032, Part 3). PTX was purchased from Sagent Pharmaceuticals (Schaumburg, IL, USA; 6mg/mL, NDC 25021-255-50). Castor oil (C5135-500G, Code 102819292, sourced from BCCM3065) and citric acid (CX1723-1, lot number 2024062632) were purchased from Sigma-Aldrich, while ethanol 200 proof (UN1170) from Decon Labs (King of Prussia, PA, USA). Milli-Q® water (18.2 MΩ·cm) was used for all preparations. The 6 × 100 mm Mustang™ balloon catheter was purchased from Boston Scientific® (Marlborough, MA, USA).

Regarding the 3D-printed components, the 3D-printed mold was fabricated using Tough 2000 resin, the custom puncher was made with Clear VA resin, the high-adhesive samples for the probe tack test were produced using Elastic 50A resin, and the mock balloons were printed with Flexible 80A resin. All resins and the Form 3B+ printer were supplied by Formlabs® (Somerville, MA, USA).

2.2 Methods

2.2.1 Formulation Preparation

HV-SA solutions were prepared, as shown in Figure 17A, at five different concentrations: 0.5%, 0.75%, 1%, 1.5%, and 2% (w/v), followed by the addition of $CaCO_3$ at a concentration of 75mM. The CA precursors were then sonicated for 15 minutes at room temperature (RT). For each formulation, 2-3 mL of the mixture was transferred to a syringe. Parafilm was used to seal the syringe tip and 1 drop per mL of food dye was added

into the solution. GDL was incorporated as a crosslinking agent at a 1:2 molar ratio relative to $CaCO_3$, with final GDL concentrations of 150 mM. The GDL was directly added to the syringe and mixed using a spatula to ensure good dissolution to form the CA hydrogel. The crosslinking process is triggered by gradual acidification induced by GDL, which dissolves slowly and lowers the pH, leading to the release of Ca^{2+} ions from $CaCO_3$. These ions subsequently cross-link the alginate chains, forming a homogeneous and stable hydrogel network. The same procedure was then applied to prepare 1:1 composite of CA and PVA (MW: 13-23 kDa) at different concentrations of PVA: 0.5%, 0.75%, 1%, 2.5%, 5% and 10% (w/v). To ensure consistency of results, triplicates (N=3) were prepared for each formulation.

For the preparation of the medium viscosity one, 1% (w/v) MV-SA solutions were prepared, followed by the addition of $CaCO_3$ at five concentrations: 15, 30, 45, 60, and 75 mM. These formulations were called 1X, 2X, 3X, 4X, and 5X, respectively, as shown in Table 3.

Table 3. Summary of tested hydrogel formulations and component concentrations.

Name	SA (mM)	$CaCO_3$ (mM)	GDL (mM)
1X	50.5	15	30
2X	50.5	30	60
3X	50.5	45	90
4X	50.5	60	120
5X	50.5	75	150

The same procedure described for the HV-SA was followed to prepare the samples, as shown in Figure 17B. The concentration of GDL was adjusted to maintain a 2:1 ratio with $CaCO_3$, resulting in final GDL concentrations of 30, 60, 90, 120, and 150 mM for the respective formulations. The same procedure was then applied to prepare 1:1 composite of CA and 5% (w/v) PVA (MW: 13-23 kDa) concentration. Again, triplicates were prepared for each formulation.

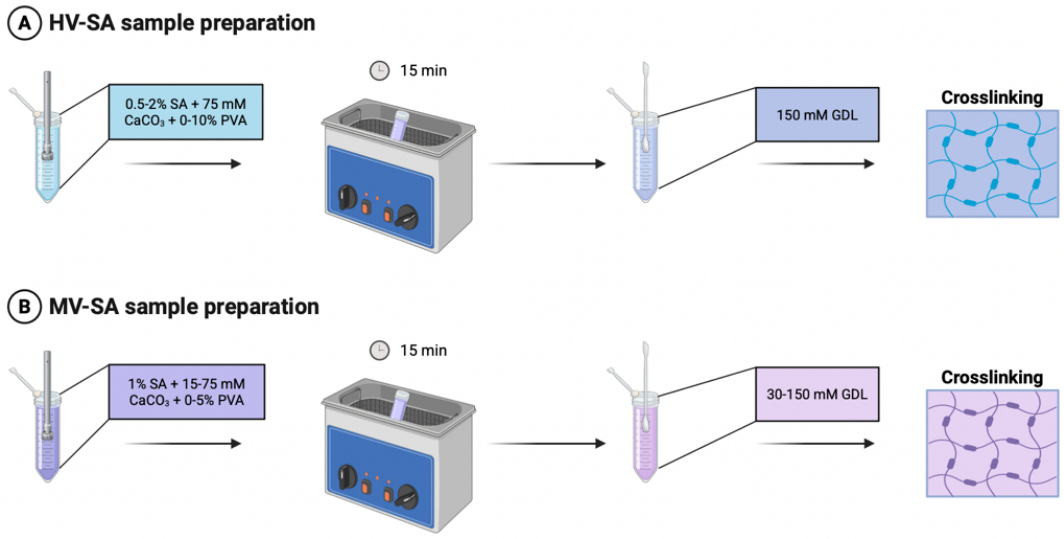

Figure 17. Workflow for the preparation process of HV-SA and MV-SA sample. Image generated with BioRender.

For drug release studies, PTX, purchased as a 6 mg/mL stock solution, was incorporated into the 4X formulation by mixing 0.1257 mL of the drug solution (corresponding to 0.7542 mg of PTX) into 3 mL of the CA precursors prior to crosslinking via GDL. This resulted in a final PTX concentration of 0.25 mg/mL in the formulation. In this case, 5% (w/v) PVA was also included in the formulation with CA precursors, testing two different types of PVA: one with low MW (13-23 kDa) and one with high MW (146-186 kDa). To evaluate the potential influence of the PTX solvent on hydrogel performance, a vehicle control was also prepared, which reproduced the solvent composition of the commercial drug batch. The solvent was obtained stirring 527 mg/mL castor oil, 49.7% (v/v) dehydrated alcohol, and 2 mg/mL citric acid. The hydrogel samples were prepared using the same procedure for the PTX-loaded formulations; however, instead of the drug, the same volume of pure solvent (0.1257 mL out of a total volume of 3 mL) was added to the formulation.

2.2.2 Evaluation of Balloon Coating Performance during Deployment

To empirically assess the quality of the hydrogel coatings, a series of practical tests were conducted using commercial balloon catheters (6 × 100 mm), with the coating applied according to the procedure proposed for intraoperative use. The balloon was inflated to 9 atm, reaching a nominal diameter of 6.03 mm, and the hydrogel was applied directly

to its surface. The coated balloon was then stored at −20 °C for 10 minutes to promote coating adhesion and facilitate handling. Next, it was placed in an oven at 55 °C for 25 minutes to ensure complete drying of the hydrogel layer. Once dry, the balloon was deflated and inserted into a 10 Fr sheath (Boston Scientific®, Marlborough, MA, USA), tool used by the surgeon during the procedure, to simulate the feasibility of the deployment closely matching all the steps required during PTA. The quality of the coating was evaluated based on visual uniformity and structural integrity.

2.2.3 Mechanical Characterization – Amplitude Sweep Test

Some samples were prepared and maintained at room temperature (RT), while others underwent a thermal cycling protocol. The objective was to obtain hydrogel samples with consistent geometry (20 mm diameter) compatible with the parallel plate geometry of the rheometer, regardless of preparation method. For RT-prepared samples, formulations were quickly injected into a custom-designed, 3D-printed plate mold, fabricated using a Form 3B+ printer (Formlabs Inc., Somerville, MA, USA), shown in Figure 18. This mold was specifically designed with wells of 20 mm diameter and variable depths (1, 1.5, and 2 mm) to directly yield uniform samples without further processing. The hydrogels were left at RT for 25 minutes to complete gelation prior to testing, as illustrated in the RT workflow in Figure 19.

Figure 18. Picture of Form 3B+ printer.
Figure adapted from Formlabs website.

For samples subjected to the thermal cycle, a different approach was necessary due to hydrogel shrinkage during the heating step. Formulations were dispensed into standard 6-well culture plates (Corning Costar, REF 3516), which allowed for thermal processing without the constraints of tight dimensional tolerances. Samples were first placed at −20 °C for 10 minutes, followed by incubation at 55 °C for 60 minutes to induce structural changes and partial drying. After thermal processing, a custom 20 mm diameter puncher, also fabricated using the Form 3B+ printer, was used to extract uniformly sized disks from the bulk hydrogel, compensating for the size reduction caused by shrinkage. This protocol is illustrated in the thermal cycle workflow in Figure 19.

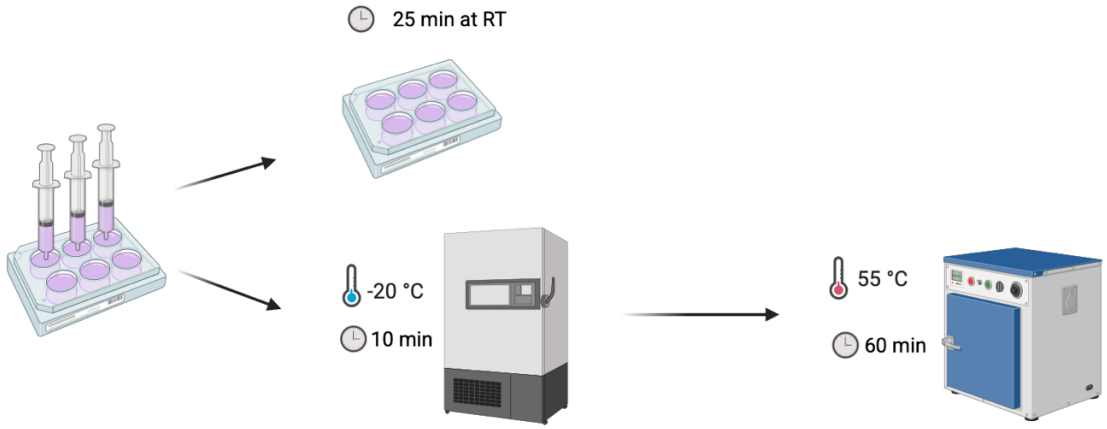

Figure 19. Workflow for the preparation process of MV-SA samples: RT vs thermal cycle. Image generated with BioRender.

Amplitude sweep tests were conducted using a Discovery HR20 rheometer showed in Figure 20 (TA Instruments – Waters LLC, New Castle, DE, USA) equipped with 20 mm smooth parallel plate geometry (TA-20/1, TA Instruments, Waters LLC, New Castle, DE, USA).

The geometry gap was adjusted for each sample to consider microscopic surface variabilities, ensuring a constant normal force of 0.5 N during the analysis. The temperature was maintained at 25 °C, while the angular frequency was set at 1 rad/s. The strain was varied continuously from 0.1% to 1000%. To obtain the value corresponding to the cross-over point, cubic spline and linear interpolation were used using TRIOS software. Cubic spline interpolation uses cubic polynomials to interpolate the points, creating a smooth curve through all data points. The fit used is:

$$y_i(x) = a_i + b_i(x - x_i) + c_i(x - x_i)^2 + d_i(x - x_i)^3 \qquad for \qquad x \in [x_i, x_{i+1}]$$

with y = G' and y = G'' through the neighboring points.

Linear interpolation, on the other hand, uses linear polynomials to interpolate the data points. The fit used is:

$$y(x) = ax + b$$

With y = G' and y = G'' through the two neighboring points only.

Figure 20. Picture of HR20 rheometer.

2.2.4 Determination of Crosslinking Time – Time Sweep Test

Sample preparation was performed at RT, following the same procedure described for the amplitude sweep test. However, in this case, the hydrogel was not injected into the custom 3D-printed mold; instead, it was deposited directly onto the lower attachment of the rheometer, immediately after the addition of GDL, to ensure a real-time monitoring of the complete crosslinking process.

Time sweep tests were conducted using again the Discovery HR20 rheometer equipped with 40 mm crosshatch parallel plate geometry (TA-40-C, TA Instruments, Waters LLC, New Castle, DE, USA). The geometry gap was adjusted for each sample to ensure adequate contact between the upper attachment and the sample surface. The temperature was maintained at 25 °C, while the angular frequency was set at 10 rad/s, for a duration of 45 minutes. The strain was maintained at 0.05%, based on previous amplitude sweep

tests, to ensure that the analysis performed occurs within the LVR of the formulations. A custom MATLAB R2024b script was developed to determine the total crosslinking time by identifying the time at which G'_{eq} is reached.

2.2.5 Evaluation of Adhesiveness – Probe Tack Test

Sample preparation was performed at RT and after thermal cycle, following the same procedures described for the amplitude sweep test.

Probe tack tests were conducted using the Discovery HR20 rheometer equipped with 20 mm smooth parallel plate geometry (TA-20/1, TA Instruments, Waters LLC, New Castle, DE, USA). A dedicated test protocol has been developed to evaluate the adhesive properties of samples through a compression-tension cycle. During the compression phase, the probe comes into contact with the sample surface at a constant speed of 10 μm/s until it reaches a normal force of 2 N. Immediately after, the tension phase begins, in which the probe retracts at a speed of 10 μm/s. The test ends when the measured force returns to 0 N, indicating complete detachment of the probe from the sample. To validate the protocol, cylindrical samples (20 mm diameter × 1 mm thickness) were fabricated using materials with different adhesive properties. A low-adhesive material was selected as a negative control: silicone samples were prepared using the Ecoflex™ 00-30 kit. The liquid resin was poured into a 6-well cell culture plate (Corning Incorporated Costar, REF 3516) and cured at RT for 24h. After treatment, samples of the desired size were obtained using the custom 3D-printed puncher described above. A high-adhesive resin was selected as a positive control, 3D printed to obtain the desired dimensions using Form 3B+ 3D printer.

2.2.6 Chemical characterization – FT-IR Spectroscopy

Technique Description

Fourier Transform Infrared Spectroscopy (FT-IR) was used to characterize the chemical structure and verify the presence of specific functional groups within the hydrogel. It is a vibrational, absorption technique widely used for qualitative analysis of materials.

Compared to other spectroscopic techniques, such as nuclear magnetic resonance, FT-IR is faster, cheaper and requires easier sample handling, although it provides less detailed information. This analysis studies the interaction between an electromagnetic radiation in the mid-infrared range (IR, 4000-600 cm^{-1}) and molecular bonds in the sample. When IR radiation hits the material, specific frequencies are absorbed, causing molecular vibrations. There are two main vibrations that can be produced: *stretching vibrations* in which there is rhythmic stretching along the bond axis that can be symmetrical or asymmetrical; *bending vibrations* that depend on changes in the bond angle. The energy transitions are detected in the final spectrum as peaks as a function of wave number. On the y-axis it is possible to represent: (I) transmittance, which is the energy that is transmitted, and in this case negative peaks will be obtained; (II) absorbance, which is the energy that is absorbed, and in this case positive peaks will be obtained. The position of the peaks in the spectrum, their shape and intensity are related to the type of chemical bond and the type of vibration. Very important is the so-called fingerprint region (1500-500 cm^{-1}), which is a complex, peak-rich region that is highly specific to single materials. As shown in Figure 21, modern FT-IR spectrometers exploit the *Michelson interferometer*, in which all signals are collected simultaneously in the form of an interferogram, and then this is converted into a spectrum using the *Fourier transform*. This provides a very rapid acquisition that allows the averaging of multiple scans, improving performance.

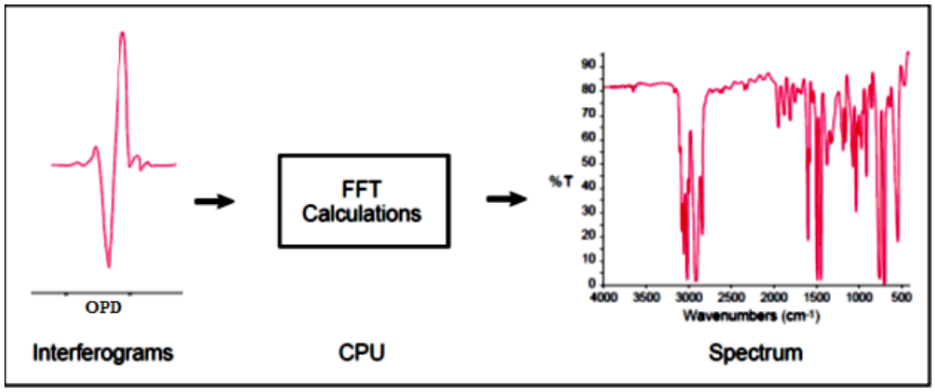

Figure 21. Scheme of operation of FT-IR machines.
This schematic shows how a Michelson interferometer-based FTIR spectrometer collects infrared signals in the form of an interferogram, which is then converted to an IR spectrum using the Fourier transform to identify functional groups in materials. Figure adapted from Shahshaha.[69]

There are two modes of operation: *transmission* and *attenuated total reflectance* (ATR). In the transmission mode, the sample is prepared in pellet form by compressing the powdered

sample together with potassium bromide (KBr), an IR-transparent material. This is a bulk analysis but is destructive. ATR involves the placement of the sample directly in contact with a high refractive index crystal (e.g., diamond or germanium), allowing analysis at the surface level (depth of 0.5-5 μm) without requiring extensive sample preparation. The IR beam reflects multiple times within the crystal, interacting with the sample with each reflection.

Sample Preparation and Experimental Settings

Two hydrogel formulations were tested: 4X and 4X + 5% PVA (MW: 13-23 kDa). For each formulation, the RT and thermal cycle protocols were followed. The samples were injected into 6-well cell culture plates (Corning Incorporated Costar, REF 3516) and frozen at −80 °C overnight. The samples were then lyophilized for 4 days using a VirTis SP Scientific Wizard 2.0 freeze dryer, at −45 °C and 0.40 mbar to ensure complete water removal.

FT-IR analysis was performed using a Thermo Scientific NICOLET™ 6700 spectrometer in ATR mode with a diamond crystal (as shown in Figure 22). Measurements were performed using the OMNIC software, with the following parameters: 125 scans per sample, 4 cm^{-1} resolution, and automatic possible residual water signal subtraction. The resulting spectra were recorded in terms of transmittance (%). A custom MATLAB R2024b script was developed to plot the data.

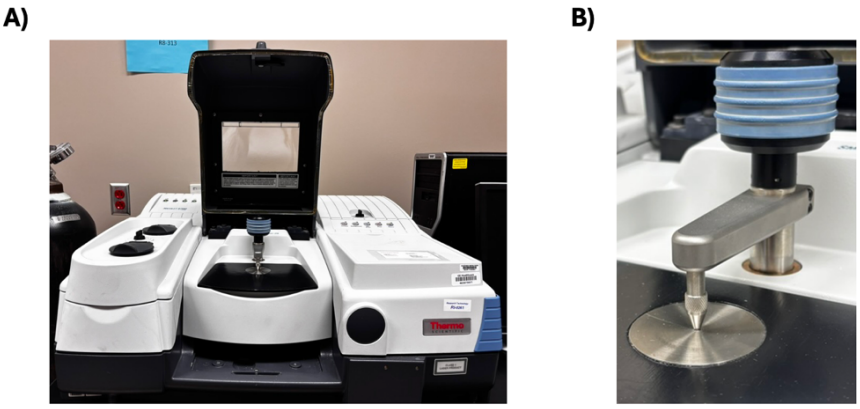

Figure 22. FT-IR spectrometer and ATR module.
(A) Thermo Scientific NICOLET™ 6700 FT-IR spectrometer used for chemical characterization of hydrogel samples; (B) ATR module with a diamond crystal, which enables surface-level analysis through multiple internal reflections, without the need for extensive sample preparation.

2.2.7 Effect of PVA on Drug Release – UV-vis Spectroscopy

Technique Description

To evaluate the potential ability of the developed hydrogel formulations to release PTX, *Ultraviolet-visible light* (UV-vis) *spectroscopy* was used. This technique is an analytical tool for evaluating the quantity of different compounds within a solution based on their ability to absorb specific wavelengths of light. Indeed, atoms, molecules or ions absorb specific wavelengths of light, causing electronic transitions between molecular orbitals. UV-vis spectroscopy uses ultraviolet and visible radiation, which are a small part of the electromagnetic spectrum. A range from 100-200 nm to 800 nm is used for this type of analysis, as shown in Figure 23. When light passes through a sample, certain molecules absorb photons that possess sufficient energy to cause electron transitions from lower to higher orbitals. This results in the generation of characteristic absorption peaks at specific wavelengths, depending on the chemical structure of the sample.

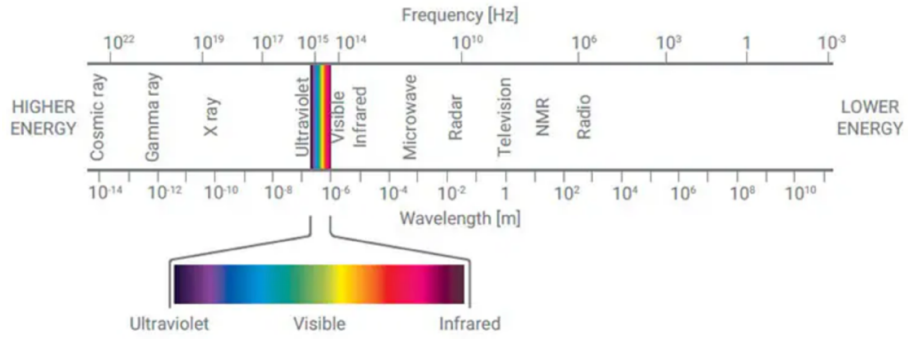

Figure 23. The electromagnetic spectrum.
This diagram shows the entire electromagnetic spectrum as a function of wavelength and frequency. There is a zoom of the region corresponding to ultraviolet (UV), visible and infrared (IR) light, commonly used in spectroscopic techniques. Figure adapted from Agilent website.

The intensity of the absorbed light is directly related to the concentration of the absorbing species, as described by *Lambert- Beer law*:

$$A = -log_{10}\left(\frac{I}{I_0}\right) = \varepsilon cl$$

Where A represents the absorbance, I is the intensity of the light measured after it interacts with the sample, I_0 is the initial intensity of the light, ε denotes the molar absorptivity (or

molar absorbance coefficient) of the material, c is the concentration of the absorbing species and l is the path length of light through the sample. Generally, ε is expressed in units of L /mol/cm, l in cm and c is expressed in mol/L; as a result, A is dimensionless. [70,71] Using this equation, UV-vis therefore enables the determination of drug concentration in a solution over time, to obtain a drug release profile. The results obtained are represented as absorption spectra, in which the wavelength of light is plotted on the x-axis, while the absorbance values are plotted on the y-axis. The higher the peaks, the greater the absorbance at those specific wavelengths.

The amount of light absorbed or transmitted during the analysis is compared with a reference called *baseline*. Typically, the baseline is a sample containing the solvent used to dissolve the sample of interest, along with any other components present. This is used to remove the background interference caused by any non-target components, and therefore its use allows for more sensitive detection, improving the accuracy and sensitivity of the analysis. The samples are placed inside a *cuvette*, a transparent container that can be made of different materials, such as glass and plastic. Generally, quartz is preferred for this analysis, due to its characteristic of to be transparent to both visible and UV light, allowing analysis to be carried out over the entire UV-vis spectrum.[71] To convert the absorbance values obtained from the analysis into actual concentrations, a *calibration curve* is required. This is achieved by preparing a series of standard solutions with known concentrations of the target material. Their absorbance is then measured at the chosen wavelength, which usually corresponds to the maximum absorbance of the sample. The resulting graph of absorbance versus concentration follows a linear trend, from which the equation can be extrapolated. Using this relation, it is then possible to extrapolate unknown concentrations in the experimental samples.

Sample Preparation and Experimental Settings

To simulate real clinical conditions, drug release tests were conducted using coated balloon models that reproduced the actual geometry and dimensions of an inflated commercial balloon (100 mm long × 6 mm in diameter). For this purpose, mock balloons were designed and 3D-printed using the Formlabs 3B+ 3D printer. The hydrogel coating was applied using the same procedure required for intraoperative use. After deposition,

the coated balloon was stored at −20 °C for 10 minutes to enhancing its adhesion to the balloon surface and ensuring it retains a firm, manipulable structure. The coated balloon was then placed in an oven at 55 °C for 20 minutes to ensure complete drying of the coating, a necessary step to allow insertion of the balloon into the sheath without damaging the hydrogel layer.

For drug release testing, the coated balloon was immersed in a glass container filled with 600 ml of Milli-Q water. Before selecting the final drug release protocol, two different configurations were tested: one using the Incu-Shaker™ 10L (Benchmark Scientific, USA) set at 37 °C and 70 rpm, and the other using a magnetic stirrer maintained at 40 °C and 60 rpm. Preliminary results showed that the second configuration provided more effective and uniform agitation of the release medium and was therefore selected for subsequent experiments. This configuration was designed to avoid a static environment and approximate the dynamic conditions of blood flow in a simplified way. Samples of the sink solution with the released PTX were collected at fixed time intervals: every 15 minutes for the first 2 hours, every 2 hours for other 6 hours, and then every 24 hours for a total of 5 days.

Collected samples were analyzed using a Cary 60 UV–Vis spectrophotometer (Agilent Technologies Inc., Santa Clara, CA, USA) operating in dual-beam mode with upper limit of detection of 4 a.u. and a baseline correction to eliminate background effect. Absorbance was measured from 200 nm to 800 nm in 1 nm increments using a quartz cuvette (QX High Precision Cell, Hellma Analytics, Müllheim, Germany) with 10 mm of optic length. For each reading, 2 mL of the sink solution are withdrawn to be measure and a % cumulative release is then calculated.

2.2.8 Morphological Characterization – SEM Analysis

Technique Description

Scanning electron microscopy (SEM) was used to study the morphology of the hydrogel coatings. This technique is widely employed in the characterization of materials due to its ability to provide high-resolution images with nanoscale detail, allowing the evaluation of structural features such as porosity and network architecture. SEM operates by directing

a high-energy electron beam onto the surface of the sample to analyze. The electrons interact with the atoms of the material, generating various signals, including back-scattered electrons and secondary electrons. The latter are collected by dedicated detectors and converted into a high-contrast images.

To perform the analysis, the samples require adequate preparation to ensure electrical conductivity. In particular, to obtain high-quality images, it is necessary to coat the surface of the sample with a thin metallic layer using a process called *sputtering*, which enables the dissipation of electronic charges that tend to accumulate on the surface of the sample during analysis. The process is based on physical vapor deposition, which is performed inside a vacuum chamber filled with an inert gas, typically argon. The deposited layer is composed of metals with high conductivity and low electron absorption power, such as gold, platinum, and palladium, which serve as target material. The target is connected to the anode, while the sample is placed on the cathode. After creating a vacuum inside the chamber, argon gas is introduced and a high-voltage electric field is applied between the anode and cathode, generating a plasma discharge. The argon ions Ar^+ are accelerated by the electric field and collide with the metal target, ejecting metal atoms from its surface. These atoms are then deposited uniformly on the surface of the sample, creating a thin coating typically ranging from 5 to 20 nm, which is sufficient to make the surface conductive without altering the native morphology. The entire process is illustrated in Figure 24.

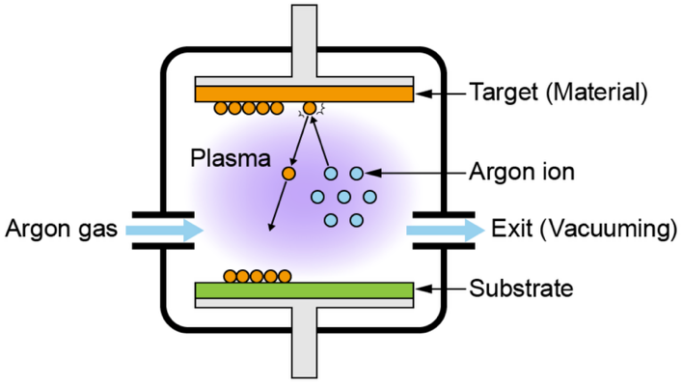

Figure 24. Schematic of the Sputtering Process.
Image adapetd from Matsusada Precision website.

This is a rapid but very complex process that requires high control of numerous parameters such as the sample-target distance, the applied current, and the type of metal

used. Alternative metallization methods, such as carbon coating or thermal evaporation, are also available. However, sputtering offers greater control over the homogeneity and thickness of the deposited film, ensuring uniform coverage even on irregular or porous surfaces.

Sample Preparation and Experimental Settings

The hydrogel formulations were injected into 6-well cell culture plates (Corning Incorporated Costar, REF 3516) and stored at −80 °C. The samples were then lyophilized for four days using a VirTis SP Scientific Wizard 2.0 freeze-dryer, operating at −45 °C and 0.40 mbar. Afterward, the samples were sectioned using a cutting blade to expose the internal cross-section. This cross-sectional surface was positioned vertically and mounted on SEM specimen mounts 45/90 (Product No. 15359, TED PELLA Inc.) using double-sided carbon adhesive tape. Carbon tape was chosen for its mild electrical conductivity, which facilitates charge dissipation during SEM analysis. A gold coating with a thickness of 7 nm was applied to the samples using a Cressington 208HR (Cressington Scientific Instruments Ltd, Watford, UK) sputter coater. Imaging was then conducted using a FEI Quanta 400F field emission SEM (Fei, Hillsboro, Oregon, USA). Initially, various magnifications ranging from 50× to 500× were tested; however, most of the selected images were acquired at a magnification of 150×.

2.2.9 Statistical Analysis and Graphs

Statistical analysis and graphing of the obtained data were performed using GraphPad Prism 10 Software. Results were expressed as mean ± standard error of the mean (Sem). One-way analysis of variance (ANOVA) with multiple comparisons and non-parametric t-test were performed to analyze date. Statistical significance was defined as follows: $p < 0.05$ (*), $p < 0.01$ (**), $p < 0.005$ (**), and $p < 0.0005$ (****).

3. Results and Discussion

The following chapter is organized into two main sections, reflecting the structure presented in the *Section 2*. The first part focuses on presenting and discussing the mechanical and physicochemical characterization of the hydrogel formulations, while the second investigates drug encapsulation within the hydrogel and release performance.

The characterization begins with an analysis of the effect of SA viscosity on both mechanical performance and coating quality, comparing the two materials previously defined as high-viscosity sodium alginate (HV-SA) and medium-viscosity sodium alginate (MV-SA). Based on the results obtained, MV-SA was selected as the optimal candidate for further formulation development. Subsequently, the impact of different $CaCO_3$ concentrations was investigated in terms of mechanical behavior and crosslinking kinetics, with the aim of identifying the optimal concentration of ions. Once the suitable $CaCO_3$ concentration was established, PVA was incorporated into the formulation to enhance coating adhesiveness, promoting stronger adhesion with vascular tissue. The potential influence of PVA on the hydrogel's viscoelastic properties was also assessed. To further optimize intraoperative applicability, the effect of the thermal cycle protocol here proposed (10 min at -20 °C + 25 min at 55 °C) on hydrogel performance was analyzed. After the mechanical characterization of the formulations, a chemical investigation was then conducted using FT-IR spectroscopy, to investigate possible covalent interactions between SA and PVA.

The second section of this chapter explores the hydrogel's ability to encapsulate and release drugs over time, using PTX as a model compound. To investigate the effect of polymer composition on release kinetics, two formulations containing PVA with different MW were tested. A drug release study was conducted in aqueous and dynamic conditions to monitor the release profile over time. To support and interpret the release behavior, a morphological analysis via SEM was performed to investigate the internal porosity and structural organization of the samples. Finally, the mechanical properties of the same drug-loaded formulations were evaluated to determine the impact of both PVA MW and PTX presence on the mechanical performance. Since PTX was supplied as a solution in an organic solvent rather than in powder form, a control formulation was also prepared by incorporating only the solvent, at the same volume used for drug loading. This allowed

for the isolation and evaluation of the solvent's impact on the mechanical properties of the hydrogel.

3.1 HV- vs MV-SA formulations

As a first step, a comparison was performed to assess the effect of SA viscosity both quantitatively, by evaluating the mechanical performance of the formulations, and qualitatively, by evaluating the uniformity of the coatings obtained on commercial uncoated balloons. Two types of SA were tested, referred to in this thesis as HV-SA and MV-SA formulations. It is important to note that these designations were chosen for the purposes of this study, and do not correspond to standardized viscosity ranges, as SA is commercially available in a wide variety of viscosity grades.

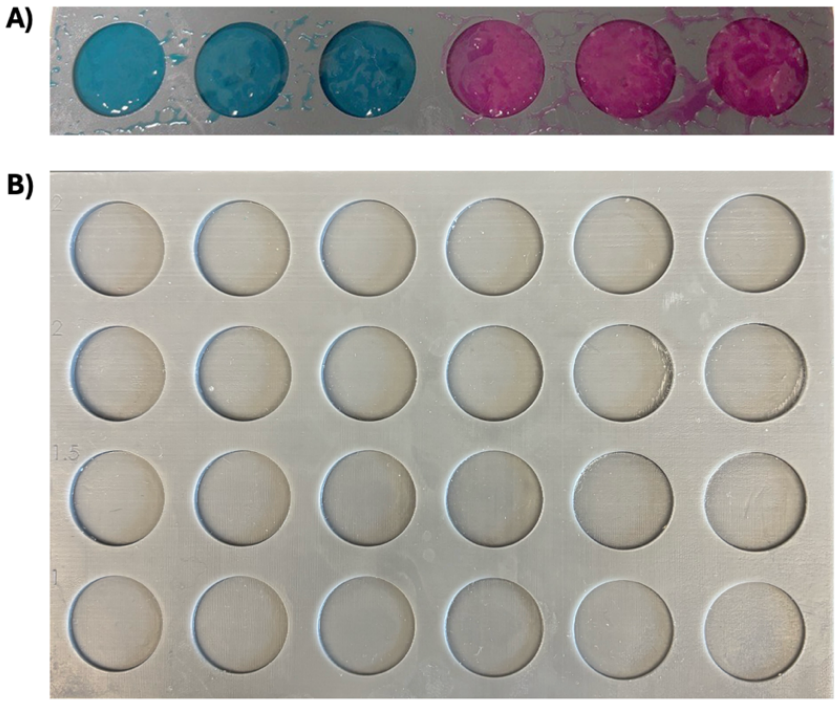

Figure 25. Picture of 3D-printed mold and resulting hydrogel samples.
A) Hydrogel samples colored with different dyes after rapid injection into the mold, B) 3D-printed mold used to produce uniform circular samples for mechanical testing.

For mechanical characterization, samples were prepared at RT using the custom 3D-printed mold shown in Figure 25B. The formulations were injected into the circular wells and evenly spread using a spatula. Two different dyes were used to visually differentiate

the various formulations, as shown in Figure 25A. In parallel, qualitative tests were performed by applying a coating onto a commercial uncoated angioplasty balloon (Mustang™ 6.00mm x 100 mm x 75 cm) from Boston Scientific®, which was inflated to 9 atm, corresponding to a final diameter of 6.03 mm. This experimental part was designed to simulate clinical application and assess the quality of the coating obtained, in terms of homogeneity and adherence.

The comparison aimed to identify the formulation offering the best uniformity, ease of application, and mechanical strength for subsequent optimization.

3.1.1 Evaluation of HV-SA: Mechanical Properties and Practical Applicability

To assess the mechanical performance of the hydrogel formulations, amplitude sweep tests were performed on HV-SA samples with increasing SA concentrations, ranging from 0.5% to 2% w/v, while maintaining a constant $CaCO_3$ concentration of 75 mM. The goal was to identify the optimal SA concentration capable of providing a hydrogel with adequate mechanical stability, ease of handling and injectability.

Figure 26A shows the trend of G' and G'' moduli as a function of oscillation strain. All formulations exhibited typical gel-like behavior, characterized by G' > G'' in the LVR and a progressive decrease in both moduli with increasing deformation, until cross-over point was reached (G' = G''). Beyond this point, G'' < G' indicating mechanical instability of the material. Among the tested samples, the 2% HV-SA formulation showed the highest G' values; however, its excessive viscosity made the material difficult to handle, resulting in difficulties in the handling during the application and high variability among triplicates. Notably, the 0.75% HV-SA formulation exhibited the highest cross-over point, indicating a greater resistance to deformation prior to mechanical failure. However, this formulation also presented considerable variability, with a Sem notably higher than that observed for the 2% sample. Statistical analysis using one-way ANOVA showed no significant differences in cross-over point values among the groups, as shown in Figure 26B, mainly due to the high variability observed. The average cross-over points (± Sem) (n =3 for each group) are summarized in Table 4:

Table 4. Mean cross-over points (± Sem) of HV-SA hydrogels.

HV-SA concentration	Cross-over point (mean ± Sem)
0.5%	1.38 ± 1.22%
0.75%	21.97 ± 30.40%
1%	4.93 ± 5.41%
1.5%	3.33 ± 2.09%
2%	6.19 ± 3.82%.

Although definitive conclusions could not be drawn based on rheological data alone, empirical observations suggested that the 1% HV-SA formulation offered the best balance between mechanical stability and injectability. Its viscosity was sufficient to maintain a stable gel structure, but still low enough to allow proper extrusion and uniform mixing, suggesting the 1% concentration as the most promising among HV-SA options.

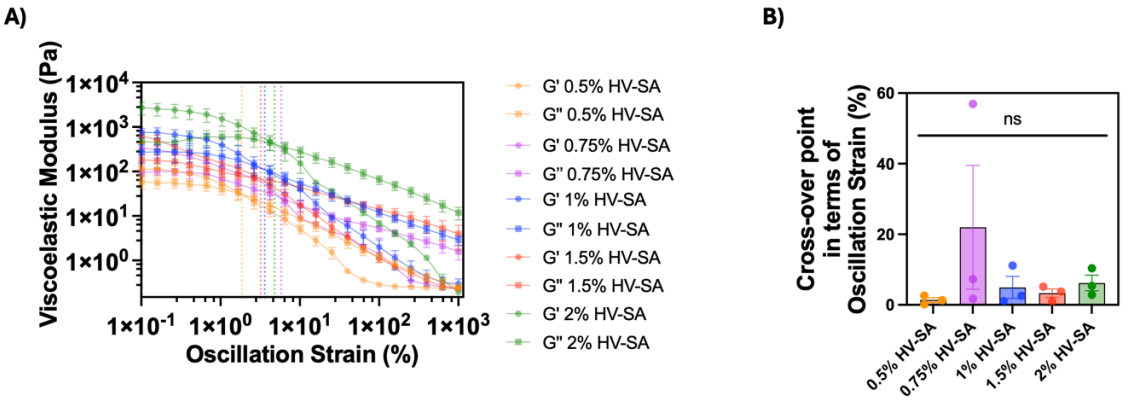

Figure 26. Amplitude sweep test of HV-SA hydrogels with increasing SA content.
A) G' and G" as a function of percentage oscillatory deformation for hydrogels HV-SA at increasing concentrations (0.5-2% w/v). The cross-over points between G' and G" are indicated by vertical dotted lines. B) One-way ANOVA of the crossover point. No statistically significant differences were observed between the samples.

To further enhance the mechanical performance of HV-SA, additional tests were conducted by incorporating PVA (MW: 13-23 kDa) in a 1:1 ratio. Various concentrations of PVA (from 0.5% to 10% w/v) were combined with increasing SA concentrations trying to identify an optimal composition. Despite the numerous experiments, the results were inconclusive: the rheological data showed high variability among the triplicates, and no

statistically significant improvements. As a result, the corresponding data and graphs were not included in the thesis.

Despite the lack of quantitative improvements, visual analysis of the samples revealed significant formulation issues. The addition of PVA to HV-SA dramatically increased the viscosity of the formulations, resulting in challenging sample preparation and leading to the formation of irregular, clustered gels, as shown in Figure 27. These results suggest that the intrinsic viscosity of HV-SA, further increased by PVA, makes this combination unsuitable for its intended application.

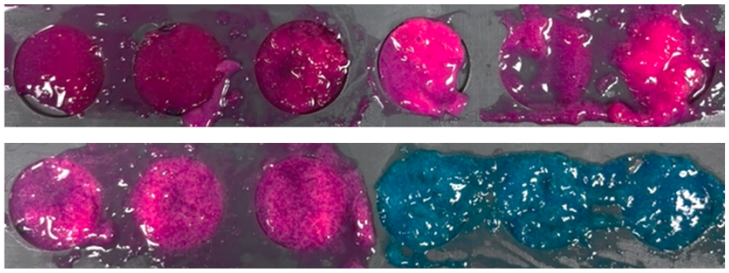

Figure 27. Macroscopic view of hydrogel samples composed of HV-SA and PVA.
The image shows the samples produced with 2% HV-SA, 5% PVA (MW: 13-23 kDa), 75 mM $CaCO_3$ and 150 mM GDL. Significant viscosity-related problems are present, leading to uneven, lumpy samples with irregular thicknesses.

Several strategies were subsequently tested to optimize the sample preparation protocol and overcome these issues. In a first approach, GDL was dissolved in milliQ water and then added to the solution, with the purpose of improving GDL dispersion inside the formulation. Nevertheless, this modification accelerated the crosslinking process, preventing the effective injection of the formulation into the 3D-printed mold. A second approach involved the use of a dual-luer system, composed of two separate syringes: one containing the CA precursors, and the other containing the GDL solution. When pressure was applied simultaneously, the two solutions mixed only after the extrusion. However, this setup caused an immediate crosslinking at the outlet, producing gel filaments instead of uniform samples. In a third approach, the CA precursors were heated to 50 °C before the addition of GDL, improving its dissolution. Still, this modification failed to improve the consistency and reproducibility of the samples. Despite multiple tests for optimizing the preparation method, the formulations remained highly viscous and difficult to process, resulting in irregular and uneven hydrogel structures. These results emphasize the

intrinsic limitations of HV-SA in this application context and its unsuitability for the creation of uniform hydrogel coatings for DCBs.

To further confirm these observations, an empirical coating test was performed using a balloon catheter (6.00mm x 100 mm x 75 cm) and a hydrogel composed of 1% HV-SA + 5% PVA (MW: 13-23 kDa), applied using the thermal cycle protocol previously described, mimicking intraoperative deployment. As shown in Figure 28, the resulting layer adhered only partially to the balloon surface, creating an irregular and fragmented coating. This outcome provides additional evidence of the limitation of HV-SA, demonstrating that the excessive viscosity of the formulation avoids the formation of continuous, uniform coating.

Figure 28. Application of HV-SA hydrogel coating on a real balloon catheter.
Image of a balloon catheter coated with a hydrogel formulation composed of 1% HV-SA and 5% PVA (MW: 13-23 kDa) in 1:1 ratio, following the thermal cycle protocol. The coating obtained has poor adhesion and uneven distribution on the surface of the balloon, confirming the practical limitations of HV-SA-based hydrogels.

Based on these findings, the investigation moved toward alternative options for hydrogel formulation. In particular, attention was shifted to MV-SA, with the aim of overcoming the issues observed whit HV-SA.

3.1.2 Evaluation of MV-SA: Mechanical Properties and Practical Applicability

After identifying the limitations associated with HV-SA, primarily related to its poor injectability, irregular sample formation, and high variability, the investigation continued with the mechanical characterization of MV-SA-based hydrogels. In this section, an amplitude sweep test was performed to evaluate the viscoelastic behavior of the formulations.

To ensure consistency with the previous experimental condition, a polymer concentration of 1% (w/v) was selected, as this value had already proven to be a good compromise between mechanical performance and processability in the HV-SA tests. In this case, the

$CaCO_3$ concentration was varied to obtain five distinct formulations, as described in Table 3 of the *Section 2*. Figure 29A shows the trend of G' and G'' moduli as a function of oscillation strain for all five formulations. Also in this case, as expected for gel-like material, all samples exhibited a first elastic response with G' > G'', followed by a progressive decrease in both moduli beyond the cross-over point, indicated by vertical dotted.

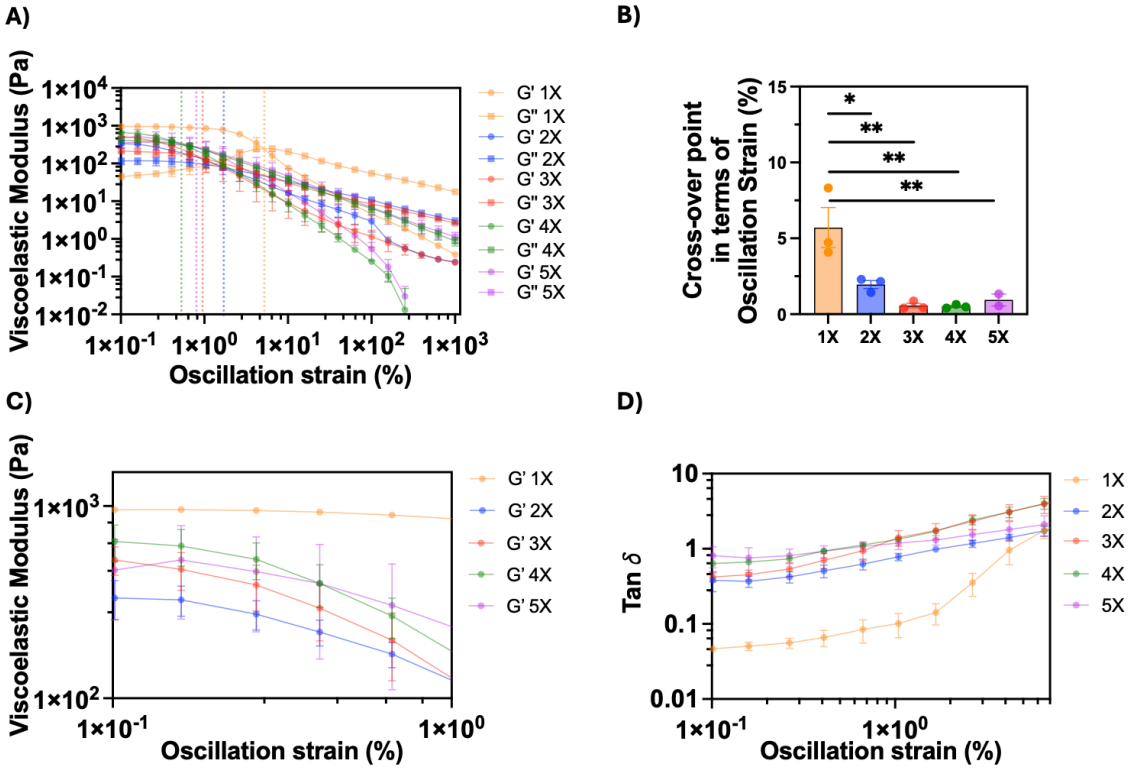

Figure 29. Amplitude sweep test of MV-SA hydrogels with increasing $CaCO_3$ content.
*A) G' and G'' as a function of percentage oscillatory deformation for hydrogels containing 1% MV-SA with increasing concentrations of $CaCO_3$ (1X: 15 mM; 2X: 30 mM; 3X: 45 mM; 4X: 60 mM; 5X: 75 mM). For each condition, GDL was added at a fixed molar ratio of 2:1 relative to $CaCO_3$ (1X: 30 mM; 2X: 60 mM; 3X: 90 mM; 4X: 120 mM; 5X: 150 mM). The cross-over points between G' and G'' are indicated by vertical dotted lines. B) One-way ANOVA of the cross-over point (*p < 0.05, **p < 0.01). C) Close-up of A), emphasizing the behavior of the viscoelastic moduli within the LVR. D) Tan δ values as a function of oscillation strain.*

The average values (± Sem) of these cross-over points (n =3 for each group) are reported in Table 5. Statistical analysis via one-way ANOVA (Figure 29B) confirmed significant differences among the formulations, indicating that formulation 1X had a significantly higher cross-over point than the others (*p < 0.05, **p < 0.01).

Table 5. Mean cross-over points (± Sem) of MV-SA hydrogels.

Formulation	Cross-over point (mean ± Sem)
1X	5.70 ± 2.28%
2X	1.95 ± 0.46%
3X	0.57 ± 0.26%
4X	0.51 ± 0.12%
5X	0.71 ± 0.55%

Although this may suggest superior mechanical strength, practical observations during testing revealed that 1X hydrogels were prone to fracturing even under moderate deformation. This fragility was supported by the tan δ values shown in Figure 29D, which represent the ratio between viscous and elastic response (G'' / G'). A very low tan δ (i.e., $0.001 < \tan\delta < 0.05$), as observed in the 1X formulation, indicates a material with minimal energy dissipation capacity.[72] Such behavior is characteristic of brittle material, meaning that once the elastic limit is exceeded, the material fails rather than deforming plastically. As a result, despite its apparent mechanical strength, the 1X formulation was considered unsuitable for the intended application and was excluded from subsequent tests.

A closer examination of the LVR (Figure 29C) provides further insight into the behavior of each formulation in the low strain region ranging from 1×10^{-1} % to 1×10^{0} % of oscillatory strain. In this range, while 1-4X formulations showed a defined initial plateau of G' followed by a gradual decline, the 5X formulation showed an irregular pattern, visibly different from the others. This behavior is likely due to an excessive content of Ca^{2+} ions during internal gelation. In optimal conditions, Ca^{2+} ions form bicomplexes by crosslinking two G blocks from different SA chains, creating a stable network. However, at higher concentrations, monocomplex formation becomes predominant, in which Ca^{2+} binds only to a single G block. These monocomplexes fail to connect the polymer chains and do not contribute to the network integrity. The result is a less densely crosslinked and mechanically unstable hydrogel, despite the abundance of ions.[51] So, despite theoretical greater performance expectations, the 5X formulation shows lower mechanical stability,

highlighting the importance of keeping an optimal Ca^{2+}/SA ratio. accordingly, the 5X formulation was also excluded from further analysis.

From a practical perspective, MV-SA-based hydrogels demonstrated significantly improved workability and ease of handling compared to HV-SA-based formulations. This allowed for the creation of more uniform and homogeneous samples, as clearly visible in Figure 30A. This qualitative observation was further supported by an empirical coating test, performed using the same coating protocol previously applied to HV-SA, using 1% MV-SA (2-4X) + 5% PVA (MW: 13–23 kDa). As shown in Figure 30B, the 4X formulation was successfully applied to an uncoated vascular balloon (Mustang™ 6.00mm x 100 mm x 75 cm) from Boston Scientific®, completely covering its surface with a uniform and continuous layer. In contrast, the 2X formulation showed evident coating discontinuities, with large, uncovered areas visible on the surface of the balloon. The 3X formulation offered intermediate performance: although better than 2X, it nonetheless presented small areas with minor discontinuities along the coating.

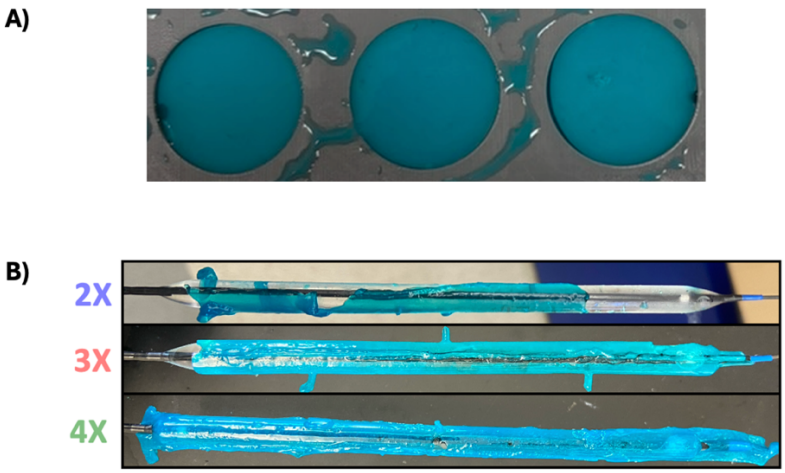

Figure 30. Images of hydrogel uniformity and balloon coatings performance.
A) Samples obtained with the 4X formulation show high homogeneity and surface uniformity. B) Balloon coating test performed with the 2X, 3X, and 4X $CaCO_3$ formulations and 5% PVA (13-23 kDa).

Despite the better performance of 4X in terms of homogenous coating application, all three formulations (2-4X) were considered for further investigation. This decision stemmed from the need to supplement the initial empirical observations with a deeper theoretical understanding of the physical-chemical behavior of the formulations. Therefore, additional experimental evaluations were designed to further investigate their suitability for balloon coating applications. These tests, described in the following sections,

were conceived as complementary to the initial analysis and aimed to provide a more comprehensive characterization of the materials.

3.2 Determination of Crosslinking Time

After the initial mechanical characterization, a quantitative evaluation of the crosslinking kinetics was of the 2-4X formulations was performed for the 2-4X formulations. The goal was to determine the time required for complete network formation, a key parameter for intraoperative applications, where rapid stabilization is essential. This evaluation was performed through time sweep tests, focusing on the evolution of G' over time under constant strain and frequency. The parameter considered was the equilibrium storage modulus G'_{eq}, defined as the value beyond which a plateau is reached, exhibiting negligible changes in stiffnes.[67] The corresponding time represents the moment when the hydrogel network is completely formed. To identify this point objectively, a custom MATLAB script was implemented to detect the instant at which the variation in G' between two consecutive measurements becomes minimal ($\Delta < 0.01$ Pa), indicating that the system has reached mechanical stability. Figure 31A shows the trend of the G' modulus as a function of time for all the three formulations (2-4X). Notably, the 2X formulation reaches lower final modulus values compared to 3X and 4X, suggesting a less structured network and therefore lower mechanical performance. This behavior is consistent with its low $CaCO_3$ content, which contributes fewer cross-linking ions to the gelation process. The average crosslinking times obtained for each formulation (n =3 for each group) are shown in Table 6. These data clearly show a correlation between $CaCO_3$ concentration and gelation time, indicating that greater ion availability accelerates crosslinking.

Table 6. Crosslinking time of 2-4X hydrogel formulations.

Formulation	Time (s)
2X	2075.5 ± 428.2 (~35 min)
3X	1957.1 ± 433.8 (~33 min)
4X	731.3 ± 104.4 (~12 min)

The statistical analysis using one-way ANOVA, shown in Figure 31B, confirmed a statistically significant difference between the three groups, with the 4X formulation showing a faster crosslinking time compared to 2X (**p<0.01) and 3X (*p<0.05). These findings highlight the potential of the 4X formulation for clinical scenarios, where it is crucial to have a material capable of quickly forming a stable network that adheres to the surface of the balloon, reducing procedural times.

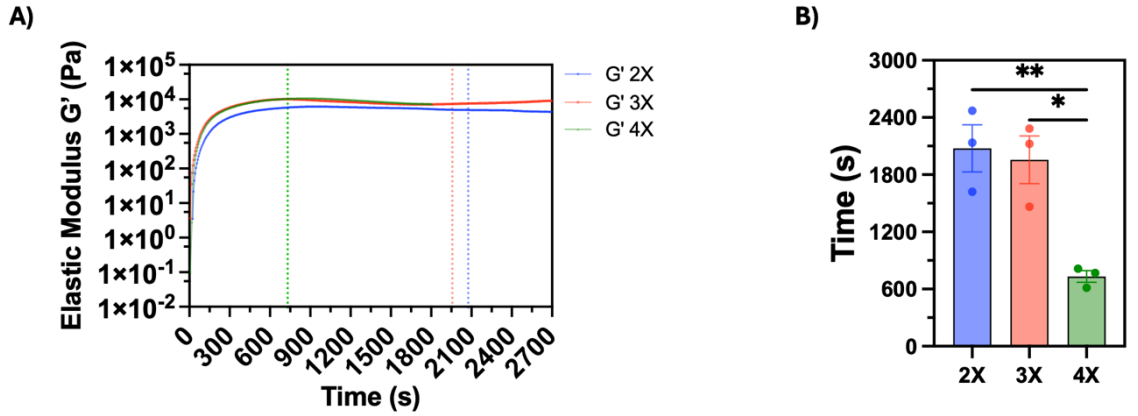

Figure 31. Time sweep test of MV-SA hydrogels at different $CaCO_3$ concentrations (2-4X).
A) Time evolution of G' for each formulation. The vertical dotted lines indicate the average time required to reach the plateau.
*B) One-way ANOVA of the crosslinking time (*p < 0.05, **p < 0.01).*

Based on the characterizations performed, the formulation containing 1% MV-SA and 60 mM $CaCO_3$ (4X) was selected for further development. This choice was based on its good mechanical performance, homogenous coating capabilities as shown in the previous section and also its fast gelation kinetics, ensuring material readiness within a clinically compatible intraoperative timeframe. Subsequent experiments focused on enhancing the adhesiveness of this optimized formulation through the incorporation of PVA. The objective was to determine whether the addition of this polymer could improve surface adhesion without compromising the mechanical stability of the hydrogel.

3.3 Evaluation of Adhesiveness

Following the mechanical and crosslinking characterization, the next step focused on evaluating their adhesive properties, a crucial requirement for ensuring coating retention within the vessel. In particular, the study investigated whether the addition of 5% (w/v)

PVA (MW: 13–23 kDa) to the 4X formulation, in a 1:1 ratio, could enhance its adhesiveness.

To achieve this goal, a probe tack test was employed. Although this test is typically performed using a universal testing machine, for practical reasons a custom protocol was developed using a rheometer, which allowed the test to be performed under controlled and reproducible conditions. The protocol was validated using two reference materials with opposite adhesive behavior: a highly adhesive material based on Elastic 50A resin and a low-adhesive material based on Ecoflex silicone. Elastic 50A resin (Formlabs Inc.) was 3D printed into disc-shaped samples and intentionally left partially uncured to ensure good adhesiveness. In contrast, Ecoflex silicone (Smooth-On Inc.) was fully cured for 24 hours in a 6-well plate, after which disc-shaped samples were obtained by cutting them with a custom 3D-printed punch. The resulting graphs, shown in Figure 32, show the trend of axial force as a function of time. The area under the curve represents the energy required to detach the sample and is therefore indicative of its degree of adhesiveness. As expected, the silicone samples showed a significantly lower area than the resin samples (10.21 ± 1.15 Ns vs. 19.45 ± 2.28 Ns, **p<0.01), demonstrating the effectiveness of the protocol in discriminating between materials with different adhesion properties.

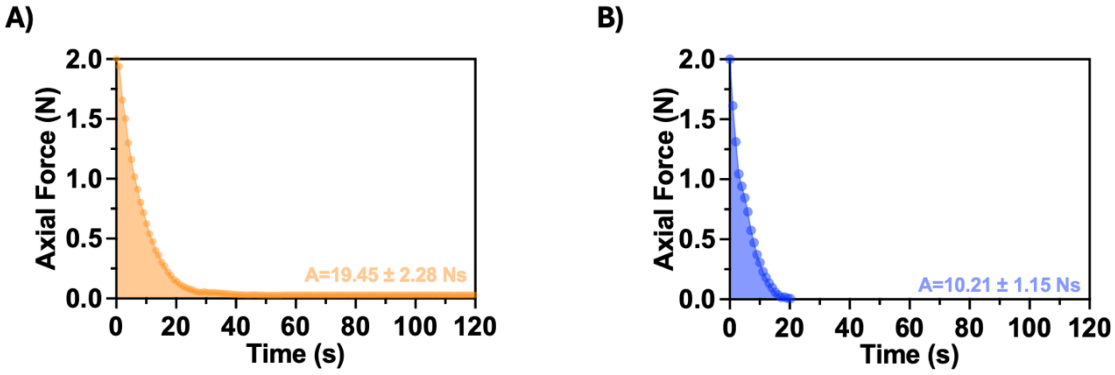

Figure 32. Validation of the custom probe tack test protocol.
A) Curve obtained from a highly adhesive sample made of Elastic 50A resin. B) Curve obtained from a low-adhesion sample composed of Ecoflex silicone.

After validation, the actual analysis of the hydrogels was performed. The samples were prepared following two distinct protocols: the first involved preparation at RT using the custom-designed, 3D-printed plate mold, as shown in Figure 25; the second involved the

thermal cycle, in which the samples were poured into a 6-well plate and then cut to the desired size using a puncher, as shown in Figure 33A,B.

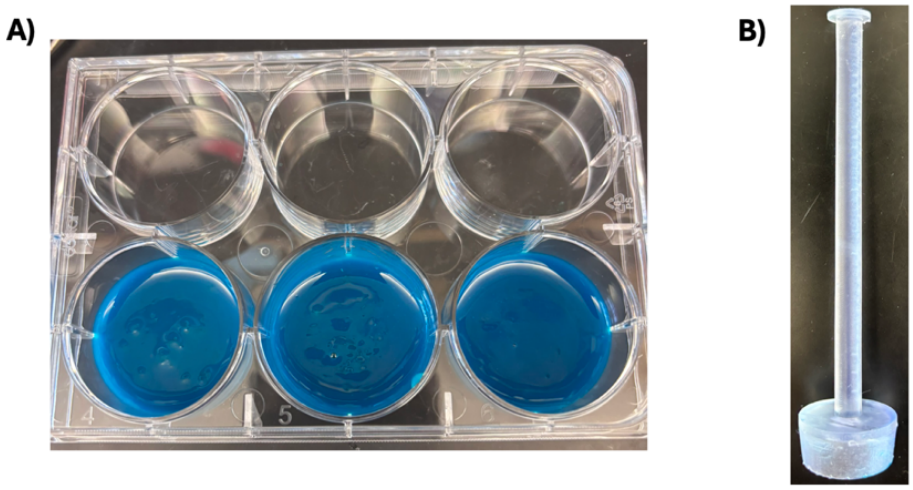

Figure 33. Sample preparation into cell culture plate and cutting tools for RT analysis.
A) Hydrogel samples placed in a 6-well plate after gelation. B) Custom cylindrical punching tool used to cut samples with a diameter of 20 mm.

However, a specific aspect relating to the samples subjected to thermal cycles requires clarification. As described in the *Section 2*, the intraoperative protocol includes a 25-minute oven drying phase, which has been identified as optimal for obtaining the desired coating characteristics. Nevertheless, the samples prepared in the 6-well plate showed a higher initial thickness at RT than the coatings formed around the balloon (3.09 mm vs. 1.73 mm, measured with a high-precision caliper). Consequently, a drying period of 25 minutes was insufficient to achieve comparable final properties. Post-heat treatment thickness measurements revealed that extending the drying time to 60 minutes resulted in a final thickness similar to that of the balloon coating (1.14 mm vs. 1.05 mm). Consequently, a drying time of 60 minutes in the oven was adopted for all samples manufactured in the 6-well plate.

The probe tack test was performed on four different groups of samples, each tested in triplicate, as shown in Figure 34: (A) the 4X formulation at RT, (B) the 4X formulation with 5% PVA (MW: 13-23 kDa) at RT, (C) the 4X formulation after thermal cycling (-20 °C / 55 °C), and (D) the 4X + 5% PVA formulation after thermal cycling.

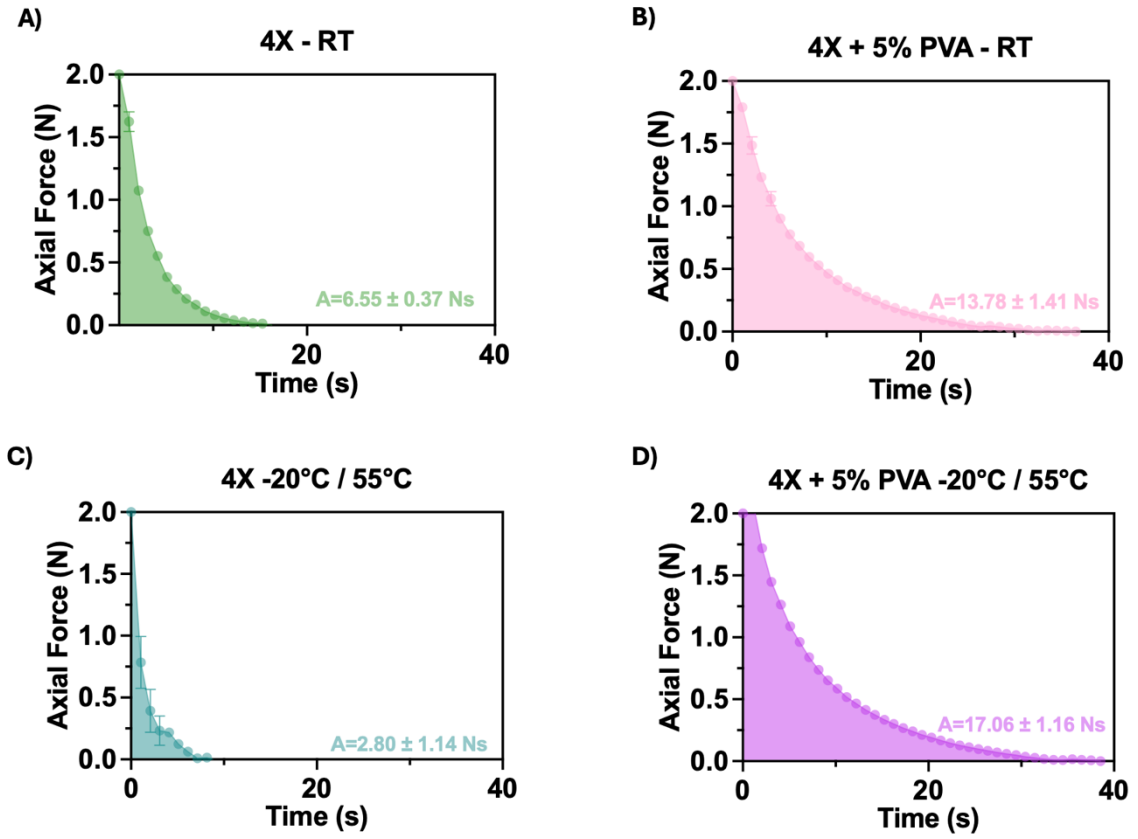

Figure 34. Probe tack test: effect of PVA and thermal cycle on hydrogel adhesiveness.
A) 4X formulation at RT, (B) 4X formulation + 5% PVA (MW: 13-23 kDa) at RT, (C) 4X formulation after thermal cycling (-20 °C for 10 min and 55 °C for 60 min), and (D) the 4X + 5% PVA formulation after thermal cycling (-20 °C for 10 min and 55 °C for 60 min).

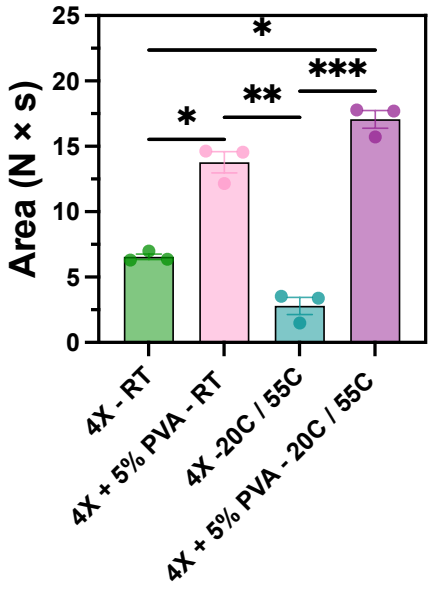

Figure 35. *One-way ANOVA of adhesion performance for 4X-based hydrogels with and without PVA. (*p < 0.05, **p < 0.01, ***p < 0.001)*

A one-way ANOVA statistical analysis was conducted to evaluate the relevant differences between the formulations, as shown in Figure 35. The results indicate that the addition of PVA significantly enhanced the adhesiveness of the hydrogel, both at RT and after thermal cycling. Interestingly, no statistically significant difference was observed between the formulations containing PVA at RT and after thermal cycling, suggesting that thermal treatment does not affect the adhesive properties conferred by PVA.

These findings support the hypothesis that PVA acts as an effective functional excipient to improve hydrogel adhesiveness. Clinically, stronger adhesion is desirable to ensure that the coating remains attached to the vascular wall after balloon deployment. In conclusion, these outcomes suggest that the 4X + 5% PVA formulation has the potential to remain stably adherent to the vascular wall after balloon deployment, one of the key performance requirements for clinical applications.

3.4 Mechanical Effect of Thermal Cycle

One of the main challenges in designing an intraoperative hydrogel coating for DCBs is ensuring that the material remains firmly adhered to the balloon surface during all stages of surgical manipulation, especially during its application to the balloon surface and during insertion of the coated balloon through the deployment sheath. To overcome this problem, as previously described, a thermal protocol was developed to stabilize the hydrogel coating directly in the operating room using a simple and quick two-step process. The first step consists of placing the coated balloon at −20 °C: this freezing phase helps to maintain the position and shape of the coating around the balloon after its application. Next, the balloon undergoes a heating phase at 55 °C, which is essential to prevent the coating from detaching during sheath insertion or catheter handling prior to the vascular procedure.

Given the need to adopt this protocol, the following section investigates the impact of the thermal treatment on the mechanical properties of the hydrogel through rheological amplitude sweep analyses. In particular, formulation 4X was tested, both with and without the addition of 5% (w/v) PVA (MW: 13–23 kDa), under two conditions: at RT

and after the thermal cycle (−20°C for 10 min followed by 55°C for 60 min) with triplicates for each condition. The objective was to determine whether thermal cycling alone, or in combination with PVA, could improve the stability and mechanical strength of hydrogels, extending their LVR and thus improving their ability to resist deformation.

Figure 36A shows the viscoelastic behavior of the 4X formulation at RT and after the thermal cycle. After treatment, noticeable increase in the cross-over point is observed, indicating improved network stability. In this condition, the elastic modulus G' remains higher than the viscous modulus G" for a broader strain range, suggesting an extension of the LVR, and, consequently, greater resistance to mechanical stress before failure. A similar trend is observed for the 4X + 5% PVA formulation, as shown in Figure 36B. In particular, the presence of PVA alone does not significantly improve the mechanical properties at room temperature; in fact, the cross-over point decreases slightly compared to the formulation without PVA. However, when combined with the thermal cycle, the formulation shows a significant improvement in mechanical performance. The Figure 36C shows a direct comparison between the thermally treated 4X and 4X + 5% PVA formulations. It can be observed that the formulation with PVA presents higher G' values across the entire interval of deformation and a wider LVR, suggesting the formation of a more cohesive and resistant polymer network. This improvement could be attributed to the combined effect of PVA and heat treatment. The freeze-thaw process may promote physical cross-linking within the PVA chains through crystallization and molecular rearrangement, improving the structural integrity of the polymer network. Furthermore, interactions between the hydroxyl groups of PVA and the carboxyl groups of CA may further stabilize the matrix, resulting in a mechanically more robust structure. The average cross-over point was quantified for all the tested conditions (n=3 for each group) and reported in Table 7:

Table 7. Mean cross-over points (± Sem) for 4X and 4X + 5% PVA formulations at RT and after thermal cycling (-20°C / 55°C).

Formulation	Cross-over point (mean ± Sem)
4X RT	**0.51 ± 0.12%**
4X -20°C / 55°C	**3.21 ± 0.27%**
4X + 5% PVA (MW:13-23 kDa) RT	**0.29± 0.07%**

4X + 5% PVA (MW:13-23 kDa) -20°C / 55°C	**9.37 ± 3.36%**

A graphical comparison is also provided in Figure 36D: statistical analysis performed using one-way ANOVA confirmed the presence of significant differences between the conditions tested. In particular, the 4X + 5% PVA formulation subjected to thermal cycles showed the highest crossover point value, significantly exceeding both the same formulation at RT (**p<0.01) and the 4X formulation with or without heat treatment (***p<0.001). This data supports the evidence that the combined effect of PVA and thermal cycling has a synergetic impact on coating performance.

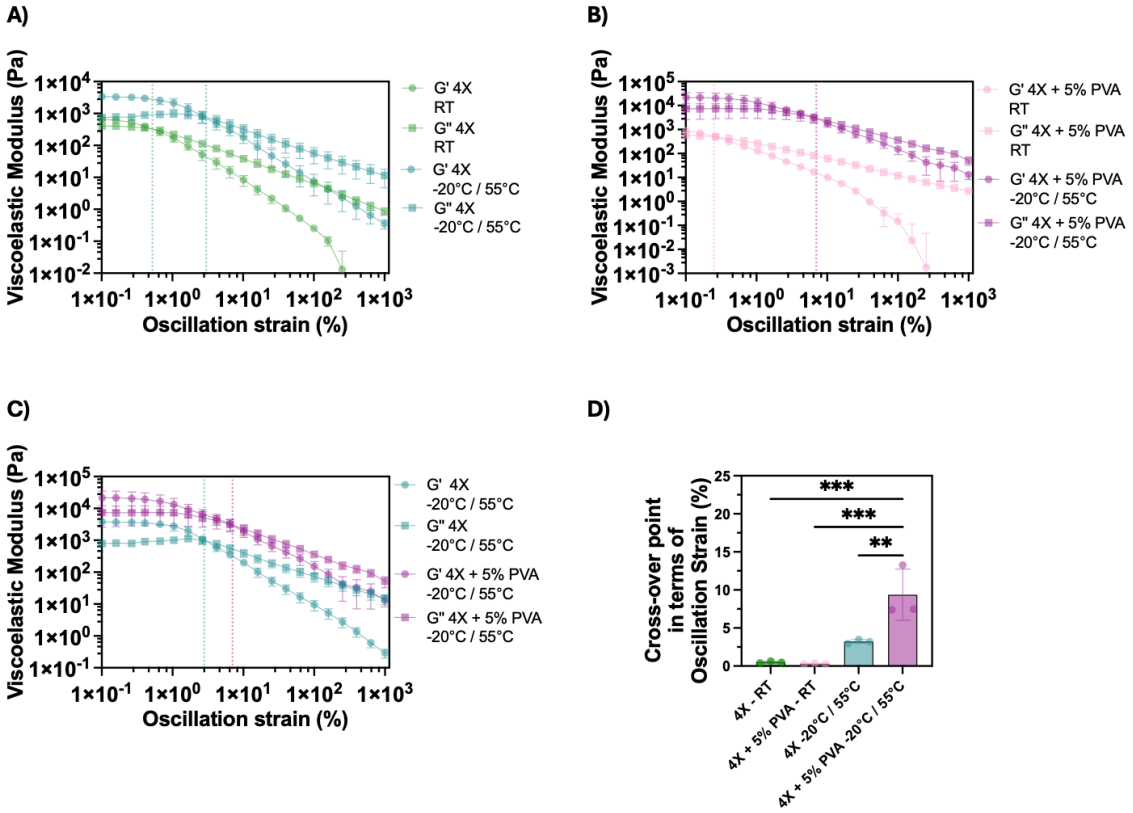

*Figure 36. Effect of PVA and thermal cycling on the mechanical properties of 4X-based hydrogel formulations. Amplitude sweep test of A) 4X formulation at RT and after thermal treatment (−20 °C for 10 min followed by 55 °C for 60 min); B) 4X + 5% PVA (MW: 13–23 kDa) formulation at RT and after thermal treatment. C) Direct comparison of thermally treated 4X and 4X + 5% PVA formulations. D) One way ANOVA of the cross-over point (*p < 0.05, **p < 0.01, ***p < 0.001).*

Overall, these results demonstrate that the combination of low MW PVA and thermal cycle not only improves the adhesion of the coating, as already demonstrated by probe tack tests, but also significantly improves its mechanical stability. In particular, the

observed expansion of the LVR is particularly relevant in a clinical context, as it reflects the material's increased ability to withstand mechanical stress during balloon deployment. Furthermore, this increased mechanical resilience is equally important after the coating has adhered to the vessel wall, where it remains exposed to physiological forces such as pulsatile blood flow and vascular wall movements, which could compromise its structural integrity and therapeutic function.

In conclusion, the 4X + 5% PVA (MW: 13–23 kDa) formulation treated with the proposed thermal protocol emerges as the most promising for intraoperative applications. It successfully combines three fundamental characteristics: a crosslinking kinetics compatible with clinical times, strong adhesion to the vessel surface, and superior mechanical and structural stability. Together, these combined properties make the system highly functional and potentially effective for real-time application as a coating for vascular balloons, able to handle the stresses during PAD procedure.

3.5 Chemical Characterization

To investigate the nature of the interactions between CA and PVA (MW: 13-23 kDa), and to assess whether the thermal cycling could induce significant structural changes in the hydrogel matrix, a chemical characterization was performed using FT-IR spectroscopy on the 4X formulation with and without 5% PVA and with and without thermal cycle. This technique allows the identification of functional groups and the detection of molecular interactions through characteristic vibrational bands. In particular, the analysis focused on evaluating the possibility that the thermal protocol could promote physical crosslinking phenomena, such as hydrogen bonds or crystallite formation, which are often reported in PVA-based systems subjected to freeze-thaw cycles.[73]

To ensure optimal spectral resolution and minimize possible signal interference from water, all the samples were lyophilized before measurement, as shown in Figure 37. This step ensured a dry and homogeneous film, suitable for reliable analysis.

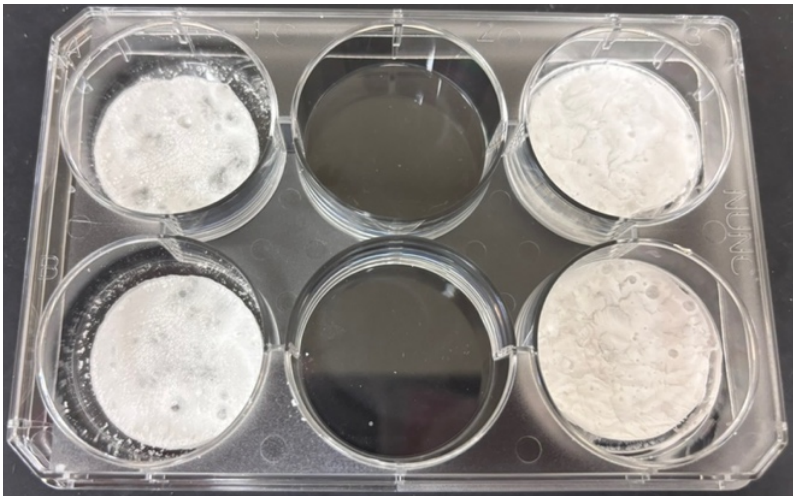

Figure 37. A representation of the lyophilized samples in a 6-well plate for FT-IR analysis.

Following FT-IR acquisition, the spectral data were processed using a custom MATLAB script, which allowed an automated comparison between samples. The main purpose of this script was to align the spectra on a common transmittance axis, allowing for reliable visual comparison between samples. This was particularly important for highlighting slight variations in peak intensity or band broadening that might otherwise be masked.

As shown in **Errore. L'origine riferimento non è stata trovata.**, spectra revealed the presence of peaks associated with functional groups characteristic of both CA and PVA. Specifically:

- 3200-3600 cm^{-1}: Broad O-H stretching band, wider in PVA-containing samples due to hydrogen bonding;[74–76]
- 2920-2940 cm^{-1}: C–H stretching, characteristic of polysaccharides and PVA;[74,75]
- 1700-1750 cm^{-1}: C=O stretching from residual acetal groups in PVA;[74]
- 1590-1515 cm^{-1}: C=O asymmetric stretching related to carboxylate groups in alginate, and broader due to the contribution of PVA;[74–76]
- 1400-1420 cm^{-1}: C=O symmetric stretching related to carboxylate groups in alginate and broader due to the contribution of PVA;[74–76]
- 1020-1100 cm^{-1}: C–O–C stretching related to glycosidic bonds in alginate;[74,76]
- 1050-1150 cm^{-1}: C–OH stretching from PVA;[74]

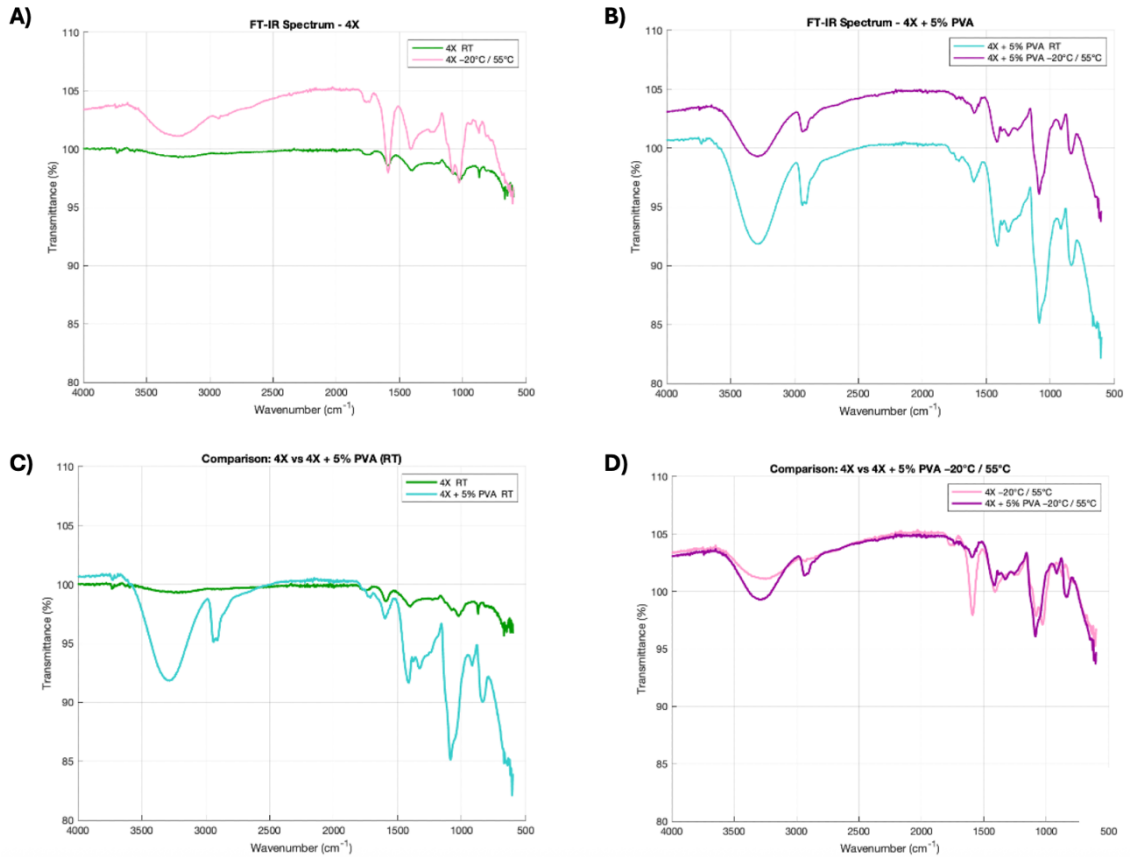

Figure 38. FT-IR spectra of hydrogel formulations with and without PVA, before and after thermal treatment. Comparison of samples at RT and thermal cycle (−20 °C for 10 min followed by 55 °C for 60 min) for both A)4X and B) 4X + 5% PVA formulations. C) Comparison of 4X and 4X + 5% PVA at RT. D) Comparison between 4X and 4X + 5% PVA after thermal cycling (−20 °C for 10 min followed by 55 °C for 60 min).

From the comparison of the spectra, two significant phenomena can be observed. First, a shift towards higher transmittances was observed after thermal protocol; this trend suggests an increase in the network density and strength of intermolecular interactions, indicative of a higher degree of molecular organization within the hydrogel network. This behavior is consistent with the known response of PVA during freeze-thaw cycles, in which water crystallization during freezing brings the polymer chains closer together. During thawing, this proximity facilitates the formation of intermolecular hydrogen bonds and microcrystalline domains. These regions act as physical crosslinking points, improving the mechanical strength of the polymer network without the formation of covalent bonds. Secondly, a reduction in the intensity of the O-H and COO^- peaks was also observed. This result is consistent with the formation of hydrogen bonds between the hydroxyl groups of PVA and the carboxylate groups of CA. The formation of these

interactions modifies the local environment and reduces the vibrational freedom of the groups involved, resulting in attenuation of IR absorption.

Overall, these results suggest that thermal treatment enhances physical interactions between CA and PVA, mainly through hydrogen bonds. The absence of new peaks associated with covalent bonding further confirms that no chemical crosslinking occurs between the two polymers under these conditions. Interestingly, some additional signals were detected in the spectra after thermal treatment. This could potentially indicate partial crosslinking of within the PVA phase; however, given their low intensity, it is not possible to conclusively determine at this stage whether they reflect genuine chemical modifications or are merely attributable to instrumental noise. Further targeted analyses would be required to clarify the origin and significance of these minor spectral features.

In conclusion, FT-IR analysis supports the hypothesis that the mechanical improvement observed in PVA-containing formulations following the thermal cycle is primarily driven by the rearrangement of the polymer chains and the potential formation of microdomains. These structural changes promote the formation of additional physical hydrogen bonds, resulting in a more compact and mechanically stable hydrogel network.

3.6 Effect of PVA on Drug Release

Following the physical-chemical characterization of the hydrogel coatings, a specific study was conducted to investigate their ability to encapsulate and release a pharmaceutical compound, specifically Paclitaxel (PTX), over time. The purpose of this investigation was not only to confirm the feasibility of incorporating the drug into the hydrogel matrix, but also to evaluate the drug release profile and how this could be modulated through variations in the formulation. In particular, attention was focused on the influence of the MW of PVA. To do this, two variants of the 4X base formulation were prepared, incorporating low (13-23 kDa) or high MW PVA (146-186 kDa). These MW were chosen to represent two extremes in polymer chain length among the available materials.

In the initial phase of the study, the effect of the MW of PVA and the presence of PTX on the mechanical properties of the coating were analyzed. As the PTX used was provided

in a commercial solubilized formulation, a specific experimental control was implemented to evaluate the effect of the excipients on the hydrogel properties. Specifically, a control solution was prepared, replicating the vehicle composition of the PTX solution while omitting the active pharmaceutical ingredient. This control allowed the independent assessment of potential solvent-induced effects, thereby minimizing confounding factors and ensuring accurate interpretation of PTX's influence on mechanical performance.

The second phase of the study focused on characterizing the drug release kinetics of the various formulations over a 5-day period, with particular attention to the impact of PVA molecular weight on sustained release behavior.

3.6.1 Influence of PVA Molecular Weight on Mechanical Behavior

To evaluate how the MW of PVA affects the mechanical behavior of the hydrogel coating, two 4X-based formulations containing low MW PVA (13-23 kDa) or high MW PVA (146-186 kDa) were prepared. After undergoing a thermal cycle (−20 °C / 55 °C), the samples were subjected to amplitude sweep tests to evaluate their viscoelastic properties and resistance to mechanical deformation.

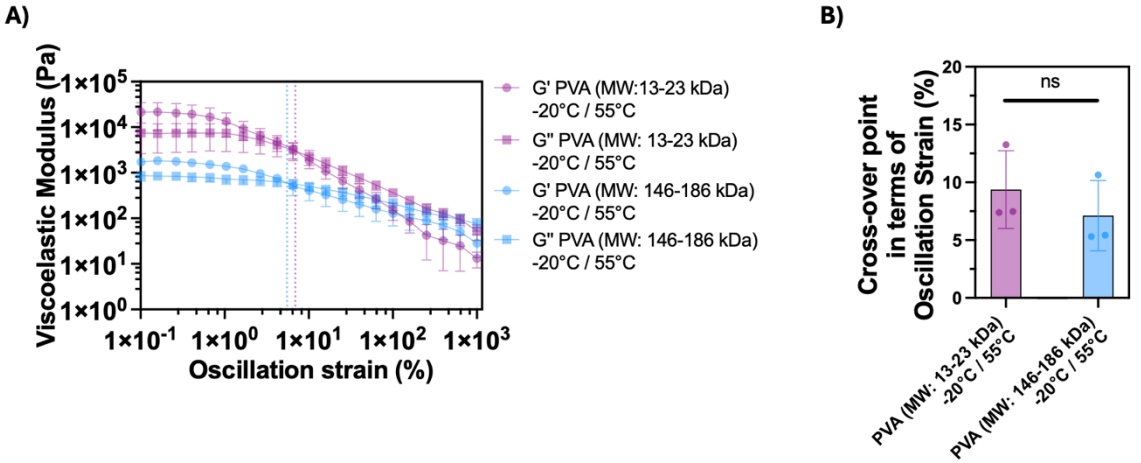

Figure 39. Amplitude sweep test of 4X-based hydrogel coatings containing low and ligh MW PVA.
A) Amplitude sweep test conducted on 4X hydrogel formulations containing PVA with low (13–23 kDa) and high (146–186 kDa) MW, both subjected to a thermal cycle (−20 °C / 55 °C). B) One way ANOVA of the crossover point.

The rheological data, presented in Figure 39A, show a clear difference in the magnitude of the modules: the formulation containing low MW PVA has significantly higher G' and

G'' values across the entire deformation range, with values approximately one order of magnitude higher than those of the formulation with high MW PVA. This suggests that the hydrogel network formed with low MW PVA is mechanically more robust and better able to withstand stress.[77] It is interesting to note that, despite the considerable difference in stiffness, the cross-over point does not differ significantly between the two groups, as confirmed by the one-way ANOVA shown in Figure 39B. The specific cross-over point values for each formulation are reported in **Errore. L'origine riferimento non è stata trovata.**:

Table 8. Mean cross-over points (± Sem) of 4X formulations with two different MW PVA after thermal cycling (-20°C / 55°C).

Formulation	Cross-over point (mean ± Sem)
4X + 5% PVA (MW:13-23 kDa) -20°C / 55°C	**9.37 ± 3.36%**
4X + 5% PVA (MW:146-186 kDa) -20°C / 55°C	**7.12 ± 3.04%**

Although it was initially expected that the use of a PVA with a higher MW would confer greater rigidity to the material,[78] the results suggest the opposite. From a structural point of view, these results suggest that low MW PVA chains, due to their reduced length, may exhibit greater mobility during the thermal cycle. This could facilitate more compact packing, better alignment, and the formation of more uniform crystalline microdomains that act as physical crosslinking points.[79] As a result, the resulting network is denser and more rigid, as evidenced by the higher G' and G'' values. In contrast, high MW PVA chains are longer, which can hinder their mobility and prevent the formation of a uniformly organized network. This could lead to a more heterogeneous and less efficient gel structure with lower resistance to deformation. The wider error bars observed in the high MW group further support this hypothesis, indicating greater variability in mechanical behavior, possibly due to uneven physical cross-linking between samples.

In conclusion, the MW of PVA has a significant influence on the viscoelastic profile of the system, not through a shift in the cross-over point, but through a marked change in the magnitude of the moduli. The superior mechanical performance of the low MW PVA formulation suggests that it may offer a more stable and resilient solution under dynamic conditions such as coating application and the subsequent deployment in the vessel.

3.6.2 Influence of PTX Loading on Mechanical Behavior

To further explore the applicability of the formulation as a drug-release coating, amplitude sweep tests were performed to evaluate how the addition of PTX, and the solvent in which it is dissolved, affects the mechanical behavior of the coating. The PTX was introduced at a concentration of 0.25 mg/mL into the 4X + 5% PVA (MW: 13-23 kDa) formulation.

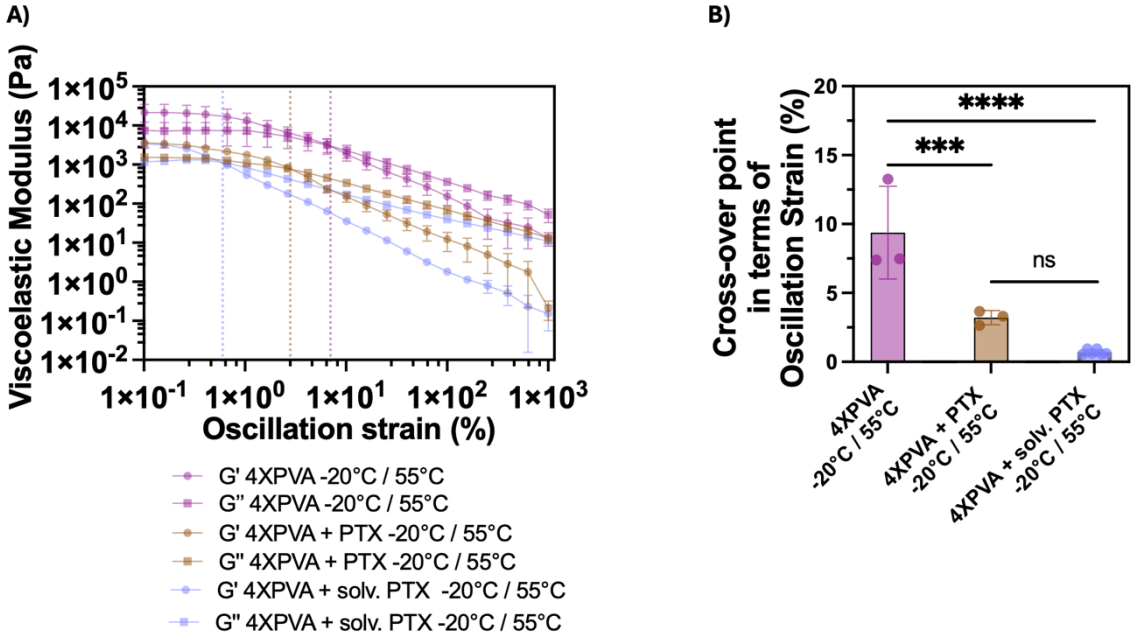

Figure 40. Effect of PTX and solvent on the viscoelastic behavior of the hydrogel coating.
*A) Amplitude sweep test of 4X + 5% PVA (MW: 13–23 kDa) after thermal cycling (−20 °C / 55 °C), with or without the addition of 0.25 mg/mL PTX or its solvent. B) One way ANOVA of the cross-over point (*p<0.05, **p<0.01, ***p < 0.001; ****p < 0.0001).*

As shown in Figure 40A, the addition of PTX into the hydrogel leads to a reduction in both cross-over point and extension of the LVR, indicating a worsening of the mechanical performance of the material. This behavior suggests that the incorporation of PTX compromises the stiffness and resilience of the network, weakening its ability to resist mechanical deformation. However, the nature of this destabilization deserved further investigation. Since the PTX used was not in powder form, but dissolved in an organic solvent, it was hypothesized that the observed decrease in mechanical properties could be attributed primarily to the solvent vehicle, rather than to the drug itself. To test this hypothesis, a control formulation was prepared by adding the same solvent, at equivalent

volume and concentration, but without the drug. The solvent used to prepare the PTX solution consisted of 527 mg/mL castor oil, 49.7% (v/v) dehydrated alcohol, and 2 mg/mL citric acid. The rheological behavior of this control group showed an even more dramatic collapse in mechanical structure, with G' and G'' values dropping by more than an order of magnitude compared with the formulation without the drug.

This trend is also confirmed by the quantitative analysis of the cross-over point, as shown in Figure 40B. One-way ANOVA demonstrates statistically significant differences between the conditions tested (****$p < 0.0001$), with a progressive reduction in the value of oscillation strain at the cross-over point. Specifically, the mean cross-over points are summarized in Table 9:

Table 9. Mean cross-over points (± Sem) of 4X + 5% PVA (MW: 13-23 kDa) after thermal cycling (-20°C / 55°C) containing PTX or solvent.

Formulation	Cross-over point (mean ± Sem)
4X + 5% PVA (MW:13-23 kDa) -20°C / 55°C	**9.37 ± 3.36%**
4X + 5% PVA (MW: 13-23 kDa) + 0.25 mg/ml PTX -20°C / 55°C	**3.20 ± 0.51%**
4X + 5% PVA (MW: 13-23 kDa) + solvent PTX -20°C / 55°C	**0.70 ± 0.20%**

In conclusion, the incorporation of PTX in its solubilized form leads to a weakening of the mechanical properties of the hydrogel, mainly due to the presence of the solvent rather than the drug itself. In particular, no statistically significant difference was observed between the formulation containing both the excipient and the drug and the one containing only the excipient, suggesting that the main effect on mechanical integrity is attributable to the excipient rather than the drug. These results underscore the importance of selecting an appropriate drug formulation strategy. In particular, the use of a powder form of PTX could prevent adverse interactions with the hydrogel network and preserve its mechanical stability, especially when physical crosslinking is the main stabilization mechanism.

3.6.3 Influence of PVA Molecular Weight on PTX Release

To evaluate the actual drug release capability of the hydrogel, a release study was conducted in an aqueous environment using UV-Vis spectroscopy. The test focused on the influence of the MW of PVA on the release kinetics of PTX, which was incorporated into the coating at a concentration of 0.25 mg/mL, corresponding to a total amount of 0.7542 mg per sample.

To closely reproduce realistic intraoperative conditions, a customized balloon phantom was fabricated using 3D printing. The dimensions of the model were selected to match those used in previous empirical tests: length of 100 mm and diameter of 6.03 mm, corresponding to the Mustang™ vascular balloon from Boston Scientific® at an inflation diameter of 9 atm. The coating procedure followed the optimized intraoperative protocol, involving a thermal cycle: the sample was frozen at −20°C for 10 minutes and then heated at 55°C for 25 minutes. To prevent direct contact between the coating and the inner walls of the container, which could potentially alter the release profile, the coated balloon was placed diagonally inside a glass container filled with 600 mL of Milli-Q water, as shown in Figure 41. This configuration ensured complete immersion of the coating.

Figure 41. Setup for PTX release from coated balloon.
Image of the glass container used for the drug release test, containing the 3D printed balloon positioned diagonally to avoid contact between the coating and the container walls.

Since PTX release is primarily governed by passive diffusion, to ensure reliable results it was essential to maintain dynamic conditions to avoid the formation of stagnant boundary. Two agitation methods were tested: a magnetic stirrer, equipped with a magnet inserted into the container to generate flow through rotary motion; and an incu-shaker, an incubator with an oscillating base designed to gently agitate the container. Preliminary tests demonstrated that the Incu-Shaker™ 10L (Benchmark Scientific, USA) at 37 °C and 70 rpm, produced insufficient agitation for effective diffusion, whereas the magnetic stirrer at 40°C and 60 rpm, provided more consistent agitation, and was therefore selected the experiment. Additionally, since it was observed that PTX is highly photosensitive and tends to degrade rapidly after exposure to light, the entire container was wrapped in aluminum foil to shield it from light.

The release profile, shown in Figure 42, display a marked difference between the two tested formulations.

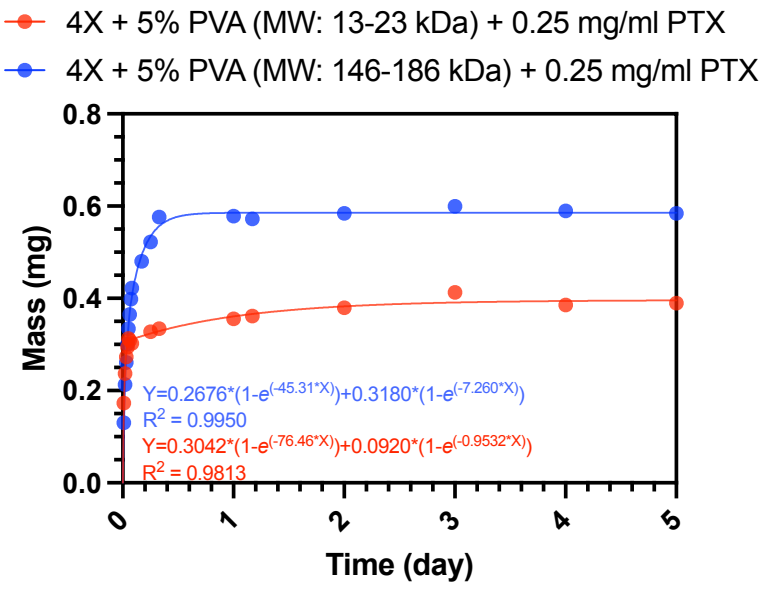

Figure 42. PTX release profiles for different PVA MW.
Release of PTX from hydrogel coatings containing low (13-23 kDa) and high (146-186 kDa) MW PVA over 5 days. The formulation with low MW PVA shows a biphasic release profile, with an initial burst followed by sustained release, while high MW PVA leads to rapid drug release within 8 hours. A nonlinear two-phase association model was used to fit the data, and the corresponding equations along with the R^2 values are shown in the graph.

The coating containing high MW PVA (146-186 kDa) showed an accelerated profile, reaching near-complete PTX release (>90%) within the first 8 hours, suggesting a rapid diffusion of the drug molecules. In contrast, the formulation with low MW PVA (13-23 kDa) exhibited a biphasic release profile, characterized by an initial burst phase,

accounting for about 30% of the total drug in the first 6 hours, followed by a prolonged, sustained release phase. After 5 days, only 53% of the 0. 7542 mg drug had been released, suggesting a greater improved drug retention capacity compared to the high MW formulation.

The observed behavior may appear counterintuitive. Typically, higher MW polymers are associated with denser crosslinked network, theoretically resulting in lower permeability and slower drug diffusion. In a study by Chen et al.[78] it was demonstrated that high MW PVA may promote the formation of a less homogeneous polymer network with internal microdefects, which can facilitate drug diffusion, leading to faster release. As a result, rather than slowing diffusion, higher MW PVA may facilitate the rapid delivery of drug molecules. In contrast, the shorter chains of low MW PVA appear to align more easily into ordered domains during heat treatment. This leads to a denser, more compact network with more uniform crystalline regions that slow the diffusion of the incorporated drug. While this hypothesis could explain the observed results, further morphological analyses, such as SEM microscopy, would be necessary to confirm the structure of the network.

In conclusion, these findings highlight that the use of low MW PVA offers a promising strategy for the controlled release of PTX from hydrogel-based coating applied to vascular balloons. The observed biphasic profile is particularly relevant in clinical settings, allowing for an initial therapeutic burst release followed by sustained drug delivery over several days, potentially reducing the need for repeated interventions. However, it is important to acknowledge the limitations of this study. The in vitro delivery system does not fully reproduce the dynamic in vivo environment. In particular, the test involves complete exposure of the coated balloon to the flow, which does not reflect the physiological scenario in which the coating should be in contact with the vascular wall. Furthermore, the absence of unidirectional flow or interaction with tissues implies that the release observed in the test is governed exclusively by passive diffusion through the hydrogel matrix, without considering potential biological factors that could influence drug transport in vivo.

3.7 Morphological Characterization

To assess the internal organization of the developed hydrogel coatings, SEM imaging was employed to analyze the microstructure of both RT and thermally treated samples. The analysis focused on different CA-based formulations: 4X, 4X + 5% PVA (MW: 13–23 kDa) and 4X + 5% PVA (MW: 146–186 kDa) MW, with or without drug loading. SEM images acquired from lyophilized cross-sections are reported in Figure 43 (A–F) for thermally treated samples and Figure 44 (G–L) for samples prepared at RT.

All the analyzed formulations exhibited globally porous with pores visibly larger than the hydrodynamic diameter of PTX molecules in solution (~2 nm), suggesting compatibility of the matrix with a diffusive-type drug release.

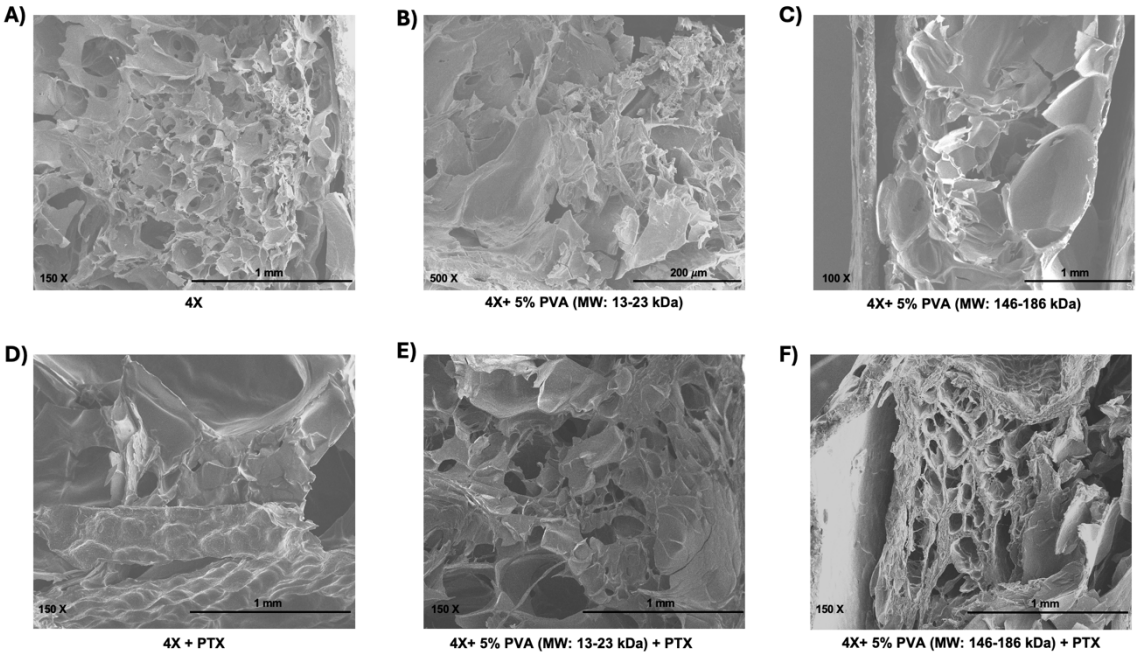

Figure 43. Representative SEM images of CA-based hydrogel formulations after thermal cycle (−20 °C / 55 °C). A) 4X, B) 4X + 5% PVA (MW: 13-23 kDa), C) 4X + 5% PVA (MW: 146-186 kDa), D) 4X + 0.25 mg/ml PTX, E) 4X + 5% PVA (MW: 13-23 kDa) + 0.25 mg/ml PTX, F) 4X + 5% PVA (MW: 146-186 kDa) + 0.25 mg/ml PTX.

Formulations containing low MW PVA (B, E, H, K) showed a more homogeneous and compact microstructure compared to those containing high MW PVA (C, F, I, L), which exhibited irregular, disorganized porosity. This observation is consistent with the hypothesis that shorter PVA chains facilitate the formation of a more ordered polymer network, while longer chains, due to the greater steric hindrance, may impair network

organization. Comparing the thermal-treated samples (A-F) with those maintained at RT (G-L), a more compact and densified porous structure was observed following thermal cycling, particularly in the presence of low MW PVA.

The addition of PTX (D-F, J-L) did not appear to induce major morphological changes in SEM images compared with the corresponding drug-free formulations. However, the PTX excipient may affect the polymer interaction.

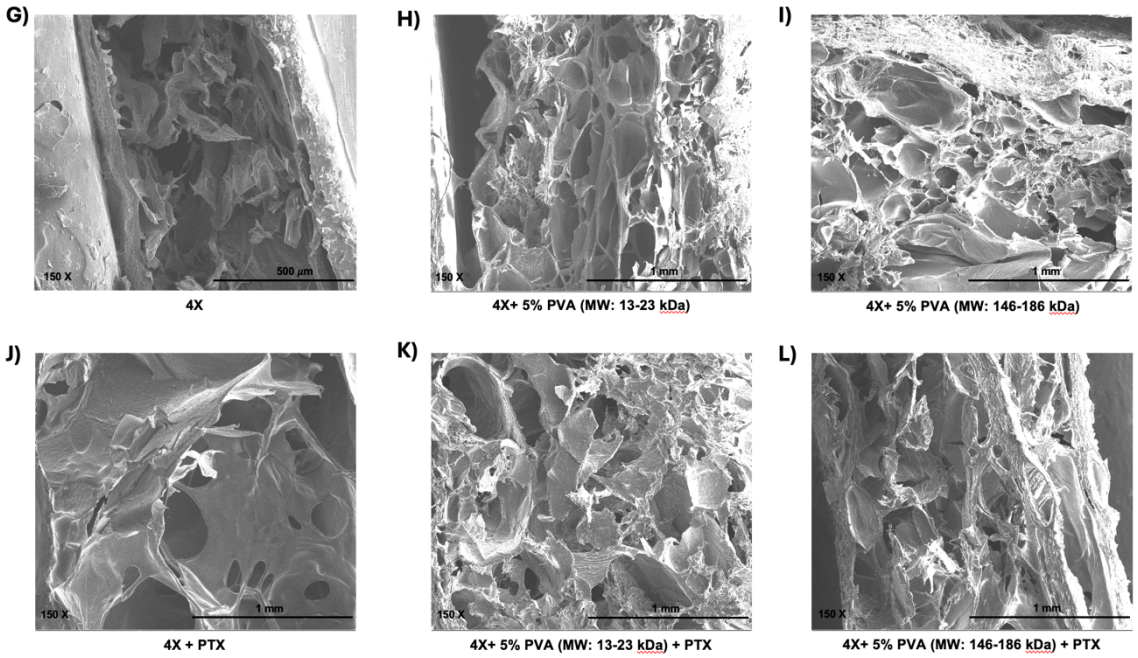

Figure 44. Representative SEM images of CA-based hydrogel formulations at RT.
G) 4X, H) 4X + 5% PVA (MW: 13-23 kDa), I) 4X + 5% PVA (MW: 146-186 kDa), J) 4X + 0.25 mg/ml PTX, K) 4X + 5% PVA (MW: 13-23 kDa) + 0.25 mg/ml PTX, L) 4X + 5% PVA (MW: 146-186 kDa) + 0.25 mg/ml PTX.

As part of the study, SEM imaging was performed to qualitatively examine the internal microstructure of the hydrogel formulations and to explore how variations in PVA MW and the presence of PTX affect the network architecture. These reference images provide a visual complement to the mechanical and drug release data, offering morphological information that supports the interpretation of the material's behavior. However, it is important to mention that the current sample preparation protocol, based on lyophilization, does not allow for optimal preservation of the native three-dimensional structure of hydrogels. The drying process can cause partial collapse of the network or introduce structural artifacts. Therefore, the SEM images presented here should be considered indicative representations rather than definitive morphological

characterizations. Although some microstructures appear consistent with mechanical performance and release profiles, the results should be interpreted with caution. To enable more accurate visualization of the microstructure of the hydrogel in its native hydrated state, future analyses may benefit from alternative imaging approaches. For example, environmental scanning electron microscopy (ESEM) allows direct imaging of hydrated samples without the need for complete dehydration, thus reducing structural alterations; this technique has been successfully applied to various hydrogel systems,[80] including alginate-based ones.[81] Another alternative is cryo-scanning electron microscopy (cryo-SEM), which preserves water content through rapid freezing, demonstrating its effectiveness in maintaining the native architecture of alginate hydrogels.[82] Another option is critical point drying, a method already tested in the preparation of PVA-based hydrogels to minimize collapse during dehydration.[83]

4. Conclusion

This thesis presents the development and characterization of a hydrogel-based coating designed for applications on uncoated balloons, with the aim of improving mechanical stability, adhesion to the vascular wall, and enabling tunable drug release for intraoperative procedures. Through the combination of CA and PVA, a formulation was optimized to meet physicochemical and pharmacological requirements.

Among the formulations tested, the 4X hydrogel (1% MV-SA, 60 mM $CaCO_3$, 120 mM GDL) was identified as the most suitable in terms of handling, coating quality and crosslinking kinetics, key parameters to ensure the feasibility of intraoperative use of the formulation. To enhance adhesion to biological tissues, 5% (w/v) low MW PVA (13-23 kDa) was incorporated in the hydrogel. This composition demonstrated improved adhesiveness and good mechanical performance after being subjected to thermal cycling, paving the way for being used as a local drug delivery platform after deployment in the vessel. FT-IR spectroscopy revealed no chemical crosslinking between CA and PVA, suggesting that the stability of the network was achieved primarily through physical interactions. The release profile of the drug PTX was evaluated using different PVA types with varying MWs: low MW PVA enabled a biphasic release pattern, with an initial burst release and a second controlled phase over time. SEM analysis confirmed the presence of an interconnected pore structure in all conditions tested, with larger pore sizes consistent with a diffusion-controlled release mechanism. To evaluate the practical applicability of the system under physiological conditions, another Master Candidate student, Cesare Farina developed a simple simulated circulatory model to conduct various experiments. The setup included a peristaltic pump used to perfuse PBS through a mock vessel, mimicking blood flow. These experiments demonstrated that the hydrogel coating adhered to the inner wall of the tube and remained in place for over 24 hours under continuous flow conditions without losing its structural integrity. In addition, he performed ex vivo validation using porcine vascular tissue, which confirmed the strong adhesion of the coating to the vessel walls, further supporting its translational potential. Together, these results validate the final formulation as a promising candidate for intraoperative vascular drug delivery.

Current findings support the hydrogel system as a valid platform for intraoperative delivery of vascular drugs. The optimized composition allows for rapid preparation and application directly at the site of surgery, making it particularly suitable for real-time procedural use. The design achieves a balance between prolonged retention in the lesion to ensure therapeutic efficacy and subsequent bioresorption, thus reducing the risk of a long-term foreign body response. Additionally, the platform offers the possibility of customizing therapy through the incorporation of multiple drugs. This could be realized through a multilayer architecture, in which each layer is engineered to release distinct agents, such as antiproliferative or antithrombotic agents. This strategy would improve therapeutic precision and offer a modular approach to addressing multifactorial vascular pathologies.

However, several approaches are needed for further optimization and validation of the technology. One particularly promising approach involves the chemical conjugation of PTX to the polymer network to achieve better retention and prolonged release. Potential strategies may involve the use of cyclodextrin, which form inclusion complexes that can stabilize the drug, or covalent bonding using poly-L-lysine. Such modifications can mitigate burst release phenomena and optimize the local bioavailability of the drug. In parallel, future studies should aim to validate the performance of the coating through rigorous biological assays. Further investigations should incorporate in vitro assessments of cytocompatibility using vascular cell models, ex vivo evaluations under dynamic flow conditions, and in vivo investigations. These investigations will be critical to assess the cytocompatibility of the material, the biodistribution of the drug once released, and its ability to maintain adhesion under pulsatile flow conditions. Moreover, in view of potential clinical translation, efforts should also be directed at adapting and integrating the coating system with commercial balloon platforms. This includes assessing the scalability of the manufacturing process, batch-to-batch reproducibility, regulatory compliance and sterility standards required for medical devices.

In conclusion, this work defines an adaptable hydrogel coating platform with proven mechanical integrity, adhesive properties, and controlled drug release potential. Although further research is required to fully characterize the biological performance and optimize the system for clinical translation, the research provides a comprehensive and promising

basis for the development of next-generation, patient-customized vascular drug delivery systems capable of addressing the complex therapeutic needs of PAD.

5. References

1. Roth GA, Mensah GA, Johnson CO, Addolorato G, Ammirati E, Baddour LM, Barengo NC, Beaton AZ, Benjamin EJ, Benziger CP, Bonny A, Brauer M, Brodmann M, Cahill TJ, Carapetis J, Catapano AL, Chugh SS, Cooper LT, Coresh J, Criqui M, DeCleene N, Eagle KA, Emmons-Bell S, Feigin VL, Fernández-Solà J, Fowkes G, Gakidou E, Grundy SM, He FJ, Howard G, Hu F, Inker L, Karthikeyan G, Kassebaum N, Koroshetz W, Lavie C, Lloyd-Jones D, Lu HS, Mirijello A, Temesgen AM, Mokdad A, Moran AE, Muntner P, Narula J, Neal B, Ntsekhe M, Moraes de Oliveira G, Otto C, Owolabi M, Pratt M, Rajagopalan S, Reitsma M, Ribeiro ALP, Rigotti N, Rodgers A, Sable C, Shakil S, Sliwa-Hahnle K, Stark B, Sundström J, Timpel P, Tleyjeh IM, Valgimigli M, Vos T, Whelton PK, Yacoub M, Zuhlke L, Murray C, Fuster V. Global Burden of Cardiovascular Diseases and Risk Factors, 1990–2019. J Am Coll Cardiol. 2020 Dec 22;76(25):2982–3021.

2. Turner EA, Atigh MK, Erwin MM, Christians U, Yazdani SK. Coating and Pharmacokinetic Evaluation of Air Spray Coated Drug Coated Balloons. Cardiovasc Eng Tech. 2018 Jun;9(2):240–250.

3. Hirsch AT, Criqui MH, Treat-Jacobson D, Regensteiner JG, Creager MA, Olin JW, Krook SH, Hunninghake DB, Comerota AJ, Walsh ME, McDermott MM, Hiatt WR. Peripheral Arterial Disease Detection, Awareness, and Treatment in Primary Care. JAMA. 2001 Sep 19;286(11):1317–1324.

4. Ajoolabady A, Pratico D, Lin L, Mantzoros CS, Bahijri S, Tuomilehto J, Ren J. Inflammation in atherosclerosis: pathophysiology and mechanisms. Cell Death Dis. Nature Publishing Group; 2024 Nov 11;15(11):1–16.

5. Suzuki J ichi, Shimamura M, Suda H, Wakayama K, Kumagai H, Ikeda Y, Akazawa H, Isobe M, Komuro I, Morishita R. Current therapies and investigational drugs for peripheral arterial disease. Hypertens Res. 2016 Apr;39(4):183–191.

6. Gornik HL, Beckman JA. Peripheral Arterial Disease. Circulation [Internet]. 2005 Apr 5 [cited 2024 Sep 24];111(13).

7. Narayanan S, Boologapandian V. How to Approach a Patient With Peripheral Arterial Disease. Indian Journal of Vascular and Endovascular Surgery. 2018 Dec;5(4):274.

8. Olin JW, Sealove BA. Peripheral Artery Disease: Current Insight Into the Disease and Its Diagnosis and Management. Mayo Clin Proc. 2010 Jul;85(7):678–692.

9. 2024 ACC/AHA/AACVPR/APMA/ABC/SCAI/SVM/SVN/SVS/SIR/VESS Guideline for the Management of Lower Extremity Peripheral Artery Disease: A Report of the American College of Cardiology/American Heart Association Joint Committee on Clinical Practice Guidelines.

10. Bevan GH, White Solaru KT. Evidence-Based Medical Management of Peripheral Artery Disease. ATVB. 2020 Mar;40(3):541–553.

11. Vartanian SM, Conte MS. Surgical Intervention for Peripheral Arterial Disease. Circulation Research. 2015 Apr 24;116(9):1614–1628.

12. Idhris M, Woodman A, Rasheed M, Ahmad S. Research Status and Future Trends of Angioplasty: A Bibliometric Analysis in CiteSpace. Ibnosina Journal of Medicine and Biomedical Sciences. 2023 Sep;15(03):135–144.

13. Se W, Gl W, Ap C. Percutaneous transluminal angioplasty versus operation for peripheral arteriosclerosis. Report of a prospective randomized trial in a selected group of patients. Journal of vascular surgery [Internet]. J Vasc Surg; 1989 Jan.

14. Kudagi VS, White CJ. Endovascular Stents: A Review of Their Use in Peripheral Arterial Disease. Am J Cardiovasc Drugs. 2013 Jun;13(3):199–212.

15. Kansal A, Long CA, Patel MR, Jones WS. Endovascular treatment of femoro-popliteal lesions. Clinical Cardiology. 2019 Jan;42(1):175–183.

16. Alraies MC, Darmoch F, Tummala R, Waksman R. Diagnosis and management challenges of in-stent restenosis in coronary arteries. World Journal of Cardiology. 2017 Aug 26;9(8):640.

17. Kovačič APM, Caprnda M, Mrhar A, Kubatka P, Locatelli I, Zolakova B, Gaspar L, Prosecky R, Kruzliak P, Staffa R, Rodrigo L, Radonak J, Petrovič D. Impact of drugs on venous thromboembolism risk in surgical patients. Eur J Clin Pharmacol. 2019 Jun 1;75(6):751–767.

18. Makin A, Silverman SH, Lip GYH. Peripheral vascular disease and Virchow's triad for thrombogenesis. QJM. 2002 Apr;95(4):199–210.

19. Restenosis: Repeat Narrowing of a Coronary Artery | Circulation [Internet].

20. Zhu H, Kong L, Zhu X, Ran T, Ji X. pH-Responsive Nanoparticles for Delivery of Paclitaxel to the Injury Site for Inhibiting Vascular Restenosis. Pharmaceutics. Multidisciplinary Digital Publishing Institute; 2022 Mar;14(3):535.

21. Rensing BJ, Vos J, Smits PC, Foley DP, van den Brand MJBM, van der Giessen WJ, de Feijter PJ, Serruys PW. Coronary restenosis elimination with a sirolimus eluting stent; First European human experience with 6-month angiographic and intravascular ultrasonic follow-up. European Heart Journal. 2001 Nov 1;22(22):2125–2130.

22. Local Paclitaxel Delivery for Treatment of Peripheral Arterial Disease | Circulation: Cardiovascular Interventions [Internet]. [cited 2025 May 23]. 2

23. Qamar SUR, Spahić L, Benolić L, Zivanovic M, Filipović N. Treatment of Peripheral Artery Disease Using Injectable Biomaterials and Drug-Coated Balloons: Safety and

Efficacy Perspective. Pharmaceutics. Multidisciplinary Digital Publishing Institute; 2023 Jul;15(7):1813.

24. Sun G, Liu J, Jia X, Xiong J, Ma X, Zhang H, Guo W. Long-term Outcomes of the AcoArt II-BTK Trial: Drug-Coated Balloon Angioplasty Compared With Uncoated Balloons for the Treatment of Infrapopliteal Artery Lesions. J Endovasc Ther. 2024 Dec 18.

25. Liistro F, Angioli P, Porto I, Ducci K, Falsini G, Ventoruzzo G, Ricci L, Scatena A, Grotti S, Bolognese L. Drug-Eluting Balloon Versus Drug-Eluting Stent for Complex Femoropopliteal Arterial Lesions: The DRASTICO Study. J Am Coll Cardiol. 2019 Jul 16;74(2):205–215.

26. Kundu A, Moliterno DJ. Drug-Coated Balloons for In-Stent Restenosis-Finally Leaving Nothing Behind for US Patients. JAMA. 2024 Mar 26;331(12):1011–1012.

27. Gray WA, Granada JF. Drug-coated balloons for the prevention of vascular restenosis. Circulation. 2010 Jun 22;121(24):2672–2680.

28. Keefe N, Shull T, Botea L, McGinigle K. Drug-Coated Balloon versus Drug-Eluting Stent: The Debate of Leave Nothing Behind. Semin Intervent Radiol. 2023 Jun 16;40(2):161–166.

29. Verde N, Ciliberti G, Pittorino L, Ferrone M, Franzese M, Russo M, Cioppa A, Popusoi G, Salemme L, Tesorio T, Di Gioia G. Contemporary Use of Drug-Coated Balloons for Coronary Angioplasty: A Comprehensive Review. J Clin Med. 2024 Oct 19;13(20):6243.

30. Park SJ, Shim WH, Ho DS, Raizner AE, Park SW, Hong MK, Lee CW, Choi D, Jang Y, Lam R, Weissman NJ, Mintz GS. A paclitaxel-eluting stent for the prevention of coronary restenosis. N Engl J Med. 2003 Apr 17;348(16):1537–1545.

31. Axel DI, Kunert W, Göggelmann C, Oberhoff M, Herdeg C, Küttner A, Wild DH, Brehm BR, Riessen R, Köveker G, Karsch KR. Paclitaxel Inhibits Arterial Smooth Muscle Cell Proliferation and Migration In Vitro and In Vivo Using Local Drug Delivery. Circulation. American Heart Association; 1997 Jul 15;96(2):636–645.

32. Mauri L, Hsieh W hua, Massaro JM, Ho KKL, D'Agostino R, Cutlip DE. Stent Thrombosis in Randomized Clinical Trials of Drug-Eluting Stents. New England Journal of Medicine. Massachusetts Medical Society; 2007 Mar 8;356(10):1020–1029.

33. Cavallaro G, Licciardi M, Caliceti P, Salmaso S, Giammona G. Synthesis, physico-chemical and biological characterization of a paclitaxel macromolecular prodrug. European Journal of Pharmaceutics and Biopharmaceutics. 2004 Jul 1;58(1):151–159.

34. Haeri A, Osouli M, Bayat F, Alavi S, Dadashzadeh S. Nanomedicine approaches for sirolimus delivery: a review of pharmaceutical properties and preclinical studies.

Artificial Cells, Nanomedicine, and Biotechnology. Taylor & Francis; 2018 Oct 31;46(sup1):1–14.

35. di Palma G, Sanchez-Jimenez EF, Lazar L, Cortese B. Should paclitaxel be considered an old generation DCB? The limus era. Rev Cardiovasc Med. 2021 Dec 22;22(4):1323–1330.

36. Gurgoglione FL, De Gregorio M, Benatti G, Donelli D, Vignali L, Solinas E, Tadonio I, Denegri A, Covani M, Dallaglio G, Cortese B, Niccoli G. Paclitaxel-Coated Versus Sirolimus-Coated Eluting Balloons for Percutaneous Coronary Interventions: Pharmacodynamic Properties, Clinical Evidence, and Future Perspectives. Future Pharmacology. Multidisciplinary Digital Publishing Institute; 2024 Dec;4(4):775–787.

37. Paclitaxel-Coated Balloon vs Uncoated Balloon for Coronary In-Stent Restenosis: The AGENT IDE Randomized Clinical Trial | Cardiology | JAMA | JAMA Network [Internet].

38. Zeller T, Micari A, Scheinert D, Baumgartner I, Bosiers M, Vermassen FEG, Banyai M, Shishehbor MH, Wang H, Brodmann M, IN.PACT DEEP Trial Investigators. The IN.PACT DEEP Clinical Drug-Coated Balloon Trial: 5-Year Outcomes. JACC Cardiovasc Interv. 2020 Feb 24;13(4):431–443.

39. Zeller T, Baumgartner I, Scheinert D, Brodmann M, Bosiers M, Micari A, Peeters P, Vermassen F, Landini M, Snead DB, Kent KC, Rocha-Singh KJ, IN.PACT DEEP Trial Investigators. Drug-eluting balloon versus standard balloon angioplasty for infrapopliteal arterial revascularization in critical limb ischemia: 12-month results from the IN.PACT DEEP randomized trial. J Am Coll Cardiol. 2014 Oct 14;64(15):1568–1576.

40. Rykowska I, Nowak I, Nowak R. Drug-Eluting Stents and Balloons—Materials, Structure Designs, and Coating Techniques: A Review. Molecules. 2020 Oct 11;25(20):4624.

41. Faenger B, Heinrich A, Hilger I, Teichgräber U. Drug loss from Paclitaxel-Coated Balloons During Preparation, Insertion and Inflation for Angioplasty: A Laboratory Investigation. Cardiovasc Intervent Radiol. 2022;45(8):1186–1197.

42. Anderson JA, Lamichhane S, Fuglsby K, Remund T, Pohlson K, Evans R, Engebretson D, Kelly P. Development of Drug-Coated Balloon for the Treatment of Multiple Peripheral Arterial Segments. J Vasc Surg. 2020 May;71(5):1750-1757.e7.

43. Fuglsby K, Anderson JA, Engebretson D, Lamichhane S. Development of an automated micropipette coating method for drug-coated balloons. Journal of Biomedical Materials Research Part B: Applied Biomaterials. 2020;108(5):2258–2275.

44. Farah S, Domb AJ. Crystalline paclitaxel coated DES with bioactive protective layer development. J Control Release. 2018 Feb 10;271:107–117.

45. Torii S, Kolodgie FD, Virmani R, Finn AV. IN.PACT™ Admiral™ drug-coated balloons in peripheral artery disease: current perspectives. Med Devices (Auckl). 2019 Feb 12;12:53–64.

46. Faenger B, Heinrich A, Hilger I, Teichgräber U. Drug loss from Paclitaxel-Coated Balloons During Preparation, Insertion and Inflation for Angioplasty: A Laboratory Investigation. Cardiovasc Intervent Radiol. 2022;45(8):1186–1197.

47. Drug-Eluting Balloon | Circulation: Cardiovascular Interventions [Internet]. [cited 2025 May 28].

48. Kaule S, Minrath I, Stein F, Kragl U, Schmidt W, Schmitz KP, Sternberg K, Petersen S. Correlating coating characteristics with the performance of drug-coated balloons--a comparative in vitro investigation of own established hydrogel- and ionic liquid-based coating matrices. PLoS One. 2015;10(3):e0116080.

49. Consigny PM, Barry JJ, Vitali NJ. Local delivery of an antiproliferative drug with use of hydrogel-coated angioplasty balloons. J Vasc Interv Radiol. 1994;5(4):553–560.

50. Glazier JJ, Hirst JA, Kiernan FJ, Fram DB, Eldin AM, Primiano CA, Mitchel JF, McKay RG. Site-specific intracoronary thrombolysis with urokinase-coated hydrogel balloons: acute and follow-up studies in 95 patients. Cathet Cardiovasc Diagn. 1997 Jul;41(3):246–253.

51. Wang SC, Du ST, Hashmi S, Cui SM, Li L, Handschuh-Wang S, Zhou X, Stadler FJ. Understanding Gel-Powers: Exploring Rheological Marvels of Acrylamide/Sodium Alginate Double-Network Hydrogels. Molecules. 2023 Jun 20;28(12):4868.

52. Rosiak JM, Yoshii F. Hydrogels and their medical applications. Nuclear Instruments and Methods in Physics Research Section B: Beam Interactions with Materials and Atoms. 1999 May 2;151(1):56–64.

53. Li J, Mooney DJ. Designing hydrogels for controlled drug delivery. Nat Rev Mater. Nature Publishing Group; 2016 Oct 18;1(12):1–17.

54. Stojkov G, Niyazov Z, Picchioni F, Bose RK. Relationship between Structure and Rheology of Hydrogels for Various Applications. Gels. Multidisciplinary Digital Publishing Institute; 2021 Dec;7(4):255.

55. Chamkouri H. A Review of Hydrogels, Their Properties and Applications in Medicine. AJBSR. 2021 Feb 3;11(6):485–493.

56. Lee KY, Mooney DJ. Alginate: Properties and biomedical applications. Progress in Polymer Science. 2012 Jan 1;37(1):106–126.

57. Wilkinson J, Wade A, Thomas SJ, Jenner B, Hodgkinson V, Coyle C. Randomized clinical trial: a double-blind, placebo-controlled study to assess the clinical efficacy and safety of alginate-antacid (Gaviscon Double Action) chewable tablets in patients

with gastro-oesophageal reflux disease. Eur J Gastroenterol Hepatol. 2019 Jan;31(1):86–93.

58. Dodero A, Pianella L, Vicini S, Alloisio M, Ottonelli M, Castellano M. Alginate-based hydrogels prepared via ionic gelation: An experimental design approach to predict the crosslinking degree. European Polymer Journal. 2019 Sep 1;118:586–594.

59. Russo R, Malinconico M, Santagata G. Effect of cross-linking with calcium ions on the physical properties of alginate films. Biomacromolecules. 2007 Oct;8(10):3193–3197.

60. Ben Djemaa I, Boulmedais F, Auguste S, Tarnowska M, Andrieux S, Drenckhan-Andreatta W. Glucono-Delta-Lactone-Induced Alginate Gelation: New Insights into the Effect of the Cross-Linker Carrier Type on the Hydrogel Mechanics. Langmuir. 2024 May 21;40(20):10492–10501.

61. Growney Kalaf EA, Flores R, Bledsoe JG, Sell SA. Characterization of slow-gelling alginate hydrogels for intervertebral disc tissue-engineering applications. Materials Science and Engineering: C. 2016 Jun;63:198–210.

62. Zhong Y, Lin Q, Yu H, Shao L, Cui X, Pang Q, Zhu Y, Hou R. Construction methods and biomedical applications of PVA-based hydrogels. Front Chem. 2024 Feb 15;12:1376799.

63. Aruldass S, Mathivanan V, Mohamed AR, Tye CT. Factors affecting hydrolysis of polyvinyl acetate to polyvinyl alcohol. Journal of Environmental Chemical Engineering. 2019 Oct 1;7(5):103238.

64. Stauffer SR, Peppast NA. Poly(vinyl alcohol) hydrogels prepared by freezing-thawing cyclic processing. Polymer. 1992 Sep 1;33(18):3932–3936.

65. A Basic Introduction to Rheology [Internet].

66. Whaley JK, Templeton C, Anvari M. Rheological Testing for Semisolid Foods: Traditional Rheometry. Rheology of Semisolid Foods [Internet]. Springer, Cham; 2019 [cited 2025 May 7]. p. 63–96.

67. Weng L, Chen X, Chen W. Rheological Characterization of in situ Crosslinkable Hydrogels Formulated from Oxidized Dextran and N-Carboxyethyl Chitosan. Biomacromolecules. 2007 Apr;8(4):1109–1115.

68. Budelmann D, Schmidt C, Meiners D. Tack of epoxy resin films for aerospace-grade prepregs: Influence of resin formulation, B-staging and toughening. Polymer Testing. 2022 Oct 1;114:107709.

69. Shahshahan S. Characterization of Functional Groups on the Surface of Sonicated Carbon Nanotubes by Optical Spectroscopy Methods. 2016.

70. Chen Z, Deutsch TG, Dinh HN, Domen K, Emery K, Forman AJ, Gaillard N, Garland R, Heske C, Jaramillo TF, Kleiman-Shwarsctein A, Miller E, Takanabe K,

Turner J. UV-Vis Spectroscopy. In: Chen Z, Dinh HN, Miller E, editors. Photoelectrochemical Water Splitting: Standards, Experimental Methods, and Protocols [Internet]. New York, NY: Springer; 2013. p. 49–62.

71. Khalid K, Ishak R, Chowdhury ZZ. Chapter 15 - UV–Vis spectroscopy in non-destructive testing. In: Otsuki A, Jose S, Mohan M, Thomas S, editors. Non-Destructive Material Characterization Methods.

72. Yan C, Pochan DJ. Rheological properties of peptide-based hydrogels for biomedical and other applications. Chem Soc Rev. 2010 Sep;39(9):3528–3540.

73. Wan W, Bannerman AD, Yang L, Mak H. Poly(Vinyl Alcohol) Cryogels for Biomedical Applications. In: Okay O, editor. Polymeric Cryogels: Macroporous Gels with Remarkable Properties [Internet]. Cham: Springer International Publishing; 2014. p. 283–321.

74. Esposito L, Barbosa AI, Moniz T, Costa Lima S, Costa P, Celia C, Reis S. Design and Characterization of Sodium Alginate and Poly(vinyl) Alcohol Hydrogels for Enhanced Skin Delivery of Quercetin. Pharmaceutics. 2020 Nov 27;12(12):1149.

75. Remaggi G, Catanzano O, Quaglia F, Elviri L. Alginate Self-Crosslinking Ink for 3D Extrusion-Based Cryoprinting and Application for Epirubicin-HCl Delivery on MCF-7 Cells. Molecules. 2022 Jan 27;27(3):882.

76. Sodium Alginate Hydrogel Carrier with Calcium Carbonate as Calcium Source for Ibuprofen Release - Lin - 2023 - Macromolecular Chemistry and Physics - Wiley Online Library.

77. Hu X, Liang R, Li J, Liu Z, Sun G. Mechanically strong hydrogels achieved by designing homogeneous network structure. Materials & Design. 2019 Feb 5;163:107547.

78. Chen Y, Li J, Lu J, Ding M, Chen Y. Synthesis and properties of Poly(vinyl alcohol) hydrogels with high strength and toughness. Polymer Testing. 2022 Apr 1;108:107516.

79. Contributions of Polymer Chain Length, Aggregation and Crystallinity Degrees in a Model of Charge Carrier Transport in Ultrathin Polymer Films | Macromolecules.

80. Martinez-Garcia FD, Fischer T, Hayn A, Mierke CT, Burgess JK, Harmsen MC. A Beginner's Guide to the Characterization of Hydrogel Microarchitecture for Cellular Applications. Gels. 2022 Aug 26;8(9):535.

81. Mansfield J, Eiselt P, Yeh J, Mooney DJ. Environmental SEM Study of Sodium Alginate Beads. Microscopy and Microanalysis. 1999 Aug 1;5(S2):300–301.

82. Koch M, Włodarczyk-Biegun MK. Faithful scanning electron microscopic (SEM) visualization of 3D printed alginate-based scaffolds. Bioprinting. 2020 Dec 1;20:e00098.

83. Trieu HH, Qutubuddin S. Polyvinyl alcohol hydrogels I. Microscopic structure by freeze-etching and critical point drying techniques. Colloid Polym Sci. 1994 Mar 1;272(3):301–309.

Appendix

Time sweep test

```
% === List of Excel files to process ===
fileList = {
    '2x_sample1.xlsx', '2x_sample2.xlsx', '2x_sample5.xlsx', ...
    '3x_sample1.xlsx', '3x_sample2.xlsx', '3x_sample3.xlsx', ...
    '4x_sample1.xlsx', '4x_sample2.xlsx', '4x_sample4.xlsx'
};

% === Parameters for plateau detection ===
windowSize = 15;          % number of points in each window
maxRelStd = 0.01;         % max relative standard deviation (1%)
minConsecutiveWindows = 15; % number of stable windows required

for i = 1:9
    % --- Load data ---
    data = readmatrix(fileList{i});
    time = data(:,1);
    G_prime = data(:,2);

    % --- Sliding window analysis ---
    N = length(G_prime);
    stableIdx = [];
    plateau_start_times = [];
    plateau_values = [];
    plateau_start_idxs = [];
    plateau_lengths = [];
    plateau_stds = []; % To store the standard deviation of each
plateau

    for j = 1:(N - windowSize + 1)
        window = G_prime(j : j + windowSize - 1);
        rel_std = std(window) / mean(window);

        if rel_std < maxRelStd
            stableIdx(end+1) = j; %#ok<AGROW>
        else
            if length(stableIdx) >= minConsecutiveWindows
                plateau_start_idx = stableIdx(1);
                plateau_start_time = time(plateau_start_idx);
                plateau_value =
mean(G_prime(plateau_start_idx:plateau_start_idx + windowSize -
1));
                plateau_length = length(stableIdx);
                plateau_std =
std(G_prime(plateau_start_idx:plateau_start_idx + windowSize -
1)); % Standard deviation of plateau

                % Save the detected plateau
```

```
                plateau_start_idxs(end+1) = plateau_start_idx;
%#ok<AGROW>
                plateau_start_times(end+1) = plateau_start_time;
%#ok<AGROW>
                plateau_values(end+1) = plateau_value;
%#ok<AGROW>
                plateau_lengths(end+1) = plateau_length;
%#ok<AGROW>
                plateau_stds(end+1) = plateau_std; %#ok<AGROW>
            end
            stableIdx = []; % Reset to search for new plateaus
        end
    end

    % --- Find the most stable plateau (smallest std) ---
    if ~isempty(plateau_stds)
        [~, min_std_idx] = min(plateau_stds); % Get index of the
plateau with smallest std
        best_plateau_idx = plateau_start_idxs(min_std_idx);
        best_plateau_time = plateau_start_times(min_std_idx);
        best_plateau_value = plateau_values(min_std_idx);
        best_plateau_std = plateau_stds(min_std_idx);
    else
        best_plateau_idx = NaN;
        best_plateau_time = NaN;
        best_plateau_value = NaN;
        best_plateau_std = NaN;
    end

    % --- Plot ---
    fig_num = ceil(i / 3);
    subplot_num = mod(i-1, 3) + 1;
    figure(fig_num);
    subplot(3,1,subplot_num);

    plot(time, G_prime, 'o-', 'DisplayName', 'Experimental
data');
    hold on;

    % Draw all detected plateaus
    if ~isempty(plateau_start_times)
        for k = 1:length(plateau_start_times)
            yline(plateau_values(k), '--g', 'DisplayName',
sprintf('Plateau %d', k));
            xline(plateau_start_times(k), '--r', 'DisplayName',
sprintf('Start %d', k));
            fill([plateau_start_times(k), plateau_start_times(k)
+ windowSize, plateau_start_times(k) + windowSize,
plateau_start_times(k)], ...
                 [min(G_prime), min(G_prime), max(G_prime),
max(G_prime)], 'g', 'FaceAlpha', 0.1, 'EdgeColor', 'none');
        end
    end
```

```
    % Highlight the most stable plateau
    if ~isnan(best_plateau_time)
        yline(best_plateau_value, '-b', 'LineWidth', 2,
'DisplayName', 'Most Stable Plateau');
        xline(best_plateau_time, '-m', 'LineWidth', 2,
'DisplayName', 'Best Start');
    end

    xlabel('Time (s)');
    ylabel("G' (Pa)");
    title(sprintf('File: %s', fileList{i}), 'Interpreter',
'none');
    legend('Location','southeast');
    grid on;

    % --- Annotate results ---
    if ~isnan(best_plateau_time)
        txt = sprintf("Most Stable Plateau: Start=%.1f s,
Value=%.2f Pa, Std=%.2f", best_plateau_time, best_plateau_value,
best_plateau_std);
    else
        txt = "No stable plateau detected";
    end
    text(0.05 * max(time), 0.9 * max(G_prime), txt, ...
        'FontSize', 9, 'BackgroundColor', 'white');

    % --- Clean up variables for next iteration ---
    clear stableIdx plateau_start_idxs plateau_start_times
plateau_values plateau_lengths plateau_stds
end
```

FT-IR Spectroscopy

```
clear all

clc



% === Load FTIR data from CSV files ===

Alg_RT = readmatrix('Alg_4X_RT.CSV');

Alg_60min = readmatrix('Alg_4X_60min.CSV');

Alg_PVA_RT = readmatrix('Alg_4X_PVA_RT.CSV');

Alg_PVA_60min = readmatrix('Alg_4X_PVA_60 min.CSV');
```

```
% === Extract columns and clean zeros ===
wavenumber1 = Alg_RT(:,1);
intensity1 = Alg_RT(:,2);
intensity1(intensity1 == 0) = NaN;

wavenumber2 = Alg_60min(:,1);
intensity2 = Alg_60min(:,2);
intensity2(intensity2 == 0) = NaN;

wavenumber3 = Alg_PVA_RT(:,1);
intensity3 = Alg_PVA_RT(:,2);
intensity3(intensity3 == 0) = NaN;

wavenumber4 = Alg_PVA_60min(:,1);
intensity4 = Alg_PVA_60min(:,2);
intensity4(intensity4 == 0) = NaN;




% === Create main comparison figure ===
% === Plot 1: Alg 4X ===
figure;
hold on;
plot(wavenumber1, intensity1, 'Color', [0 0.6 0], 'LineWidth',
1.5);
plot(wavenumber2, intensity2, 'Color', [1 0.6 0.8], 'LineWidth',
1.5);
set(gca, 'XDir', 'reverse');
xlabel('Wavenumber (cm^{-1})');
ylabel('Transmittance (%)');
```

```
title('FT-IR Spectrum - 4X');
legend({'4X  RT', '4X -20°C / 55°C'}, 'Location', 'northeast');
grid on;
box off;
ylim([80 110]);
saveas(gcf, 'ftir_4X.png');
saveas(gcf, 'ftir_4X.pdf');

% === Plor 2 2: Alg 4X + 5% PVA ===
figure;
hold on;
plot(wavenumber3,   intensity3,   'Color',   [0.2   0.8   0.8],
'LineWidth', 1.5);
plot(wavenumber4, intensity4, 'Color', [0.6 0 0.6], 'LineWidth',
1.5);
set(gca, 'XDir', 'reverse');
xlabel('Wavenumber (cm^{-1})');
ylabel('Transmittance (%)');
title('FT-IR Spectrum - 4X + 5% PVA');
legend({'4X + 5% PVA  RT','4X + 5% PVA -20°C / 55°C'}, 'Location',
'northeast');
grid on;
box off;
ylim([80 110]);
saveas(gcf, 'ftir_4X_PVA.png');
saveas(gcf, 'ftir_4X_PVA.pdf');

% === Pairwise comparison: RT ===
figure;
hold on;
```

```
plot(wavenumber1, intensity1, 'Color', [0 0.6 0], 'LineWidth', 2);

plot(wavenumber3, intensity3, 'Color', [0.2 0.8 0.8], 'LineWidth', 2);

set(gca, 'XDir', 'reverse');

xlabel('Wavenumber (cm^{-1})'); ylabel('Transmittance (%)');

title('Comparison: 4X vs 4X + 5% PVA (RT)');

legend({'4X  RT', '4X + 5% PVA  RT'}, 'Location', 'northeast');

grid on; box off;

ylim([80 110]);

saveas(gcf, 'ftir_comparison_RT.png');

saveas(gcf, 'ftir_comparison_RT.pdf');


% === Pairwise comparison: 60 min ===

figure;

hold on;

plot(wavenumber2, intensity2, 'Color', [1 0.6 0.8], 'LineWidth', 2);

plot(wavenumber4, intensity4, 'Color', [0.6 0 0.6], 'LineWidth', 2);

set(gca, 'XDir', 'reverse');

xlabel('Wavenumber (cm^{-1})'); ylabel('Transmittance (%)');

title('Comparison: 4X vs 4X + 5% PVA −20°C / 55°C');

legend({'4X −20°C / 55°C', '4X + 5% PVA −20°C / 55°C'}, 'Location', 'northeast');

grid on; box off;

ylim([80 110]);

saveas(gcf, 'ftir_comparison_60min.png');

saveas(gcf, 'ftir_comparison_60min.pdf');
```